Experimental Study on the Compression of Entrapped Air Pockets in Stormwater Tunnel Systems

by

Gabriel Maciel Leite

A thesis submitted to the Graduate Faculty of
Auburn University
in partial fulfillment of the
requirements for the Degree of
Master of Science

Auburn, Alabama
August 4, 2012

Keywords: stormwater hydraulics, air pockets, experimental investigation, numerical modeling

Approved by

José Goes Vasconcelos Neto, Chair, Assistant Professor of Civil Engineering
Prabhakar Clement, Professor of Civil Engineering
Xing Fang, Associate Professor of Civil Engineering

To Luana, which she gave strength and protection

when I needed the most.

Abstract

Stormwater storage tunnels may undergo rapid filling pipe conditions during extreme rain events. Such conditions are relevant as adverse conditions may develop, such as surging due to entrapment and compression of entrapped air pockets. Operational issues such as structural damage, geysering and return of conveyed water to grade, among others, have been linked to air pocket entrapment. This work presents results from experimental investigations on pressure surges caused by sudden air pocket entrapment. Steady flow was supplied in a pipeline in such a way that pressurized flows existed at the upstream end while the downstream end experienced free surface flow due to free discharge conditions at the downstream end. A combination of flow rates and slopes resulted in several gradually varied flow profiles at the discharge, with various volumes of atmospheric air at the discharge end. By sudden closing the downstream discharge valve, an air pocket was entrapped and surges were recorded. To emulate conditions in which surge relief is provided during air pocket compression, valve maneuvering also included cases with partial valve obstruction. Among the obtained results, one can notice significantly different surges for cases with and without pressure relief (e.g. with total or partial obstruction), and that the larger is the obstruction degree the larger are the surges. Such findings are useful in the development of numerical models to simulate rapid filling of stormwater tunnels incorporating these findings.

Acknowledgement

I will begin to be intensely grateful to my advisor, Doctor Vasconcelos, for giving the time I need for my recuperation and to have so much confidence in my research. Thank you so much, professor, for believe that I would pass this obstacle in my life. I would also thank my friend, Kyle Moynihan, for helping me to build the apparatus experimental and collecting the data.

I would like to express my genuine gratitude to my family (Salomão, Ciene, Osmarina, Louise and Lorena) that without your security and support, I will have never achieved and succeeded. I will be enormous grateful to the Doctor Clement and to your church for providing a place for my parents and my friends to stay and helping so much in times of need. Thank you very much to all the people (Bernardo, David, Scoot, Sherry, Matthew, Kyle, Sushban, Nirajan, Manoj, Tom Hart, Luana, Lenilza, Salomão, Ciene, José Goes, Denise, Derong, Xiaolong, Sam and if I forgot somebody, please forgive me) who visited in the hospital and the rehabilitation center, I really appreciated all your kindness. I would be hugely grateful to everyone that helped me get up and continue to live my life. Thank you all very much for my friends and my family without you I wouldn't be living this fulfilling moment of my graduation.

Luana, my dear friend, you showed me that is possible to realize my dreams and ambitions. You transformed my life without I even noticed. I already found someone with best kindness and immense sympathy in the world. My luck and my destiny is to have known you.

Table of Contents

List of Figures

List of Tables

Chapter one - Introduction

Stormwater drainage systems are designed to drain the excess of superficial water derived from rain or ground water from the city pavements. Among other components, this system is includes main and secondary conduits, also referred as stormwater sewer system, that receive the runoff captured by the inlets at dropshafts. The dimension (e.g. diameter of conduits) of stormwater sewer systems often reflects flows from rain events with relatively low return periods and with the assumption that the system will operate in a free surface regime. However, in the case of a rapid filling during an intense rain, the conveyance capacity of the system may be exceeded and a pressurized flow regime will occur in the conduit. This is observed from the smallest conduits at the upstream end of the urban catchment until the largest conduits such as stormwater storage tunnel systems.

In this process, the air phase initially present in the conduits can also become entrapped and pressurized, resulting in a two-phase flow condition. The transition between the two phases has been linked to structural problems in drainage systems and the geysering phenomenon. Guo and Song (1991) show pictures of geysers that occurred in Minnesota stormwater drainage system pointing that these events resulted in undesirable flooding and pollution problems. Zhou et al. (2002) pointed out similar issues and infrastructure damage caused by intense rain events in the city of Edmonton in 1995.

The knowledge about this problematic is still very scarce and limited, mainly in the interaction of the two phases in an extreme inflow condition. This study aims to contribute in the better understanding of the issues in drainage systems during intense rain events focusing on the effects generated by entrapped air pockets. To attain this objective, research was conducted involving numerical and experimental investigations in order to represent more precisely the effects of sudden air pockets entrapment and associate pressures surges in an unventilated system.

The following sections include a description of flow in stormwater sewers as two-phase flows, considering all possible interactions between air and water in rapid filling scenarios. Also,

these flows also are unsteady due to the nature of the rainfall-runoff generation process, and a section on unsteady flow formulation for these systems is presented.

1.1. Stormwater systems described in two-phase flow framework

Air presence in stormwater system flows is of great relevance to the analysis of these in unsteady conditions. Air may become an issue in hydraulic systems when the filling rate reaches a certain level that leads to the entrainment and/or entrapment of air in the pressurized portions of the flow. These rapid inflow conditions are central to the hydraulic analysis of these systems since operational issues that have been reported to date in stormwater systems are generally associated with intense rain events. The effects of the air presence in the closed conduits are mainly three (Pozos, 2007):

1. High air compressibility can generate higher pressures than the pipeline walls resistance, causing the rupture of the conduit (Wylie and Streeter, 1993);
2. Air volume alter system dynamics, and can lead to change in the flow characteristics, velocity and discharge, and have been traced to episodes such as geysering (Vasconcelos and Wright, 2011);
3. The air accumulation in the intermediate or high points with no ventilation can form a partial blockage in flows, creating additional energy losses and in cases of stormwater tunnels loss of storage capacity, which may lead to premature overflow episodes.

Stormwater flows are said to be single phase if water phase fills the entire conduit volume; when air phase is also present, they are classified as biphasic or two-phase flows. When small air bubbles and pockets are traveling in conduits due to drag forces caused by the water flow, this volume of air tends to accumulate in the high points of the conduit, a problem that is of relevance in the context of water main design; in other instances air pockets may be generated from the air volume originally present in the tunnel that is entrapped by the water flow, as shown in Vasconcelos and Wright (2006). Figure 1.1 exemplifies a mechanism of air pocket entrapment

based on reflection of inflow fronts off of system boundaries predicted by numerical simulation. As it is presented below, classification of two-phase flows generally involves a clear identification of the two phases in the conduits, which occupy distinct places in the pipe cross section. Adequate representation of these conditions in numerical models requires two-phase flow modeling approaches (Vasconcelos et al, 2011). However, for some applications where very small air bubbles are well-distributed in the entire pipe cross section, flows may be regarded as homogenous, and a valid modeling alternative is to represent such conditions in a single-phase flow framework. In these circumstances, modeling can be done considering a single phase fluid and adjusting the acoustic wave velocity calculation, among other relevant flow parameters such as density and bulk modulus of elasticity (Wylie and Streeter, 1993).

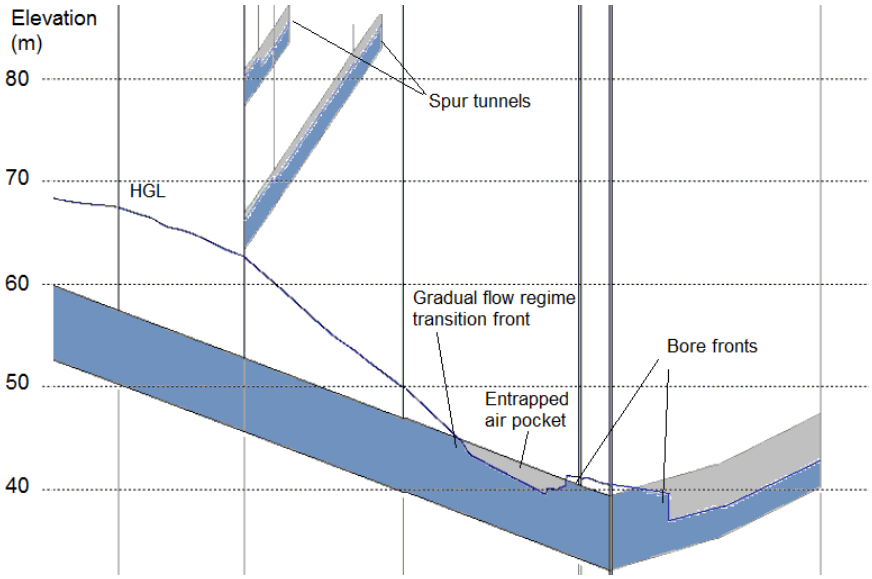

Figure 1.1: Air pocket entrapment at low point shaft predicted by numerical simulation

Air accumulation in the closed conduits affects the behavior of the flow, and may cause additional head losses and reduction of acoustic wave propagation speed (Wylie and Streeter, 1993). This topic has been of research interest since the decade of 1940's, with the studies by Kalinske and Bliss and Kalinske and Roberts on the motion of air bubbles and the air

entrainment in hydraulic jumps. Benjamin (1968) performed studies on the motion of air cavities in closed conduits in the context of gravity current flows. Wallis (1969) presents a comprehensive study on unsteady two-phase flows proposed a classification based in the morphological arrangement of the components of the two-phase flow. This study also indicates that the classification can often be revealed through visual or photographic observations but it can't define completely the flow regime due to other independents criteria such as the turbulence of the system. The relative proportion of air and water flowing through the pipeline depends on the slope and the quantity of air. The presence of air in water flows receives different denominations depending on the relative size of the cavity, as illustrated in the Figure 1.2.

Falvey (1980) described the flow patterns for two-phase horizontal flows:

- Bubble Flow - Air forms in bubbles at pipe crown that has approximately the same velocity as the water flow; it is denominated as "Front Flow" if the bubbles are dispersed;
- Plug flow - The air bubbles combine in plugs and rapid alternation between air flow and water flow is observed in cross sections;
- Stratified flow - The air and water flow creates a horizontal interface separation and both are flowing downstream;
- Wave flow- Surface waves appear in stratified flow if air flow is increased;
- Slug flow - Air pocket are large enough to close half of the pipe cross section. The air slug travels with velocity higher than the average water flow velocity.
- Annular flow - Water flows as a film on the pipeline wall, while air phase flows with greater velocity at the conduit center.
- Spray flow – For even higher air flow velocity, the water film is broken by shear and carried away in water droplets.

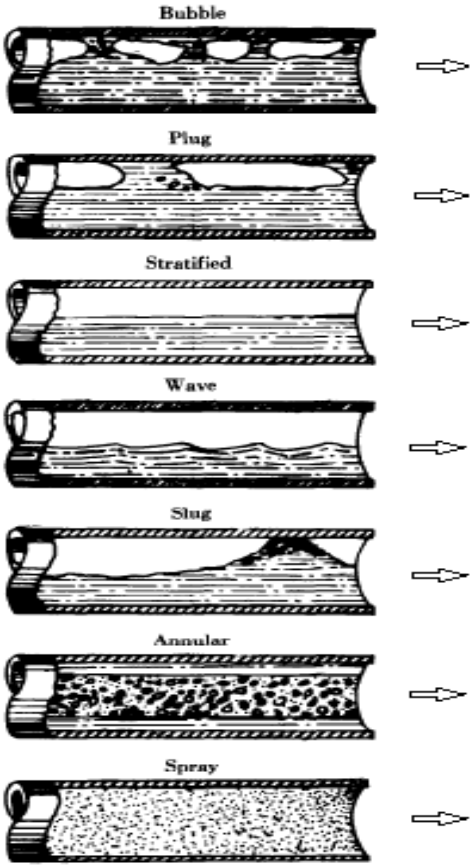

Figure 1.2: Horizontal, two-Phase flow patterns (Falvey, 1980)

In stormwater system flows, anticipated two-phase flows are either slugs or bubbles flow, depending on inflow conditions, and system geometry characteristics such as pipeline slope. The definition of bubbles and slug sizes varies between researchers. Bubbles are identified by Wisner et al. (1975) as ellipsoidal shaped air cavities with the size varying from 1 mm to 5 mm. In the case of Pozos (2007), bubbles are identified as air cavities with the longitudinal length less than or equal to the diameter of the pipe. On the others hand, air slugs and pockets are defined by Pozos (2007) as an air cavities with longitudinal length greater than the diameter of the pipe. Falvey (1980) describe that the transition from bubble flows to slug flows occurs when the bubble diameter is one-half of the conduit diameter.

1.2 Modeling Framework of rapid filling pipe problems

Because of potential operational issues in stormwater systems undergoing rapid filling events, numerical models have been developed to anticipate the magnitude of pressure surges and/or simulate the filling process of these systems, particularly in the context of large stormwater tunnel systems (Song, et al., 1983; Cardle and Song, 1988; Vasconcelos, et al. 2006; Politano, et al. 2007; among others). While most current models neglect effects of entrapped air in these systems, in the scope of the present investigations the inclusion of these are essential. This section presents a brief summary of the mathematical framework used in the development of the numerical model of this thesis.

1.2.1. Air phase modeling

While there are different alternatives to simulate the behavior of entrapped air pockets that includes one-dimensional, discretized formulations as presented by Issa and Kempf (2003), Trindade and Vasconcelos (2011), among others, the simplest formulation that has been used to date is based on the application of the ideal gas law. This alternative has been used by Martin (1976), Li and McCorquodale (1999), Zhou, et al. (2002), among others.

The ideal gas law was Clapeyron in the XIX century, who demonstrated that there was an inversely proportional relationship between pressure and volume of a gas. Krönig, in 1856, demonstrated that these results can also be derived from kinetic theory of gases. In an isothermal process, a gas pressure, volume, and temperature are related by equation (1.1).

$$PV = nRT \tag{1.1}$$

which P is the pressure, V is the volume, n is the amount gas substance (in moles), R is the ideal, or universal gas constant, and T is the temperature.

While the ideal gas law is good approximation to the behavior of real gases at any pressure or any temperature, it has various limitations that one example was the negation of both molecular size and intermolecular attraction. However, for the process involving air entrapment in water flows in closed conduits, the ideal gas law has been applied successfully to describe pressure changes upon air compression/expansion cycles. This equation, expressed in terms of an ordinary differential equation on time, is enforced during the water flow simulation at air-water interfaces.

1.2.2. Water phase modeling

Time-independent water flows, in which none of its fundamental characteristics such as pressure and velocity are varying in time, are classified as steady flows. However, due to the nature of rainfall-runoff generation, stormwater flows present significant variation over time, and thus are referred to as unsteady flows. The one-dimensional formulation of these unsteady flows requires a mathematical model based on the fundamental laws of mass and linear momentum conservation, as presented below.

1.2.2.1. Momentum equation

The theoretical foundation of the momentum equation is in Newton's second law, which states that the sum of the forces acting on a control volume must be balanced by varying the amount of linear movement amount of it. Essentially, in water flows, three forces are predominant: weight; frictional forces; and pressure forces. Figure 1.3 illustrates a typical free-body diagram over a control volume for application of equation of motion in a closed conduit.

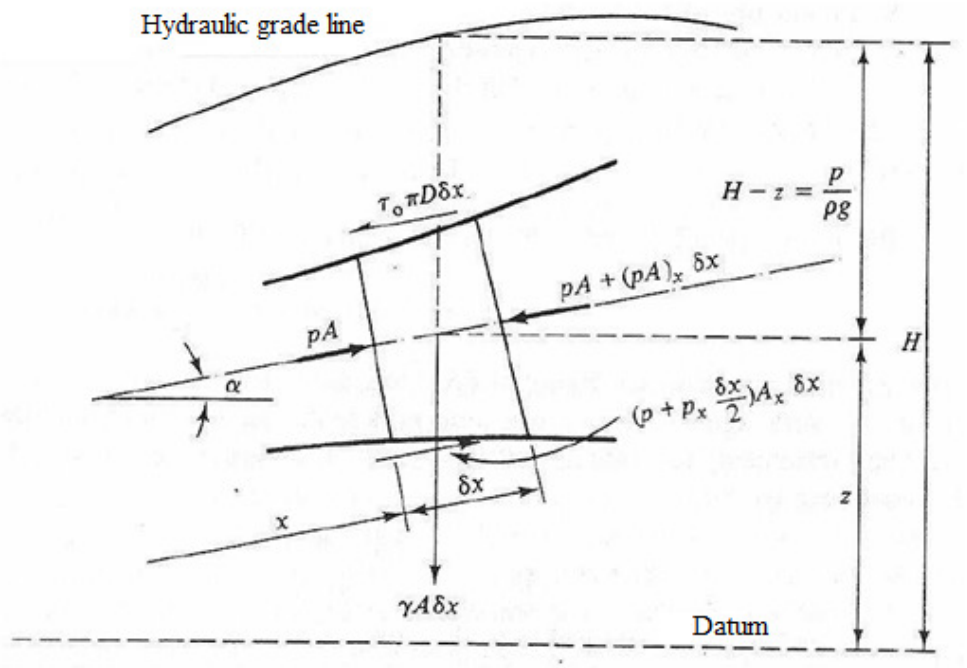

Figure 1.3: The equation of motion for a control volume (Wylie and Streeter, 1993)

The application of Newton's 2nd law in the control volume presented in Figure 1.3 results in equation (1.2):

$$pA - \left[pA + \frac{\partial (pA)}{\partial x}\delta x\right] + \left(p + \frac{\partial p}{\partial x}\frac{\delta x}{2}\right)\frac{\partial A}{\partial x}\delta x - \tau_o \pi D \delta x - \rho g \delta x A sin(\alpha) = \rho A \delta x \frac{dV}{dt} \quad (1.2)$$

Where p is pressure in the control volume, δx is the length of the control volume, ρ is water density, A is the cross-sectional area, D is the pipe diameter, V is the velocity in the section, g is the gravity, and H is the height hydraulic grade line, τ_o is the shear tension, x is the position on the length, z is the elevation of the pipe center and t is the time.

Provided that δx is sufficiently small, all terms which in the order $(\delta x)^2$ become negligible. This results in equation (1.3).

$$\frac{\partial p}{\partial x}A + \tau_o \pi D + \rho g A sin(\alpha) + \rho A \frac{dV}{dt} = 0 \quad (1.3)$$

Despite shear forces be dependent of local acceleration terms (Wylie and Streeter, 1993), particularly in fast transient (waterhammer) applications, for simplicity it is assumed the validity of the Darcy-Weisbach equation relating a pressure drop caused by friction, the friction factor and the velocity head as defined by equation (1.4):

$$\Delta p = \frac{\rho f L}{D}\frac{V^2}{2} \quad (1.4)$$

If this pressure drop is caused by shear forces, one may write:

$$\Delta p \frac{\pi D^2}{4} = \tau_o \pi D L \quad (1.5)$$

From this relationship, an expression for the shear tension is obtained:

$$\tau_o = \frac{\rho f V|V|}{8} \quad (1.6)$$

Since velocity V is a function of both time and space, its total differential can be defined as:

$$\frac{dV}{dt} = \frac{\partial V}{\partial t} + V\frac{\partial V}{\partial x} \quad (1.7)$$

When equations 1.6 and 1.7 are used in equation 1.3, relation (1.8) is derived:

$$\frac{\partial p}{\partial x}\frac{1}{\rho} + V\frac{\partial V}{\partial x} + \frac{\partial V}{\partial t} + g sin(\alpha) + \frac{fV|V|}{2D} = 0 \quad (1.8)$$

As pointed out by Wylie and Streeter (1993), for low Mach flows this expression may be expressed by the expression below of the momentum conservation:

$$\frac{\partial p}{\partial x}\frac{1}{\rho}+\frac{\partial V}{\partial t}+gsin(\alpha)+\frac{fV|V|}{2D}=0 \tag{1.9}$$

Further manipulation includes represent the pressure terms in terms of the piezometric head H. The relationship between pressure p and piezometric head H is:

$$p=\rho g(H-z) \tag{1.10}$$

with z as the elevation of the CV.

Therefore, one derives:

$$\frac{\partial p}{\partial x}=\rho g\left(\frac{\partial H}{\partial x}-\frac{\partial z}{\partial x}\right)=\rho g\left(\frac{\partial H}{\partial x}-sin(\alpha)\right) \tag{1.11}$$

which is substituted into the equation 1.9 to derive an alternative expression for the momentum equation:

$$\frac{\partial V}{\partial t}+g\frac{\partial H}{\partial x}+\frac{fV|V|}{2D}=0 \tag{1.12}$$

Equation 1.9 and 1.12 are applicable for any one-dimensional, homogeneous, low Mach fluid flows. Further simplification of this expression is possible, yielding an ordinary differential equation that forms the basis for the Rigid Column Model.

1.2.1.2. Continuity Equation

The one-dimensional continuity equation expresses mass conservation in pipeline flows. The control volume geometry is represented by Figure 1.4, where the upstream boundary of the control volume is located in section x. The mass conservation law establishes that the net inflow into the control volume equals to the rate of mass increase, expressed by equation 1.13:

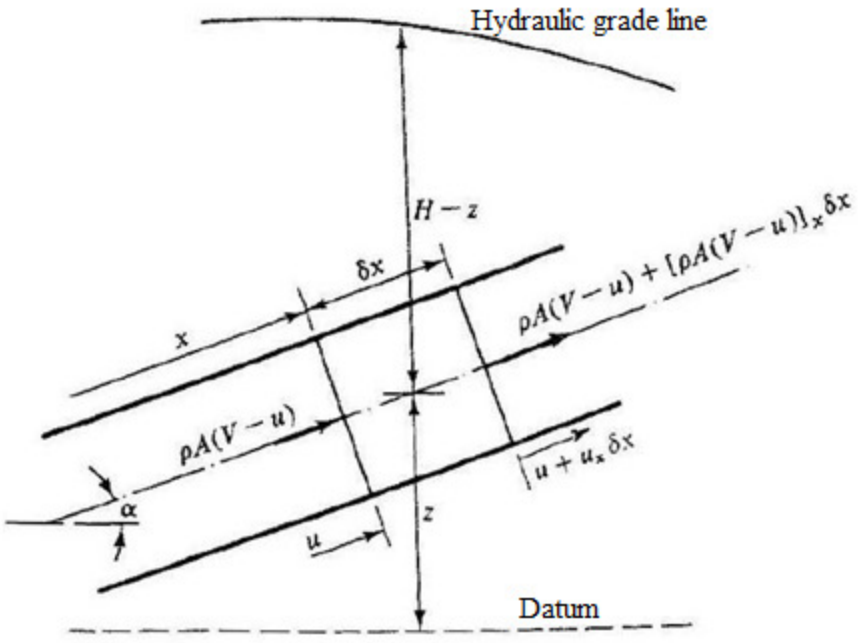

Figure 1.4: Control volume for continuity equation (Wylie and Streeter, 1993)

$$-\frac{\partial}{\partial x}[\rho A(V-u)]\delta x = \frac{d}{dt}(\rho A \delta x) \tag{1.13}$$

Where u is the velocity in the conduit wall velocity and the differential operator d/dt that appears in equation in equation 1.13 is expressed as:

$$\frac{d}{dt} = u\frac{\partial}{\partial x} + \frac{\partial}{\partial t} \tag{1.14}$$

The growth rate of the length of the control volume is given by the formula (1.15).

$$\frac{d}{dt}\delta x = \frac{\partial u}{\partial x}\delta x \tag{1.15}$$

Taking these expressions into equation 1.12 results in:

$$\frac{\partial}{\partial x}[\rho A(V-u)]\delta x + \delta x \frac{d}{dt}(\rho A) + \rho A \frac{d}{dt}(\delta x) = 0 \tag{1.16}$$

Further manipulations leads into

$$\frac{\partial}{\partial x}(\rho AV) - \frac{\partial}{\partial x}(\rho Au) + \frac{d}{dt}(\rho A) + \rho A \frac{\partial u}{\partial x} = 0 \tag{1.17}$$

$$\frac{\partial}{\partial x}(\rho AV) - \frac{\partial}{\partial x}(\rho Au) + u\frac{\partial(\rho A)}{\partial x} + \frac{\partial(\rho A)}{\partial t} + \rho A \frac{\partial u}{\partial x} = 0 \tag{1.18}$$

Assuming that the last term on the left hand side of equation 1.18 is zero, equation 1.19 or 1.20 are obtained as expressions of the continuity equation for compressible flows.

$$\frac{\partial(\rho A)}{\partial t} + \frac{\partial(\rho AV)}{\partial x} = 0 \tag{1.19}$$

$$\frac{\partial(\rho A)}{\partial t} + V\frac{\partial(\rho A)}{\partial x} + \rho A \frac{\partial(V)}{\partial x} = 0 \tag{1.20}$$

Wylie and Streeter (1993) proceed with equation 1.20, and using the concept of acoustic wave speed (the celerity of pressure wave propagation in closed conduit flows) defined as $a^2 = \frac{K/\rho}{1+(K/A)(\Delta A/\Delta p)}$, (with ρ as density and K the fluid's bulk modulus of elasticity) showed that for Mach number flows, one can express the unsteady continuity as:

$$\frac{\partial H}{\partial t} + \frac{a^2}{g}\frac{\partial V}{\partial x} = 0 \tag{1.21}$$

One relevant observation is that the equations (e.g. 1.12 and 1.21) have been derived with the assumption of unsteady, pressurized flows. During rapid inflow scenarios is likely that portions of the system will be pressurized, but others would be operating in unsteady, free surface flows. In the latter case, Saint-Venant would be applicable. Stormwater tunnel models may either apply either equation at these flow regions, tracking the position where pressurization interface exists, or apply conceptual models such as the Preissmann slot (Cunge and Wegner,

1964) or TPA (Vasconcelos, et al. 2006) and use a single equation in the two flow regime domains. The approach in this study involves tracking the location of the pressurization interfaces over time.

1.3. Thesis Outline

Chapter Two includes the literature review for this research, focusing in recent investigation on two-phase flow characterization; air effects in unsteady closed conduit flows; experimental investigations on rapid inflow conditions in stormwater systems; and numerical modeling approaches to extreme flow conditions in stormwater systems. Chapter three presents the perceived knowledge gaps and research objectives. Chapter Four includes the methodology of the work, including a description of the experimental apparatus construction, experimental program, and numerical modeling strategy. Chapter Five presents research results and a discussion of research findings that are of practical relevance for the design of stormwater conveyance systems. Finally, Chapter Six presents the conclusions of this research and it gives recommendations for subsequent studies.

Chapter two - Literature Review

The literature review is divided in three subsections to facilitate the understanding current stage of the research on extreme flows in stormwater systems including air effects. The initial section presents two-phase flow investigations in the context of air cavity motion and shape in closed conduits. The second section presents the research on rapid filling flows in closed conduits and effects of entrapped air, both in the context of sloping water pipelines and stormwater systems. Finally, the last section presents some of the numerical modeling alternatives to simulate the flows including the transition between free surface and pressurized conditions, which are anticipated in stormwater systems undergoing rapid filling.

2.1 Air cavity motion and shape in closed conduit flows

The advance of an air cavity into a pressurized flow is an example of a gravity current problem, and has been studied by a number of researchers as early as the decade of 1960's. An important contribution was the work presented by Benjamin (1968), who considered the advance of an air cavity into a horizontal pipeline water flow as it was emptied. Among other important contributions, this work demonstrated an important relationship between the thickness of the gravity current and the celerity of its advance. A follow-up study presented by Wilkinson (1981) demonstrated that no-slip effects and surface tension, which were not accounted for in Benjamin's work had an influence the air cavity shape and celerity.

Research by Baines (1991) included the advance of an air cavity in an emptying pipeline considering slope effects. It was observed that increased slopes resulted in a larger celerity of the air pocket for the narrow range of slopes considered. Moreover, it was observed a variation of air pocket thickness along its length. It also expressed that the air pocket shape at the air-water interface front is very depending on the air quantity that enters into the conduit, and that under certain conditions a led to gulping at the water outlet, which broke the integrity of the advancing air cavity, generating discrete air pockets.

Goldring (1983) analyzed the air voids caused by the downshaft-tunnel bend water flow of middle size diameter. He noticed that there was a range between air and water flows to an air void become stable in the bend. A related problem was presented by Hager (1999), who investigated air cavity shape formed as water discharged freely from a horizontal pipeline. The on systematic experiments assumed the Froude number in the outlet as the controlling variable. This studied modified the Boussinesq equation and proposed equations to represent the shape of the cavity profile and the downstream end depth ratio for various flow conditions. Figure 2.1 represents a portion of the experimental two-phase flow apparatus, which has a discharge setup that resembles the one used in the present research.

Figure 2.1: Two-Phase flow apparatus (Hager, 1999)

2.2. Rapid filling flows in closed conduits and effects of entrapped air

One of the pioneering studies involving unsteady pipeline flows with air was presented by Holley (1969), who conducted analytical and experimental studies in order to investigate the type and magnitude of surges that can happen in pipe system that contains several check structures. The author suggested that that the storage and release of air cavities inside the pipeline can cause head surges initiation in the system.

Martin (1976) proposed a model based on the lumped inertia approach that combined air modeling based on the ideal gas law. This model was developed to determine the magnitude of the pressure surges caused by compression of air cavities at the pipeline discharge. The model shows that the presence of entrapped air may lead to peak surge pressures that are many times larger than the driving pressure in the water flow due to air compressibility. This model proposed ideas that later served as basis for important studies, such as Zhou, et al. (2002) and De Martino et al. (2008). A schematic of key parameters of Martin (1976) model is presented in Figure 2.2.

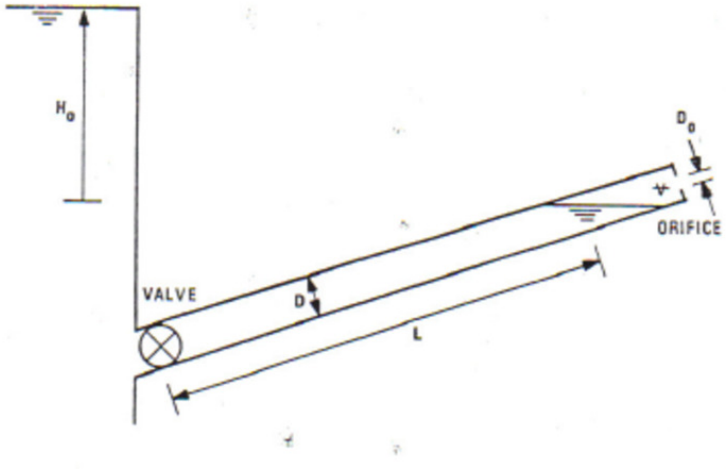

Figure 2.2: Schematic of key parameters used in Martin (1976) model.

Possibly, the first numerical model of water main filling simulation was designed by Liou and Hunt (1996). It applied to the filling of long water mains with variations in topographic profiles, but the model does not account explicitly for air phase effects. According to the authors, the model is applicable as long as the flow velocity is higher than the celerity of an intruding air cavity, such as the ones discussed in section 2.1. In these conditions, a rigid column model was proposed and implemented, assuming perfect air ventilation and that the inflow front remains well defined and vertical, resembling a water piston. As the inflow front advances over an sloped terrain, increasing frictional forces slow its advance. The authors compared the model predictions with experimental results obtained with a small diameter pipeline submitted to a high

driving head and obtained good agreement. Figure 2.3 presents a sketch of the key variables used by this model in an undulating water main.

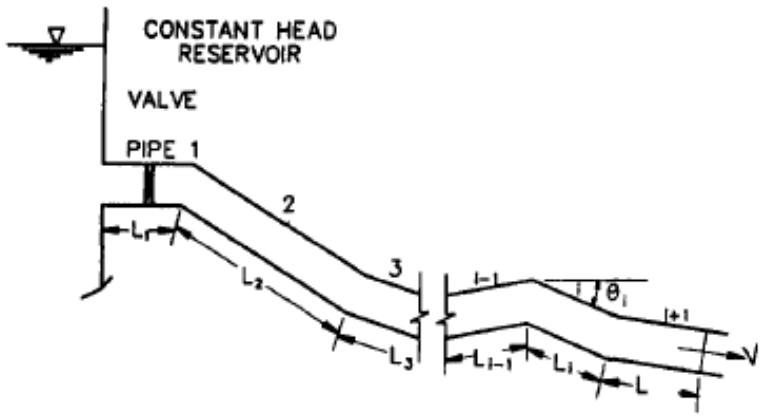

Figure 2.3: Sketch of key variables used by Liou and Hunt (1996) model for water mains.

Izquierdo et al. (1999) presented a numerical model to simulate the filling of pipelines based on the momentum equation, considering the hypothesis of water accumulation in the lower points of the water pipeline, which would lead to air pockets entrapment upon flow startup at the upstream end of the system. Air pockets were located between the points of water accumulation and they were highly compressed by the surrounding water columns as the flow was initiated. The authors concluded that the smaller air pockets volumes led to greater the pressure surges upon flow initiation, a result in agreement with the earlier work by Martin (1976). The model assumes that the transition interface between phases remains well defined and that the entrapped air does not intrude on the water advance. While Izquierdo (1999) improved Liou and Hunt (1996) model by adding the capability of air pocket compression during a rapid filling event, it still has applicability limitations. One is the lack of air ventilation on the formulation, a feature that could be present in anticipated in stormwater systems in terms of vertical shafts and/or manholes. A follow-up experimental study presented by Fuertes, et al. (2000) assessed the validity of Fuertes, et al. (1999) model using an experimental apparatus comprised by a pipe with 6.90 m of length and a small internal diameter of 18.8 mm, shown in Figure 2.4. Good agreement

between experiments and numerical predictions was observed, as presented in Figure 2.5. An important remark is that experimental conditions included only cases with high ratios of driving pressure head over pipe diameter, which are not representative for flows in stormwater systems.

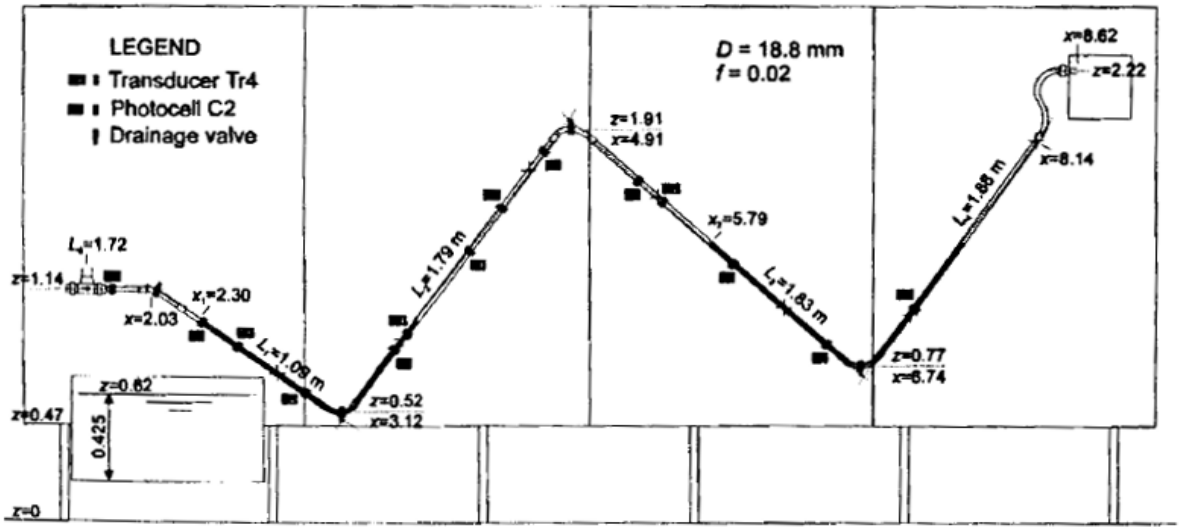

Figure 2.4: Characteristics of the installation (Fuertes et al., 2000)

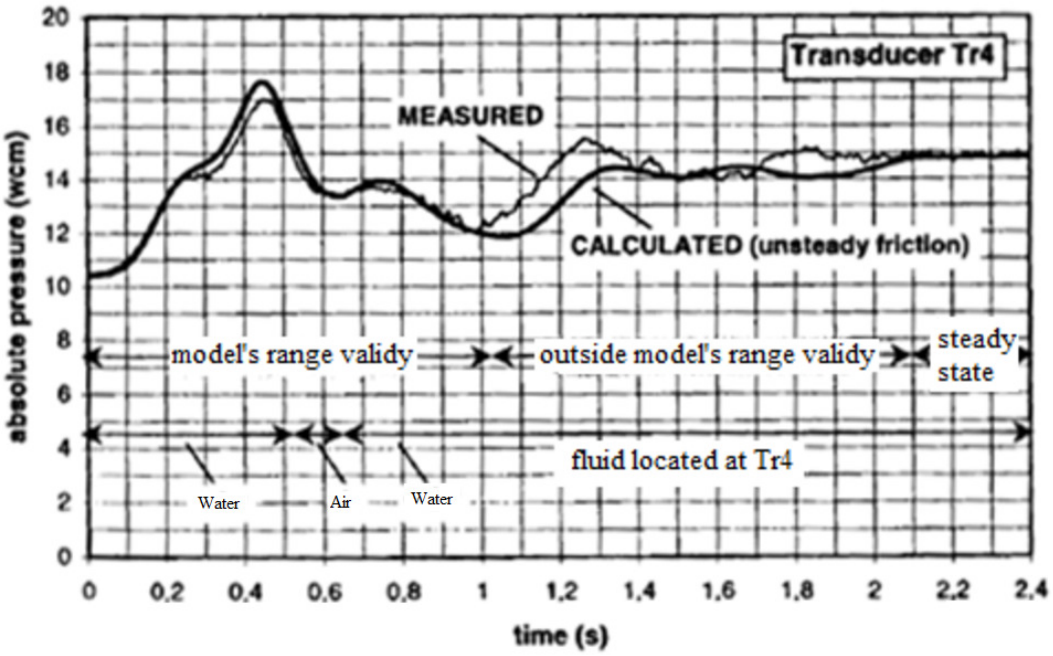

Figure 2.5: Comparison between the model of Izquierdo et al. (1999) and the measured values (Fuertes et al., 2000).

Li and McCorquodale (1999) constructed an experimental model to simulate the pressure transients due to the transition from the free-surface to the pressurized flow in the context of rapid filling pipeline flows. The study of consisted of the 12.12 m long pipeline and the diameter was 152 mm, connecting upstream to open-channel section and downstream to a reservoir tank. This research analyzes continuously surges due to the entrapped air pocket and considers the movement of the air bubbles, which consists an in important innovation. The authors also proposed a numerical model that extended and refined the previous one proposed by Hamam and McCorquodale (1982) that adopted the hypothesis of a stationary bubble. One limitation of this study is that it doesn't consider the effect of a ventilation system acting in the air cavity for storm sewers. Figure 2.6 presents schematics of their experimental apparatus.

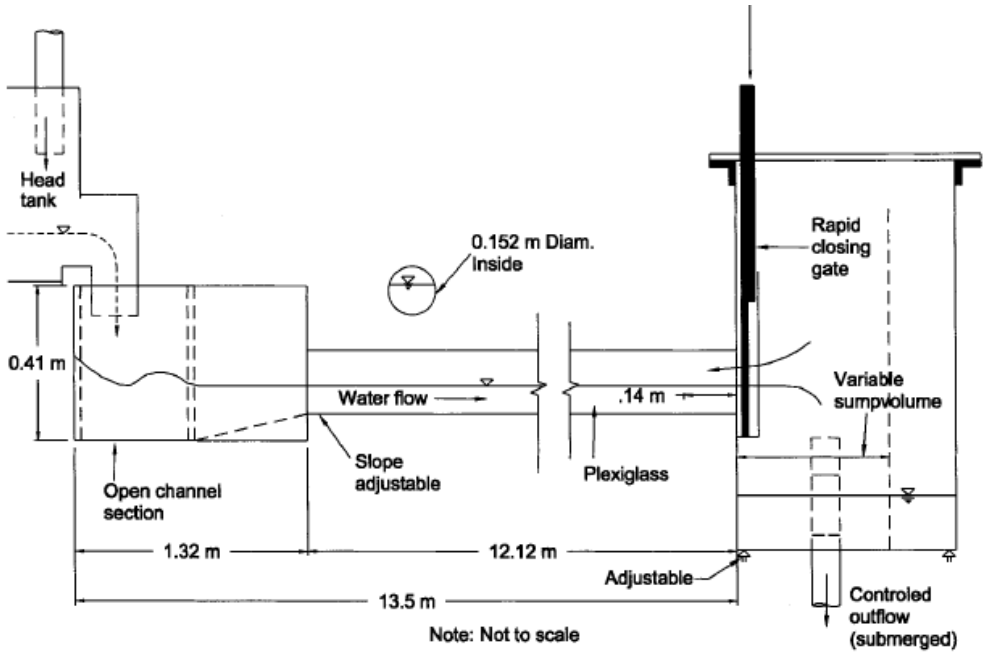

Figure 2.6: Experimental model layout by Li and McCorquodale (1999).

Another relevant work was presented by Zhou et al. (2002), which included an experimental study of the rapid filling of a short and horizontal conduit with 10 meter of length and 35 mm of diameter. One important goal was to estimate the effects of the air ventilation to the observed transient pressures with the goal of obtaining the peak pressure. The authors also proposed a numerical model based on the lumped inertia approach with the additional consideration of the air pressurization effects. A limitation of Zhou et al. (2002) study is the use of a small pipeline diameter and a very large driving pressure head/diameter ratio, which are not representative conditions that would be observed in actual stormwater systems. The numerical model uses the same assumption as Liou and Hunt (1996) and Izquierdo, et al. (1999) model of a well-defined inflow interface; the authors assume a vertical inflow front in the filling process. A follow-up work by Zhou et al (2004) introduced a vertical pipe in the apparatus in order to investigate the effect of the vertical conduit in the air-water flow condition, but the behavior of

the system and the results did not change considerably. Figure 2.7 exemplified a sketch of experimental apparatus used Zhou et al. (2002).

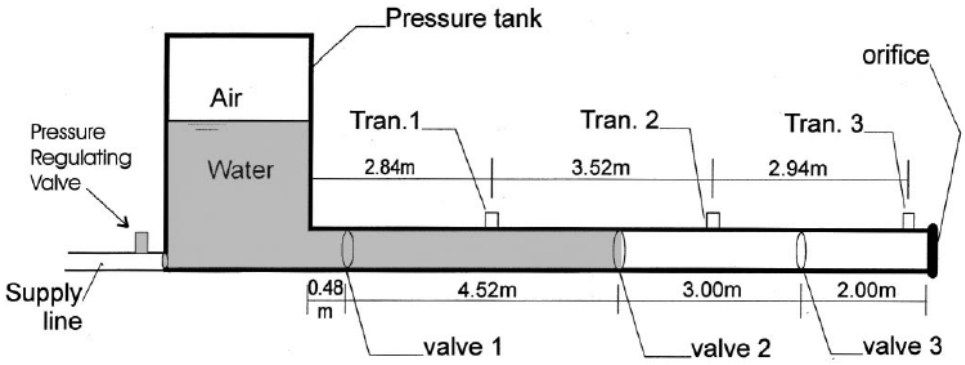

Figure 2.7: Diagram of experimental apparatus (Zhou et al., 2002).

Aimable and Zech (2003) conducted experiments that agreed with the experiment proposed by Li and McCorquodale (1999) for the formation of air pockets in sewers. Their apparatus consisted of pipe with two manholes of 0.2 m and 0.144 m diameter spaced 5.0 m along the pipeline. The downstream reach initially flowed in a steady pressurized state and the two other parts were in free surface conditions. The study shows that a sudden increase in the pressure at the downstream end generated a flow regime transition front, and confirmed the mechanism of pocket motion described by Li and McCorquodale (1999).

Arai and Yamamoto (2003) performed experiments in apparatus 1/50 scale of actual underground drainage system. The experimental apparatus have the pipeline of 0.198 m diameter and a length of 122.08 m to investigate the effects of the air pressurization when there is flow already on the system. Their results indicate that the air pocket presence accelerates the transition from free surface to pressurized flow, suppress the tube oscillation and increases the maximum pressure and increases air releases.

Despite many of these previous studies resulted in numerical models that are constructed with the assumption of well-defined air-water interfaces, in conditions when the driving pressure head/diameter relationship is not high this assumption of may not be accurate. Guizani, et al. (2005) conducted numerous experiments on the filling of water pipelines with different inflow conditions and slopes. In all cases the filling front shape resembled a wedge, similar to a dam-break front propagating within the pipe. In this research, it was point out that a vertical interface would be an applicable supposition only if the flow rate within the conduit is very large.

More recently, De Martino, et al. (2008) reported an experimental installation to analyses the water flow transients that was caused by the expulsion of the air pocket. The De Martino, et al. (2008) utilized a galvanized steel pipe was around 70 m long, a diameter of 53 mm and the downstream end an air venting orifice. In this research, the pressure oscillation through an orifice was studied and it was closely related to the ones observed by Zhou et al. (2002). This study avoided the difficulty of assuming a vertical air-water interface by orienting the pipe flow and direction of air compression vertically. De Martino, et al. (2008) showed that the driving pressure head and orifice diameter are more important factors toward the pressure surge magnitude than the length of the air pocket.

However relevant, one argues that these extreme conditions used in most of past investigations are too extreme and not representative of the situations anticipated in stormwater systems in rapid filling scenarios where air pockets may become entrapped and compressed. In addition to this, important air pocket formation mechanisms, such as the one generated by the reflection of water flow fronts within the system downstream boundaries has not been sufficiently executed and tested to this date to assess the magnitude of surges that are anticipated following these entrapment mechanisms. These are outstanding research questions that are addressed by the present work.

2.3. Numerical modeling of stormwater drainage systems in extreme flow conditions

As mentioned previously, numerical modeling has been an important tool to analyze the behavior of stormwater systems, particularly large below-grade stormwater tunnels, under rapid inflow conditions that are anticipated in intense rain events. These models provide information as to what are the anticipated pressure surges, elevations of HGL at selected location, flow rates and other relevant results for designers. A common assumption is that flows are single-phase, and unsteady. These models' ability to incorporate air phase interactions is limited partly because of the few experimental studies conducted to date on these interactions in closed conduit flows.

Because filling processes will be characterized by the transition between free surface flow conditions into a pressurized flow condition, models that need to handle both flow unsteadiness and the transition between these two flow regimes. These models are referred to in literature as Mixed Flow models or Flow Regime Transition models, and the first model was proposed by Cunge and Wegner (1964) to study the hydraulics of a tail-race tunnel in the context of a hydroelectric dam. The model used the Saint-Venant equation to perform the simulation, which is expressed below in conservative, vectorial format:

$$\frac{\partial \vec{U}}{\partial t} + \frac{\partial \vec{F}}{\partial x} = \vec{S} \tag{2.1}$$

$$\vec{U} = \begin{bmatrix} A \\ Q \end{bmatrix} \qquad \vec{F} = \begin{bmatrix} Q \\ \frac{Q^2}{A} + gAh_c \end{bmatrix} \qquad \vec{S} = \begin{bmatrix} 0 \\ gA(S_o - S_f) \end{bmatrix} \tag{2.2}$$

Where $\boldsymbol{U}$ is the vector of conserved variables, $\boldsymbol{F}$ is the vector of conserved fluxes, $\boldsymbol{S}$ is the vector of source terms, A is the flow cross sectional area, Q is the flow rate, g is gravity acceleration, h_c is the distance from the cross-section centroid and the free surface, S_o is the conduit slope and S_f is the friction head.

Because this equation becomes non-defined if the free surface width reaches zero (e.g. at pipe crown), the authors used the conceptual model proposed by Preissmann (1961). He hypothesized that if a virtual narrow slot would be added at the top of a closed conduit both pressurized and free surface flow could be analyzed by the St. Venant equations since the

resulting cross section would still have a free surface interface. This slot would allow for the surcharge pressure that would be anticipated in pressurized flow conditions. A schematic of the Preissmann slot is represented by Figure 2.8, with t_f as the slot width, h_{slot} as the water level inside the slot, corresponding to a surcharge pressure head, and *D* as the conduit diameter.

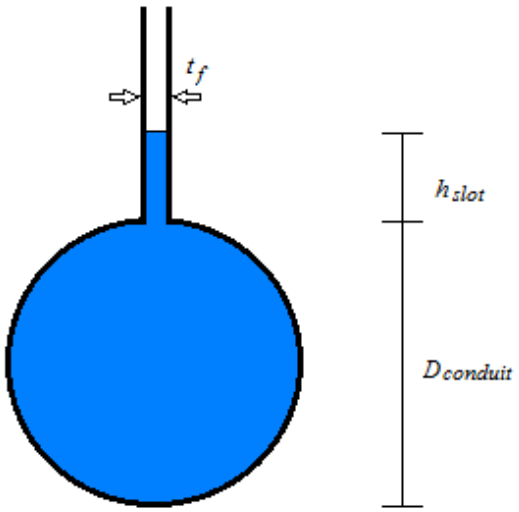

Figure 2.8: Scheme of Preissmann Slot concept

The Preissmann slot idea is simple and allows for a single set of equations to represent two flow regimes simultaneously. Moreover, these models may be implemented using sophisticated flow solvers based on non-linear schemes, with advantages in the simulation of flow discontinuities (e.g. bores) when these solvers are constructed with shock-capturing capabilities (Toro, 2001). The Preissmann slot was included in various numerical models, including versions of EPA SWMM 5 (Rossman, 2004) and HEC RAS 4.0 (Brunner, 2008). A limitation of the conceptual model is that it cannot simulate negative water pressures, as it would regenerate free surface flow conditions even in the absence of ventilation, a non-physical outcome.

Song, et al. (1983), Cardle and Song (1988), Fuamba (2002), Politano, et al. (2007) and others have proposed an alternative way to simulate unsteady flows involving the transition

between pressurized and free surface flows. These models are referred to as shock-fitting mixed flow models, and apply the set of unsteady pressurized flow equations (eq. 1.12 and 1.21) alongside with unsteady flow equations for free surface flows based (eq. 2.1 and 2.2). Explicit tracking of the pressurization interface is needed to determine the boundaries of these two flow regimes so that the appropriate set of equations may be applied. Despite of the added complexity of these models that comes from the tracking of multiple pressurization fronts and the use of two sets of unsteady flow equations, they were extensively applied in the simulation of extreme flows in stormwater tunnels since Preissmann slot models are unable to simulate sub-atmospheric flows.

The limitation that the Preissmann slot posed was overcome by a new conceptual model proposed by Vasconcelos, et al. (2006). Rather than consider a virtual slot, the authors assumed an elastic behavior for the conduit walls so that there would be a direct relationship between the pressure experienced in pressurized flows (either positive or negative/sub-atmospheric) and changes in the full-pipe cross-sectional area. This conceptual model, referred to as TPA model, has been applied in water main filling modeling (Vasconcelos, 2007; Vasconcelos, et al. 2009), stormwater tunnel systems (Lautenbach, et al. 2008), stormwater collection networks (Sanders and Bradford, 2011), and has been expanded to include effects of pressurized air phase (Vasconcelos and Wright, 2009; Trindade and Vasconcelos, 2011), as well effects of distributed cavitation (Vasconcelos and Marwell, 2011). The TPA model introduces changes to the Saint-Venant equation, resulting in the following system of partial differential equations:

$$\frac{\partial \vec{U}}{\partial t} + \frac{\partial \vec{F}}{\partial x} = \vec{S} \tag{2.3}$$

Where

$$\vec{U} = \begin{bmatrix} A \\ Q \end{bmatrix} \qquad \vec{F} = \begin{bmatrix} Q \\ \frac{Q^2}{A} + gA(h_c + h_s) \end{bmatrix} \qquad \vec{S} = \begin{bmatrix} 0 \\ gA(S_o - S_f) \end{bmatrix} \tag{2.4}$$

The term h_s represent the pressure head anticipated only in pressurized flow conditions, and is calculated as:

$$h_s = \frac{a^2}{g}\frac{(A - A_c)}{A_c} \tag{2.5}$$

With a as the acoustic wavespeed and A_c the cross-sectional area of the conduit.

In a completely different context, multiphase models have been developed to simulate the slug flow in oil or gas transport through pipelines with an example the work by Issa and Kempf (2003). However it is uncertain that these models consider all the relevant physics of stormwater hydraulics into the continuity and momentum equations, since, for instance, there is no specific term that handles pressure surcharge in the conduits.

Chapter three - Knowledge gap and Objectives

The research proposed here aims to provide insights on the interactions between entrapped air cavities inside a stormwater tunnel without air ventilation by means of experimental and numerical investigations. Based on previous related research in stormwater tunnels systems, the pertinent knowledge gaps related to air pocket entrapment and compression include:

i. The pipeline flow within system boundaries is one of the causes of air pocket formation and pressurization. However, the air pocket by the reflection of water flow fronts within the system downstream boundaries has not been sufficiently executed and tested to this date. Such cases are not anticipated to be as extreme as the conditions that have been considered in previous studies (Martin, 1976 and Zhou, et al. 2002) because of the pressure relief that shafts may provide. Yet, they are very relevant as they may result in loss of tunnel storage volumes. Of particular interest is the magnitude of the surges upon pocket entrapment and whether in such cases negative pressures will be observed;

ii. It is probable that rapid flows will produce large pressure upon the valve or blockage. If there is air pockets, this large pressure will make them smaller and compressed (Martin, 1976).

In most of situations when there is a blockage, the flow is going to elevate pressure and the water will passes even in smaller quantities. So far, no research has considered this factor, principally in the context of air pocket entrapment in stormwater tunnels. This may difficult the development and calibration of numerical models to simulate tunnel filling events accounting for air pressurization effects.

This study presents the numerical and experimental results from a constant investigation on surges caused by air pocket entrapment. The idea is to measure the magnitude of those pressure surges for varying air pocket volumes, system slopes, initial flow rates and obstruction levels caused by a discharge valve. These researchers intend to follow the conditions in which water removal causes surge decrease by varying the valve barriers. It's assumed that the knife gate valve would create conditions similar to rising water at shafts, decreasing the outflow into the shafts during the air pocket compression process. By investigating this particular flow condition, the main goal is to gain better insight of the underlying physics and with this improve current modeling approaches to this problem by better incorporating air pressurization effects. Although, this discussion of numerical and experimental models for the simulation of stormwater drainage tunnels filling indicates that there are still opportunities for improvement. Future models should include more realistic assumptions, when considering effects of air pocket pressure.

Chapter four - Methodology

This methodology chapter presents how the proposed investigation on air pockets entrapment was conducted in three main sections. The first section presents how the required experimental apparatus was designed and constructed. The second section discussion covers how the experimental program was conducted: procedures, experimental variables, conditions tested, etc. The third and last section focuses on the numerical modeling development, which aimed to replicate the conditions tested in experiments.

The fundamentals of the experimental and numerical investigation of air pocket in water flow applied similar approach to the works of Martin (1976) and Zhou et al. (2002), but with some important distinctions. In those earlier works, the flow rate was zero in the pipeline, going all the water to compress the air pocket. However, in this study, the flow rate was steady and non-zero value with a gradual transition between free surface and pressurized flows. Upon rapidly valve maneuver, a bore was generate at the valve and started to move upstream of the conduit and initiates the air cavity entrapment. As a result of the air pocket entrapment mechanism, it's assumed to be describing the actual characterized of air entrapments in authentic stormwater tunnels in which air pockets are trapped between water columns, particularly in the cases where compression occurred in parallel to pressure relief provided by partial openings at the discharge valve.

4.1. Experimental apparatus construction

The experimental apparatus was thought and designed to be a recirculation system, which the upstream reservoir would supply water flow for the pipeline until it passes the last valve and fall in downstream reservoir. Thus, there are two pumps in the downstream reservoir, which are responsible to create the system recirculation. For that reason, it was constructed the wooden material to operate such as a recirculation apparatus.

First, it was necessary to construct a wood support to elevate the upper reservoir. However, it was required to know that the wood stands the weight of a filled upper reservoir. It constructs the project design of the wood support, which it was calculated. Then, it was build the pipeline wood holders to control the slope. Since the conduit is little elastic, the wood holders also served to maintain the inflexibility of pipeline, making sure that the air pockets are in the right position. This was verified and calculated, as a result there were six pipeline holders necessary.

Next, it was required to fit the experimental apparatus pipeline, which is compound to a clear PVC pipe of 101.6-mm diameter with a length of 12 meters for horizontal and adverse slopes. Later, the experimental apparatus have to change location to another off-campus experimental laboratory, thus the new laboratory was a little smaller that the before and the experiments with favorable slopes where performed in a 10.6 meter. However, for experiments of this thesis, it isn't altered, significantly, the features of the flow. The next step was the knife gate valve that was installed in the pipeline downstream end. The knife gate valve had the function of closing almost instantaneous the water flow and entrapping the air cavity. And the last piece set up in the pipeline apparatus was the ventilation orifice that was in upstream end. The ventilation orifice was able to let air escape to allow the permanent flow and in the next step, the valve was close.

In order to establish the initial flow conditions, the upper and downstream reservoirs have, respectively, 0.66 m^3 and 0.62 m^3 of total volume. Hence, the two pumps were putted in downstream reservoir and a white pipeline was built to connect the upper reservoir to the pumps. Both of the pumps had a valve to regulate how much flow passes in the pipeline. Another valve was putted in white pipeline in order there flow couldn't come back in opposite direction. This valve also served to control the flow that reaches the upper reservoir. All of this were constructed and connected to a recirculation apparatus experimental. The Figure 4.1 demonstrates the construction of experimental apparatus.

Figure 4.1: Illustration of experimental apparatus construction.

After that, it required that flow and pressure measurements were placed and connecting with the computer. The type of the two piezoresistive pressure transducers was MEGGIT-ENDEVCO 8510-50C, the maximum pressure was 345 kPa and 0.4% of accuracy. The pressure transducers were collocated on the wall inside pipeline, one in the middle and another in the downstream end. Consequently, it was needed to finish the two holes in the conduit in order to collocated the two plastic supports, which the Figure 4.2 presents a sketch of the adapter used to connect the pressure transducers to the pipeline.

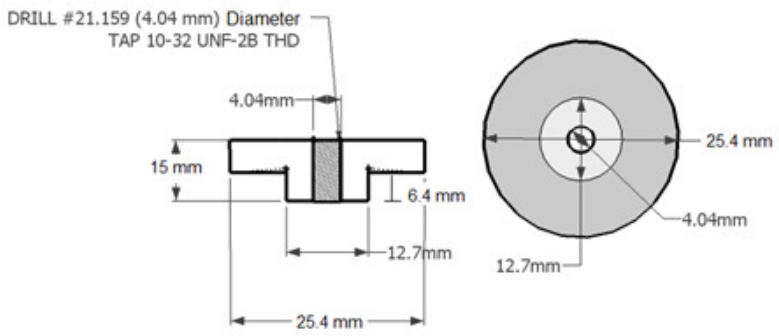

Figure 4.2: Sketch of the adapter used to connect the pressure transducers to the pipeline.

Subsequently, the two manometers were placed in the same position and opposite site that the pressure transducer. There were also required two holes that were smaller than the rubber hose linking to the manometer because it need to make pressure to haven't any sort of leakage. The paddlewheel flow was fitted in the white pipeline to observe how much the flow change in the rotation the valve.

And at last and more complicated was the MicroADV probe that has function to measure the velocity. Primary, it was thinking and constructed a wood support for MicroADV, which touch the ground, although it doesn't work. When it modified the slope, the MicroADV had little movement and it messes with the connection between the MicroADV and the conduit. The most recent idea was to support the MicroADV into the pipeline and a hole in rubber connection to fit inside the conduit where there is flow velocity. It demonstrates the wood support into the pipeline in Figure 2.3.

Figure 4.3: MicroADV wooden support.

4.2. Experimental program

4.2.1. Experimental procedure

Following the experimental construction there was a period of few weeks of experimental troubleshooting, after which the system was ready for experimental runs and for data collection. The conditions were designed to create pressurized flow in the pipeline connection with the upstream reservoir. Brink depth discharge conditions at the downstream end were designed to create conditions of free surface flows at the downstream end, and consequently free discharge conditions were anticipated with the presence of an atmospheric air cavity at the pipeline crown. The location of the air pocket intrusion would depend on a combination of flow rate and pipe

slope, and conditions were adjusted to avoid air pocket lengths exceeding more than 50% of the pipeline length.

The pipeline slopes and variable discharge rates were meant to represent a wide variety of air cavity volumes and when the knife gate valve was fully or partially closed (about 0.3 second) it formed an air pocket. Upon obstruction, water flow continued to compress the air phase due to water phase inertia, and air pocket pressure increases significantly before water flow reversed.

The pressures conditions were captured by the pressure transducers and recorded in the computer. The pressures transducers were placed in two positions: at the pipe crown in the pipeline downstream end and at half of the apparatus length at the pipe invert. These two points were carefully chosen to represent the pressure variations. First one, at pipe crown, measured the pressures variations between the air and water flow and the second one measures only water pressure to observe if there are some differences between the values or not. However, the pressures transducers yielded an analog electrical signal that is directly correlated to pressure changes, so it was necessary to place two manometers in the same point as the transducer to permit an accurate pressure conversion. The flow velocities were measured by a MicroADV probe that was located at 3.0 m from the upstream end, position that always flow in pressurized conditions. All the essential elements of the experimental apparatus are presented in Figure 4.1.

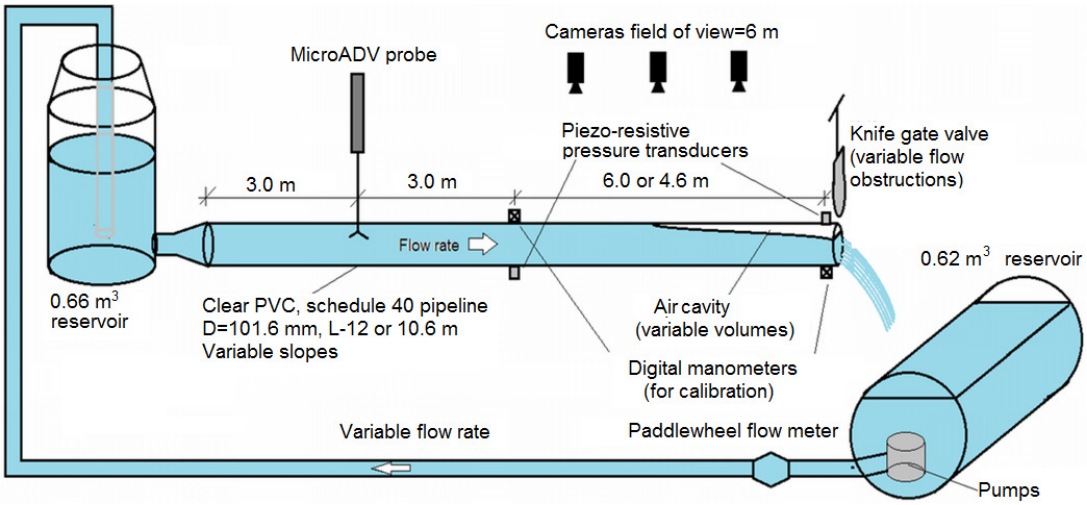

Figure 4.4: Sketch of the experimental apparatus used in the investigations

For the experimental process, it is described as following:

1. A required slope was set in the pipeline
2. Pumps were started and flow valves were opened and regulated to that a predetermined steady flow would was supplied to the upstream reservoir and into the pipeline. The choice of the water flow depended on the required volume of the air cavity that was formed at the downstream end of the pipeline;
3. Air pocket volume was measured by performing measurements of the air pocket width at the clear PVC pipe crown at regular intervals, so that a numerical integration of the resulting volume could be performed. The spacing between the stations where the air cavity width was measured varied from 0.05 m for the smallest pockets (less than 0.50 m), 0.10 m for the intermediate size pockets (up to 1.2 m) and 0.30 m for the larger pocket;
4. Three digital camcorders (1920 x 1080 resolution, 30 frames per second) were turned on to record the pocket compression process. All the important parameters like date, hour,

discharge, repetition among others relevant experimental parameters, were registered in the movies.

5. The initial pressure readings at the two manometers were recorded, as well the head at the upstream reservoir was read;
6. The two piezoresistive pressure transducers were started at a frequency of 100 Hz.
7. Velocity acquisition was provided by a MicroADV probe, sampling at a frequency of 25 Hz;
8. The knife gate valve was rapidly closed (partially or completely) obstructing the flow at the downstream end of the pipeline, and visual observations and comments were made to aid the subsequent data analysis;
9. Next, the pump flow was stopped and downstream reservoir valves were closed, separating the upper from downstream reservoir.
10. After the pressure pulses disappeared, the pressures reached an equilibrium level. The final pressure levels at the upper reservoir and at the final manometers reading were collected to the pressure transducers.

4.2.2. Experimental variables and tested range

The experimental apparatus provided focus on variables such as the slope, the flow rate and the valve obstruction. Table 1 illustrates the range of tested variables.

Table 4-1- Experimental variables and tested range

Variables	**Range tested so far**	**Normalized range**
Flow rate *(Q)*	2.08 to 5.45 L/s	$Q^*=Q/(gD^5)^{0.5}$=0.202 to 0.532
Slope (S_o)	Horizontal; 0.5% and 1.0% favorable; 1.3% and 2.7% adverse	n/a

Valve obstruction	0 mm, 8 mm and 13 mm residual opening at the knife gate valve	100%, 89% and 81% of cross section obstruction

The initial idea was to conduct 75 different initial conditions in this experimental system, but this number was re-adjusted to 60 considering that some of the conditions were not possible to create or were not relevant to the experimental program objectives. A total of 136 experimental runs were conducted considering repetitions to ensure consistency. Usually two to three such repetitions were made and results compared to verify whether pressure and/or ADV signals were comparable. When the duplicates had significant difference in values (~10%), a more repetitions were introduced.

4.3. Numerical Model – Lumped Inertia Method

A predictive numerical model based in lumped inertia was developed and its results compared to experimental results, using for the code development CodeGear Turbo Delphi that is based on the object-oriented computational language Object Pascal. The Object Pascal language is a windows-based Pascal platform which allows for a quick development of programs, and in its Turbo Delphi Express version the license was free. The idea for the numerical model development was to check whether results obtained in experiments would be reproducible in a two-phase, one-dimensional modeling framework constructed with the water phase momentum continuity equation, and the ideal gas law. The following subsections presents detail of the selected mathematical model (based on the lumped inertia approach as described in Wylie and Streeter, 1993), and the strategy used in its numerical implementation.

4.3.1. Mathematical model: Water phase momentum equation

The momentum equation for the lumped inertia approach is the simplification of the partial differential equations related to pressurized flow that leads a system of two partial differential equations (describing mass and linear momentum conservation) into only a single one ordinary differential equation for the momentum equation, allowing for a significant simplification in the solution procedure. The approach is based on the assumptions of the water incompressibility and absolute inelasticity of the conduit walls. Thus, the approach ignores the fluid accumulation in the pipeline in function of water pressure changes. Alongside with the pipe inelasticity, this implies in a linear pressure gradient at all times, and that changes to the flow conditions do propagate instantaneously through the system (infinitely large acoustic wave speed).

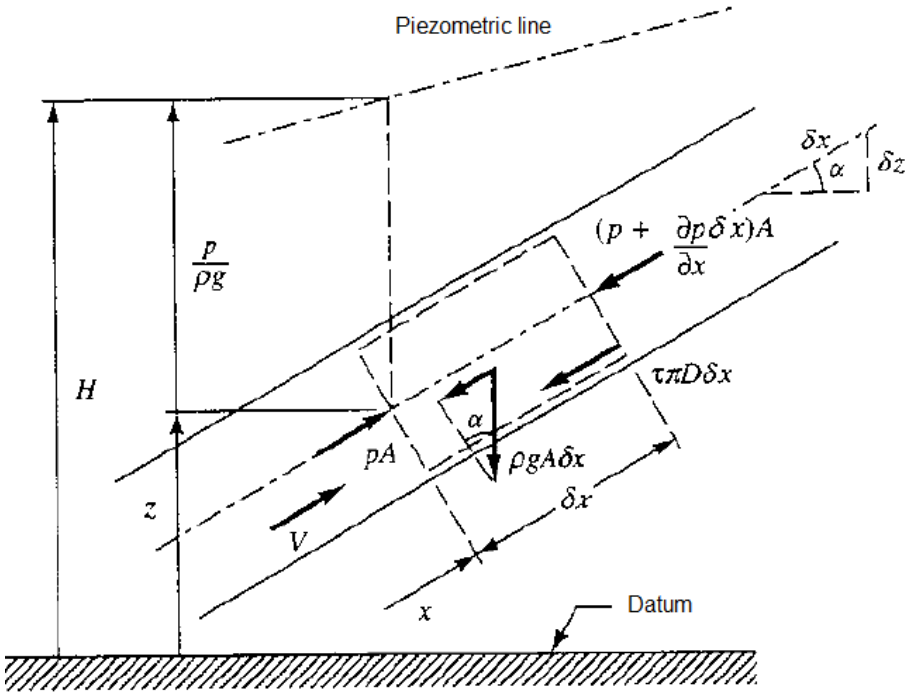

Figure 4.5: Force balance in a pipeline flow

Figure 4.2 sketches terms used in the derivation of the lumped inertia method (Wylie and Streeter, 1993). The application of the lumped inertia analysis (Wylie and Streeter, 1993) to a control volume leads to equation (4.1).

$$\frac{1}{\rho}\frac{\partial p}{\partial x} + \frac{\partial V}{\partial t} + g\sin\alpha + \frac{fV|V|}{2D} = 0 \tag{4.1}$$

where p is the control volume pressure, ρ is the water density, D is the pipeline diameter, V is the velocity, g is the gravity acceleration, α is the acoustic wave celerity, x is the position of conduit length, f is the friction loss coefficient and t is the time.

As explained, the acoustic wave celerity has an infinitely large value considering that instantaneous propagation of flow conditions. Thus, the flow velocity remains constant during the whole extension of the conduit and the equation (4.2) can be written.

$$\frac{\partial H}{\partial x} = \frac{H_{res} - H_{atm}}{L} \tag{4.2}$$

In which H_{res} is the reservoir head, H_{atm} is the atmospheric pressure head and L is the pipeline length between the reservoir and the location at which pressure is at atmospheric levels.

After this increment and some manipulation on slope effects, the momentum formula for the water column is transform in the ordinary differential equation (4.3)

$$\frac{dQ}{dt} = \frac{gA}{L}\left[H_{res} - (H_{air} - H_{atm}) - S_0 L - \left(f\frac{L}{D} + K_{local}\right)\frac{Q|Q|}{2gA^2}\right] \tag{4.3}$$

In which, Q is the water flow rate, H_{air} is the air phase pressure head, K_{local} is the localized loss coefficients.

4.3.2. Mathematical model: Description of the air phase volume

A lumped inertia air continuity equation may be formulated in terms of the amount of water flow that is admitted upstream end of the pipeline and the water discharged through the knife gate valve, computed with an orifice-like equation. It assumed that no air mass is lost or gained during the valve maneuvering process. The resulting continuity equation for the air phase is expressed in equation (4.4).

$$\frac{dV_{air}}{dt} = -Q + C_d A_{orif} \sqrt{2g(H_{air} - H_{atm})} \tag{4.4}$$

In which, V_{air} is the air phase volume, C_d is the discharge coefficient at the downstream end as the valve is being closed and A_{orif} is the discharge area as the gate valve is being closed.

4.3.3. Mathematical model: Description of the air phase pressure

It was considered that the ideal gas law is applicable for this experimental apparatus, so the energy equation for the air phase is constructed. The water flow can't escape all through the knife gate valve cavity, so the air pocket is suffered pressure and its air volume has decrease. The equation (4.5) is presented as following:

$$\frac{dH_{air}}{dt} = -k \frac{H_{air}}{V_{air}} \frac{dV_{air}}{dt} \tag{4.5}$$

in which, k is the polytropic coefficient (assumed as 1.2 in this research).

An initial calibration of the experimental values was necessary to approximate the numerical model results. The water flow utilized in the experiments contained a certain amount of fine sediments, and eventually these sediments became attached to the pipe walls. Although

PVC pipes are very smooth and sometimes it roughness has been ignored, in this particular case this was not the case due to sediment accumulation. Therefore, instead of friction factors around 0.021-0.022 anticipated for smooth PVC pipes at such flow rates, the friction factor number used in the computations that best matched the experimental results was 0.025. The local loss coefficient was considerable, mostly for the junctions, valve and a small pipe segment using two inches diameter at the upstream reservoir outlet.

The initial strategy of calculating the pressure changes assumed a totally or partially instantaneous valve closure procedure, effectively changing A_{orif} into zero right at the simulation start. However, this approach led to pressure peaks that were between 50% and 100% larger than what was observed the experimental measurements. A close examination of the movies records indicates that rather than instantaneous, the valve closure lasted between 0.18 s to 0.30 seconds (6 to 9 recording frames in a 30 FPS camera). A parabolic closure relationship was proposed to express the decrease of A_{orif} over the initial 0.20 second of the simulation based on movies.

A second adjustment was on the discharge coefficient Cd utilized in the calculations since the predicted discharges after the knife gate maneuver left a clearance for water discharge. The commonly adopted value of Cd=0.60 was consistently yielding flow rates that were much above the measurements based on the MicroADV probe velocity. This discrepancy was larger for the experiments that used a smaller discharge gap at the valve (8 mm). After matching the discharge values yielded by the model with the observations, the discharge coefficient C_d varied from a maximum of 0.40 (for some 13 mm opening down) to 0.30 (for 8 mm opening experiments).

4.3.4. Implementation of the numerical solution

The 4th Runge-Kutta method (Press et al., 1989) is a popular approach to solve one or more ordinary differential equations. This method was selected to solve equations 4.3 and 4.5, with errors per time step (Δt) is in the order of Δt^5 and the accumulated error is in the order of

Δt^4. It uses four estimates (where defined as k1, k2, k3 and k4) for the slope (rate of change) of the dependent variable and the resulting change is a weight average of these values. The 4th Runge-Kutta method is exemplified for the equation of momentum for water column.

$$f(t_n, Q_n) = \frac{dQ}{dt} = \frac{gA}{L}\left[H_{res} - (H_{air} - H_{atm}) - S_0 L - \left(f\frac{L}{D} + K_{local}\right)\frac{Q_n|Q_n|}{2gA^2}\right] \quad (4.6)$$

The Runge-Kutta considers the derivative in four intermediate points as the equations (4.7) and (4.8).

$$Q_{n+1} = Q(t + \Delta t) = Q_n + \Delta t.\left(\frac{k_1 + 2k_2 + 2k_3 + k_4}{6}\right) \quad (4.7)$$

$$t_{n+1} = t_n + \Delta t \quad (4.8)$$

Where the coefficients of the intermediate points are calculated as follows:

$$k_1 = f(t_n, Q_n) \quad (4.9)$$

$$k_2 = f\left(t_n + \frac{\Delta t}{2}, Q_n + \frac{\Delta t}{2}k_1\right) \quad (4.10)$$

$$k_3 = f\left(t_n + \frac{\Delta t}{2}, Q_n + \frac{\Delta t}{2}k_2\right) \quad (4.11)$$

$$k_4 = f(t_n + \Delta t, Q_n + \Delta t k_3) \quad (4.12)$$

Figure 4.6 illustrates an interface of numerical program that was for entering the data and showing the results.

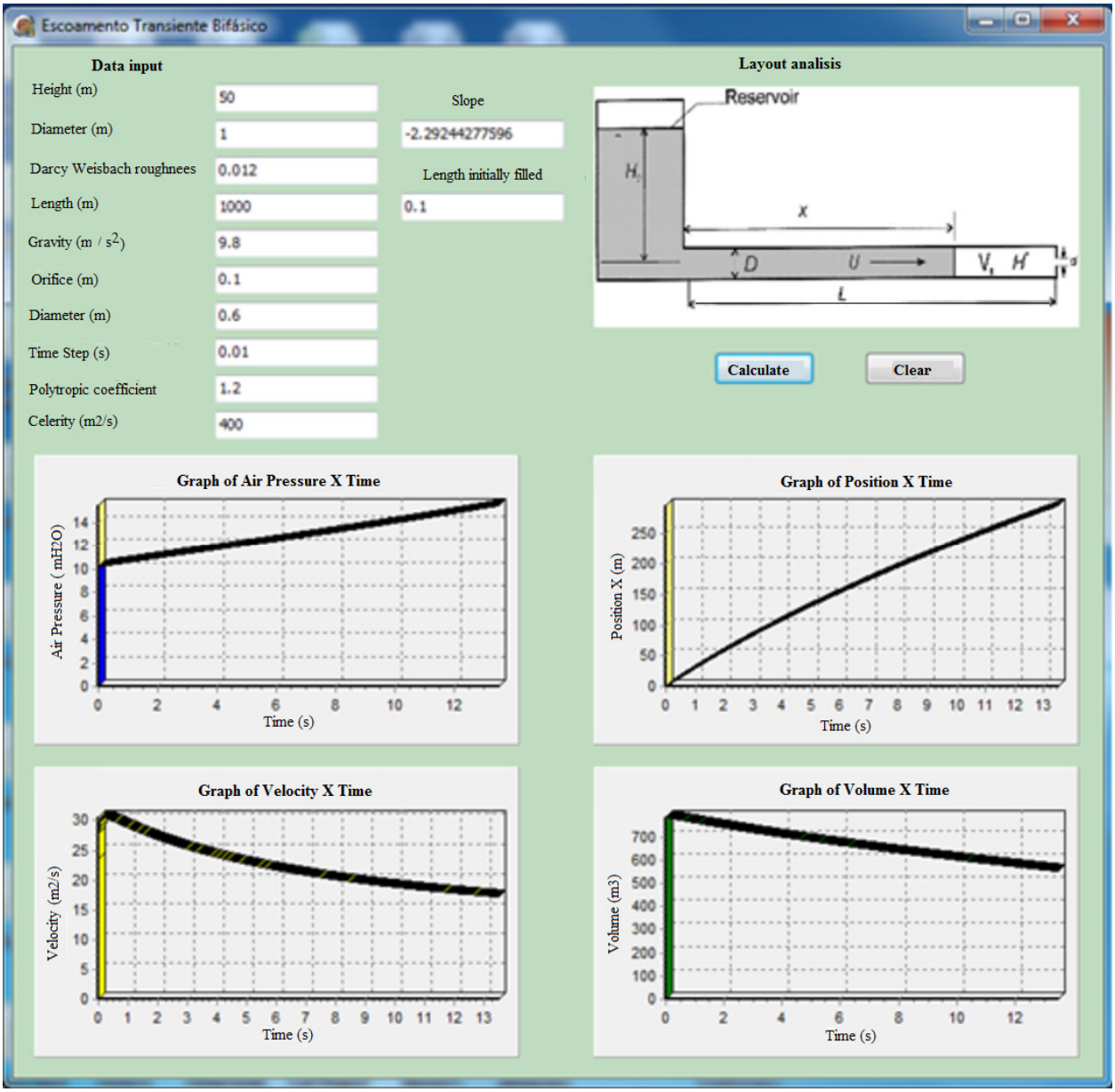

Figure 4.6: Screen capture of the numerical model interface.

Chapter five - Results

The experimental apparatus and the numerical code on the compression of entrapped air pockets in stormwater tunnels generate many results that were divided into experimental and numerical. First, it will be demonstrate the experimental data and, after that, it will be presented the numerical data, always comparing with the experimental results. Initially, it was demonstrated and discussed the results of total valve obstruction and then, the partial valve obstruction.

5.1. Experimental Results

The experiments that involved complete valve obstruction represent an extreme case of a bore reflection against a system boundary without any storage capability, thus with no pressure relief for entrapped air pockets present at stormwater tunnels. Yet, they were included because they are similar to previous experimental studies (Martin, 1976; Zhou, et al. 2002; De Martino et al., 2008) and to make comparison between the total and the partial valve obstruction.

Unlike experiments with partial valve obstruction, presented ahead, these experimental cases yielded significant down surges and sub-atmospheric pressures. An oscillatory-like pattern for the pressures and flow velocity measurements was noticed, with an oscillation period that depended on the entrapped air pocket volume. The discussion of experimental results separates the pressure and the flow velocity in different sections. A sequence of still images following a total obstruction maneuver is presented in Figure 5.1 for a horizontal slope case. The figure presents a bore that is formed at the moment of the valve total closure and propagates upstream.

After some time a curved pocket front moves back towards the valve and eventually an air pocket is spread at that portion of the pipe.

5.1.1.Total obstruction experiments - Pressure measurements

Pressure measurements at the upstream transducer ($X^*=X/L_{pipe}=0.5$) and at the downstream transducer ($X^*=X/L_{pipe}=1.0$) are presented in Figures 5.2, 5.3, 5.4 and 5.5, grouped by the flow rate/initial air pocket volume for the horizontal slope, and including all repetitions. In these charts, one notices a sudden rise in pressure was followed by an oscillation pattern in the pressure over time as the incoming flow decelerates due to the air pressure build-up caused by valve obstruction. Time is normalized by the factor $L/(g.\ D)^{0.5}$. One may also notice that the pressure peaks increase for smaller air pockets, while pressure oscillation period increased with entrapped pocket volume as anticipated by Martin (1976). The magnitude of the oscillations was strongly damped at each oscillation cycle, a feature that is further discussed in ahead in the numerical modeling results section.

The air pocket shape upon valve closure indicated a very complex configuration, with the initial air intrusion breaking into several smaller pockets, and moving within the pressurized region. Discrepancies among experimental repetitions are generally caused by the inability to enforce exactly equal initial conditions prior to valve maneuver, especially with respect to the initial air pocket volume. Figure 5.1 illustrates the sequence of pipeline still images following a total closing of last valve.

T=01m:33.35s - System initial steady condition

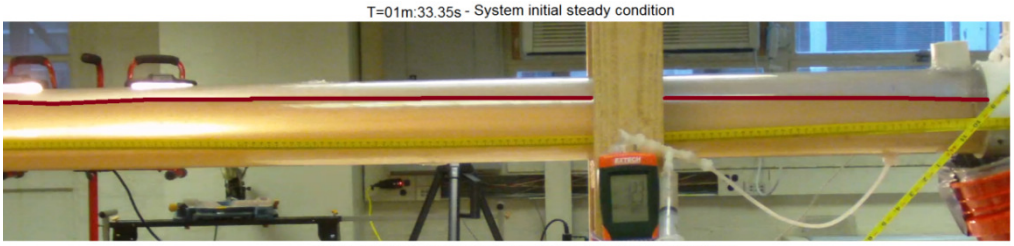

T=01m:33.51s - Knife gate valve closed, bore moving upstream

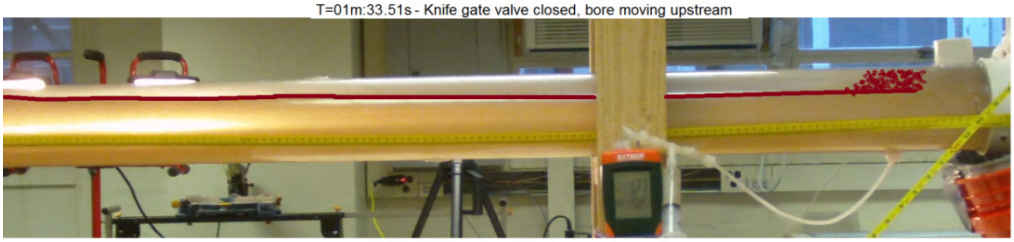

T=01m:33.78s - Pipe filling bore moving upstream

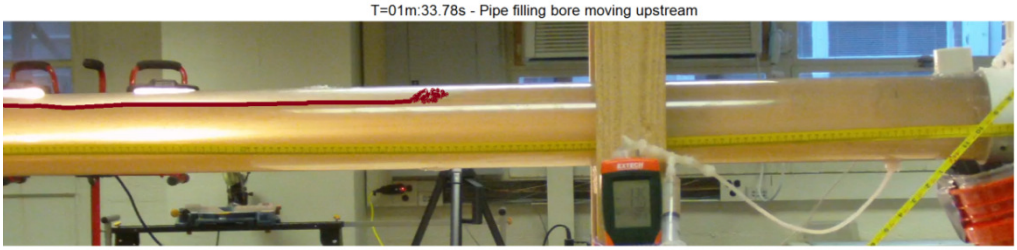

T=01:34.11s - Bore swept through the camera field of view

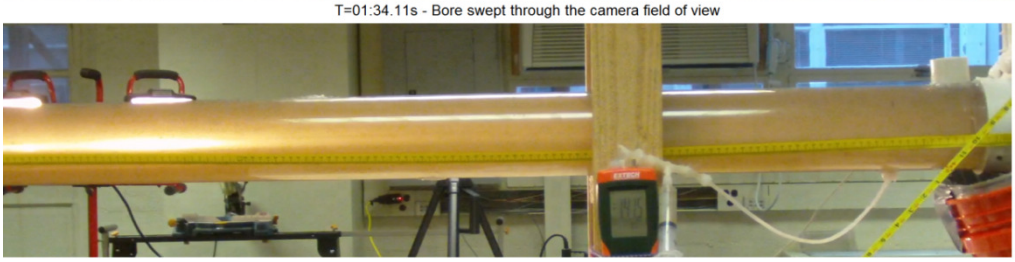

T=01m:35.95s - Discrete pockets moving toward valve

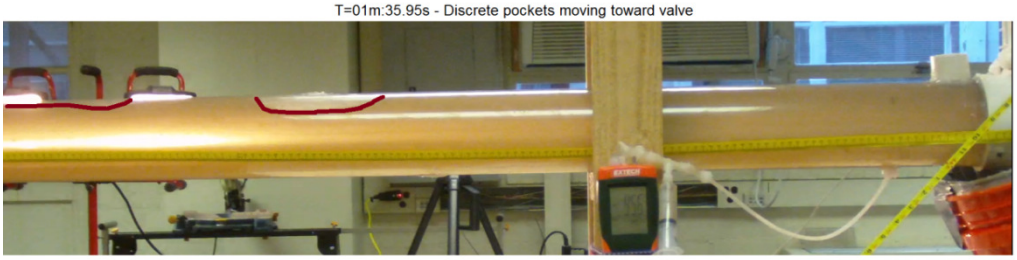

T=01m:39.21 s - Stratified conditions with no flow

Figure 5.1: Sequence of a complete valve obstruction, air pocket formation and motion. (Q*=0.44, Vair*=2.3, horizontal slope). Interface between air water phases has been artificially enhanced.

Figures 5.2, 5.3, 5.4 and 5.5 present pressure hydrographs with either two or three repetitions of the same experimental condition. These charts present variations on the resulting pressure for the tested repetitions for various air pockets as the inflow rate values varied between the cases. All the conditions presented in these figures correspond to horizontal slope experiments, and these different flow rate values resulted in different sizes of air cavities at the downstream end, as predicted by Hager (1999)

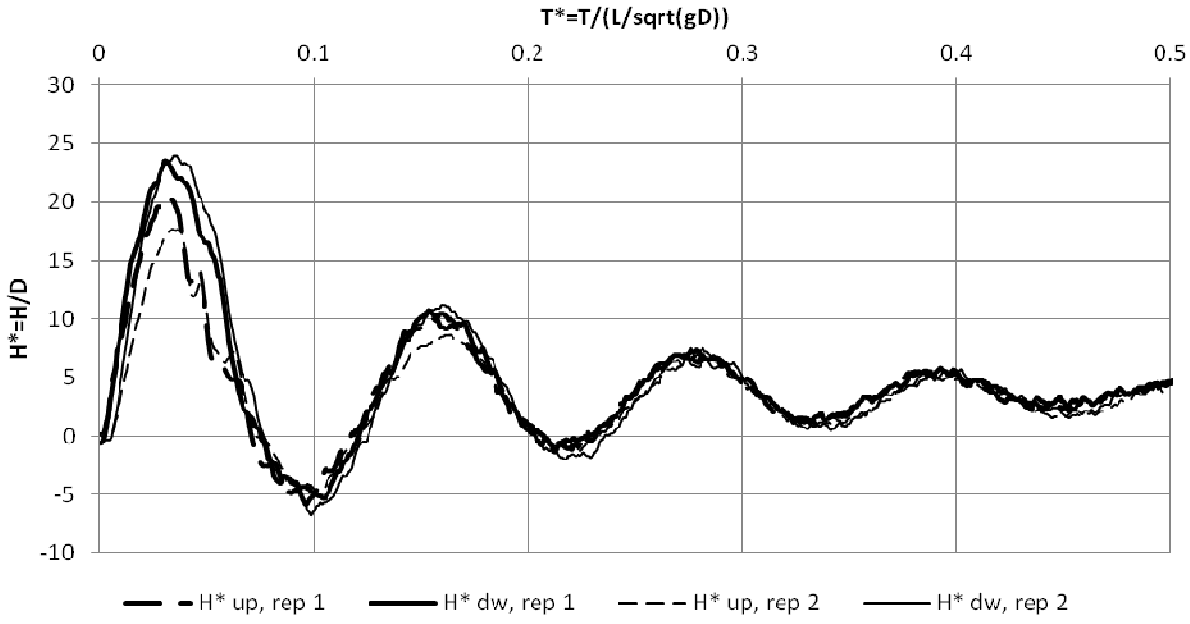

Figure 5.2: Non-dimensional pressure evolution following complete obstruction of the knife gate valve. (Q*=0.38 to 0.40, Vair*=3.4, horizontal slope). Subscripts up and dw denotes upstream pressure transducer results (X*=0.5) and downstream pressure transducer results (X*=1.0), respectively.

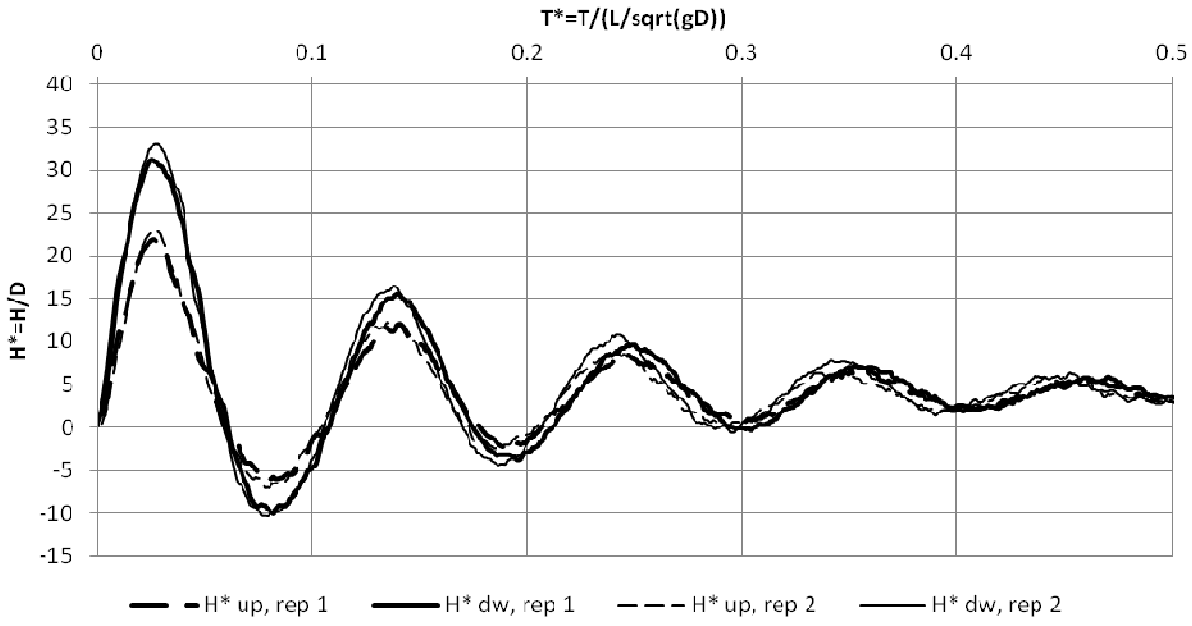

Figure 5.3: Non-dimensional pressure evolution following complete obstruction of the knife gate valve. (Q*=0.42, Vair*=2.55, horizontal slope).

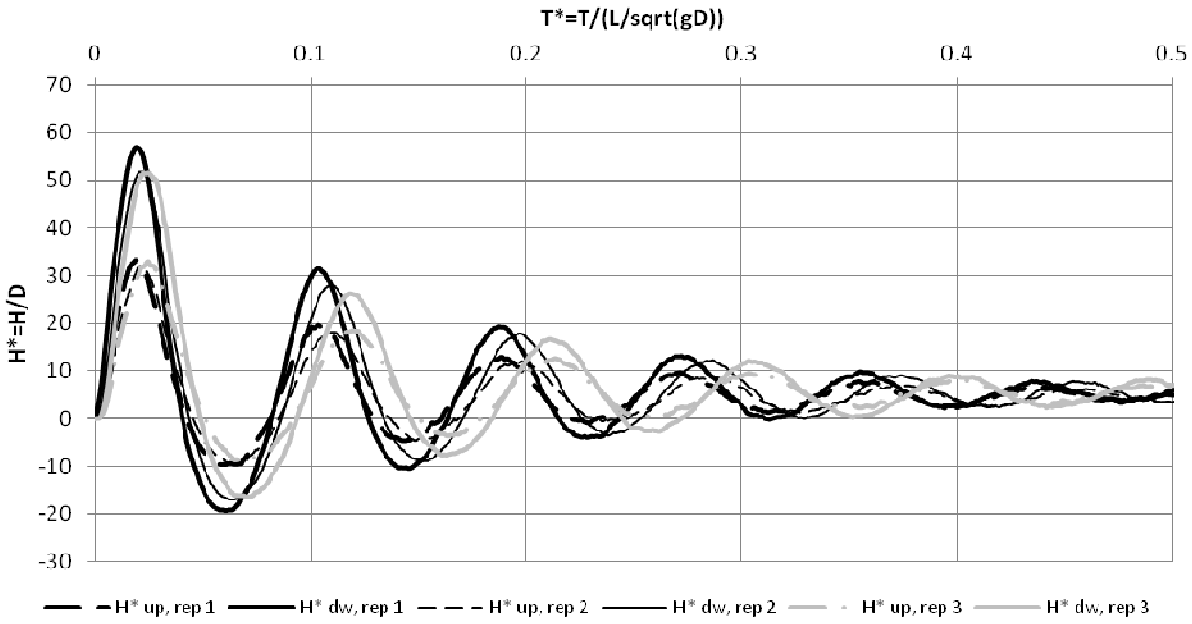

Figure 5.4: Non-dimensional pressure evolution following complete obstruction of the knife gate valve. (Q*=0.48, Vair*=1.08, horizontal slope).

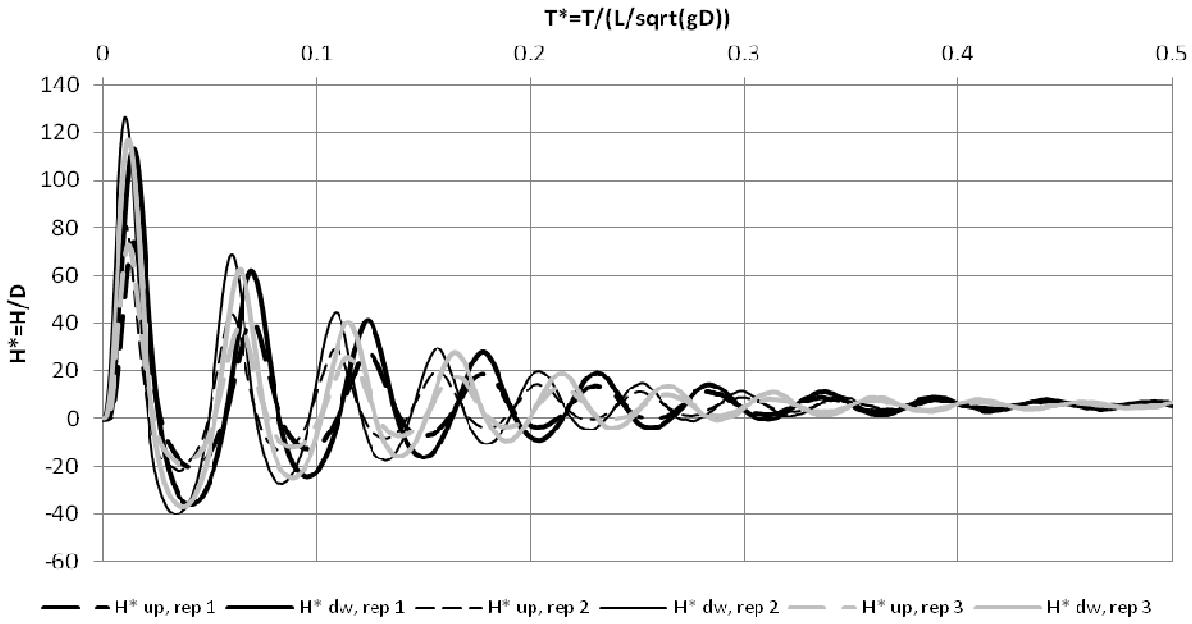

Figure 5.5: Non-dimensional pressure evolution following complete obstruction of the knife gate valve. (Q*=0.51 to 0.52, Vair*=0.38 to 0.42, horizontal slope).

Figure 5.6 and 5.7 present a comparison between the total obstruction experiments performed at various slopes while keeping the flow rate approximately the same. The flow rates considered in Figure 5.6 were the largest tested for sloped conditions, and ranged between 0.49 and 0.51. In such conditions the resulting differences in pocket volumes are very large between horizontal/adverse slope experiments and favorable slope experiments. The latter cases were associated with a large portion of the flow that could not be sustained in pressurized mode considering that large conveyance associated with the favorable slope and the brink depth discharge conditions. Thus, one notices that peak pressures associated with these favorable slope conditions are much smaller than correspondent cases for horizontal and adverse slopes.

Results in Figure 5.7 are similar to the ones presented in Figure 5.6, except that experimental conditions were such that the flow rates were much smaller (Q*=0.37-0.38). However, favorable slopes results are not presented since there was no pressurized flow in the entire pipeline for these lower flows. The results presented for adverse and horizontal slope indicate that larger peak flow rates are associated with smaller air pocket volumes, as anticipated.

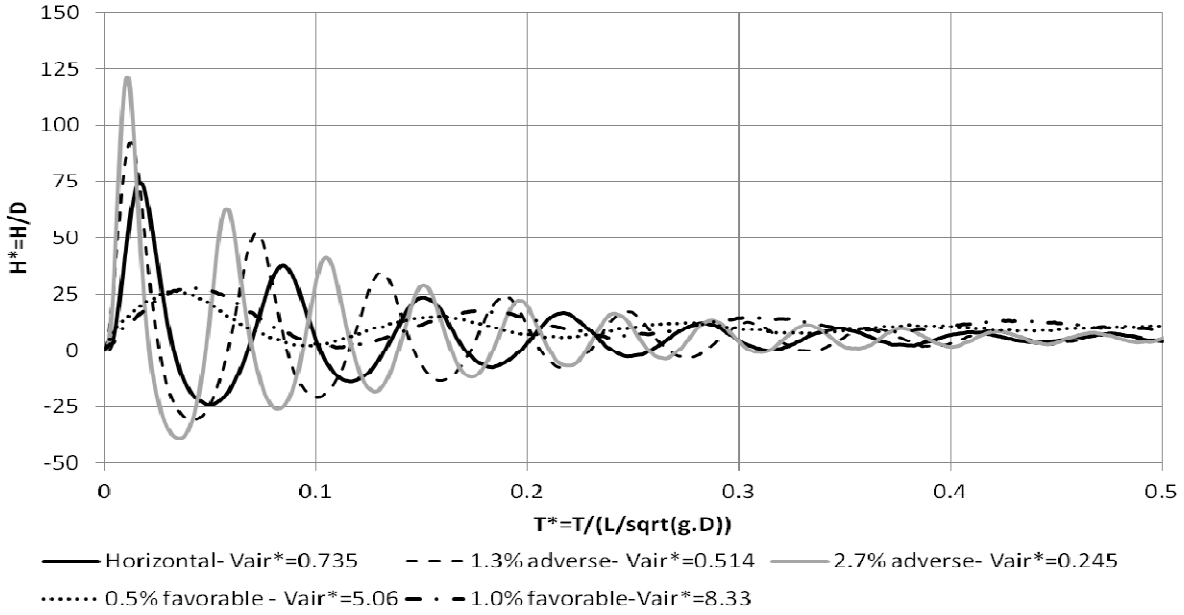

Figure 5.6: Non-dimensional pressure evolution following complete obstruction by the knife gate valve. (Q*=0.49 to 0.51, Vair*=0.13 to 0.38, varying pipe slopes)

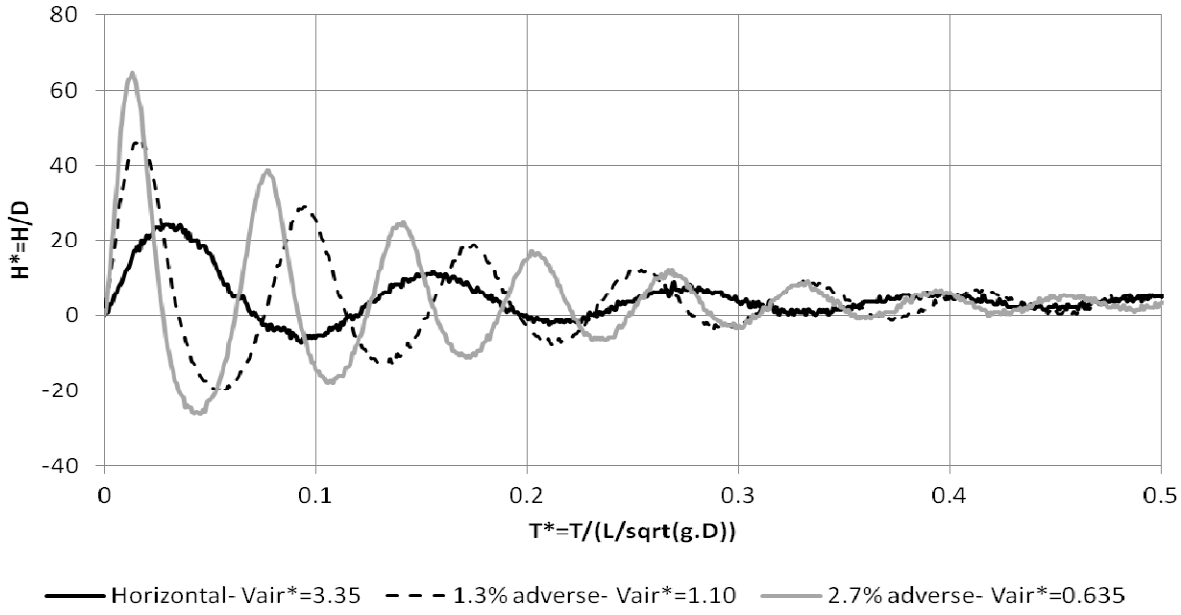

Figure 5.7: Non-dimensional pressure evolution following complete obstruction by the knife gate valve. (Q*=0.37 to 0.38, Vair*=0.64 to 3.35, varying pipe slopes)

A slight increase in the flow rate for favorable slopes (Q*~ 0.51-0.53) results in a major reduction in the air pocket cavity observed at the downstream end. A comparison between the horizontal (in this same flow rate range) and favorable slope results presented in Figure 5.8 indicate that pressure peak results and oscillaiton periods from these cases are comparable, but there seems to be a more rapid energy damping in the cases associated with favorable slope conditions. No clear explanation for that is available, but one speculates that the upward motion of the entrapped air pocket following complete valve closure could be associated with added energy losses as the resulting contraction from the pocket presence would be larger than the one anticipated for a thinned air pocket evenly spread in horizontal slope conditions.

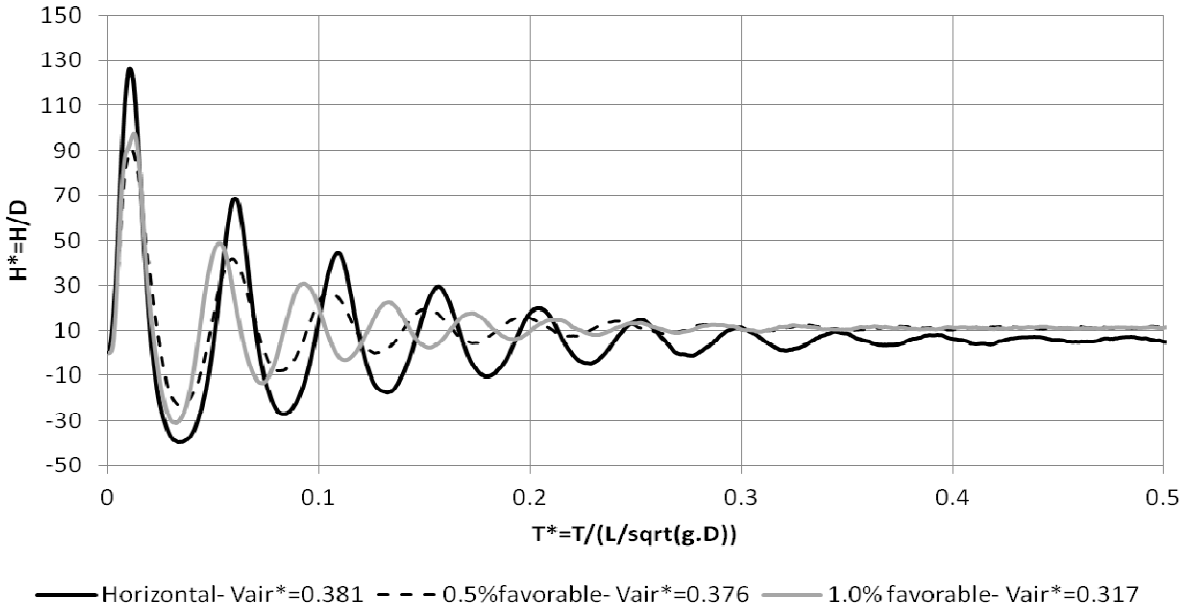

Figure 5.8: Non-dimensional pressure evolution following complete obstruction by the knife gate valve. (Q*=0.51 to 0.53, Vair*=0.317 to 0.381, varying pipe slopes)

5.1.2. Total obstruction experiments - Flow velocity measurements

The MicroADV probe was located 3 m downstream from the reservoir(X*=0.25), and prior to the valve maneuver velocity measurements were characterized by a steady value with anticipated fluctuations associated with turbulence. As the valve was closed there was a rapid drop in the flow velocities, followed by the same damped oscillation pattern observed with the pressure. Results in Figure 5.9 are presented for one of each different sizes of air pockets tested.

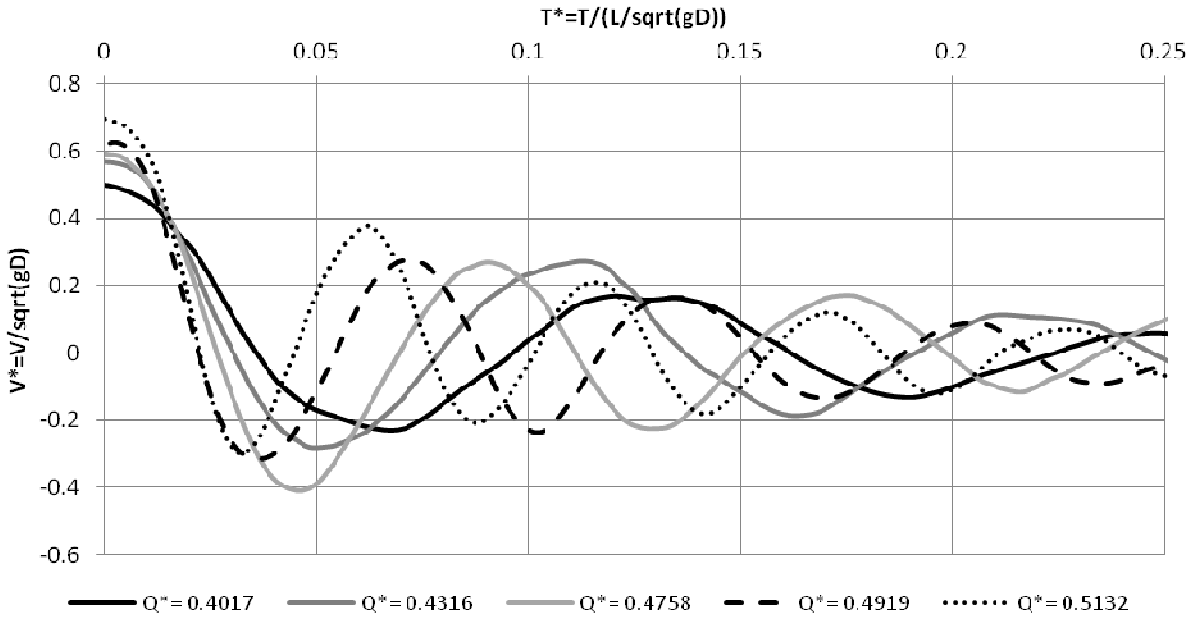

Figure 5.9: Non-dimensional velocity evolution following total obstruction by the knife gate valve, horizontal slope results.

The velocity measurements are similar to the pressure measurement results in that they also present a damped oscillatory pattern. Oscillation period was smaller for larger flow rates considering that for such conditions the entrapped air pocket volumes were smaller. This trend was also observed with other slopes tested, as shown in Figures 5.10 and 5.11 measurements for the cases of maximum adverse and favorable slopes, respectively. Velocity results obtained for the other tested slopes present the same trend and are not shown.

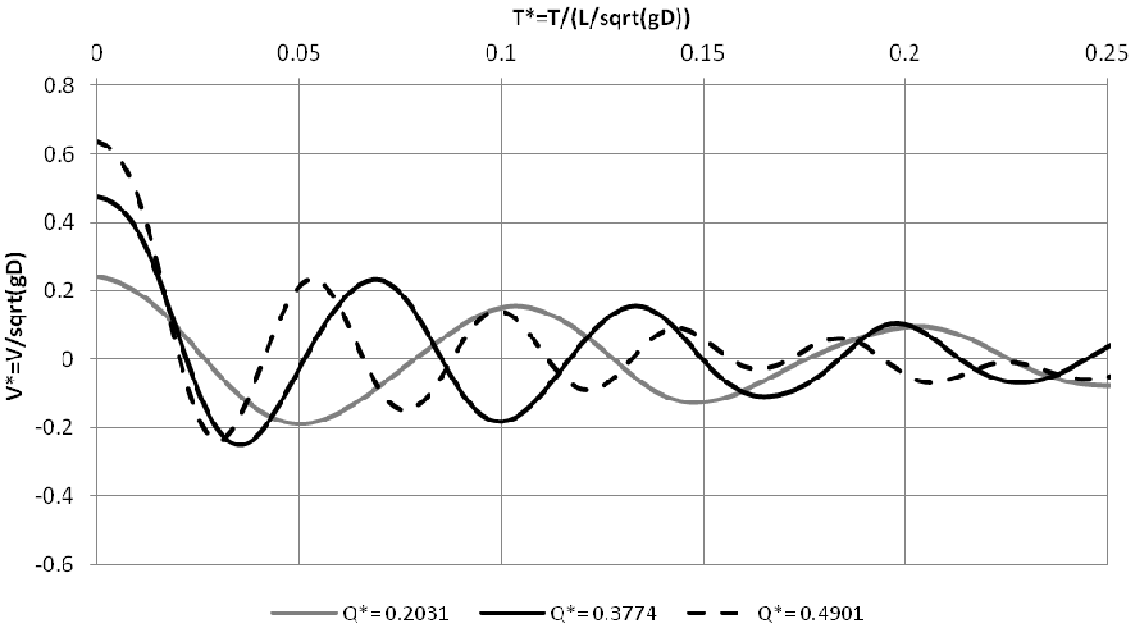

Figure 5.10: Non-dimensional velocity evolution following total obstruction by the knife gate valve, 2.7% adverse slope results.

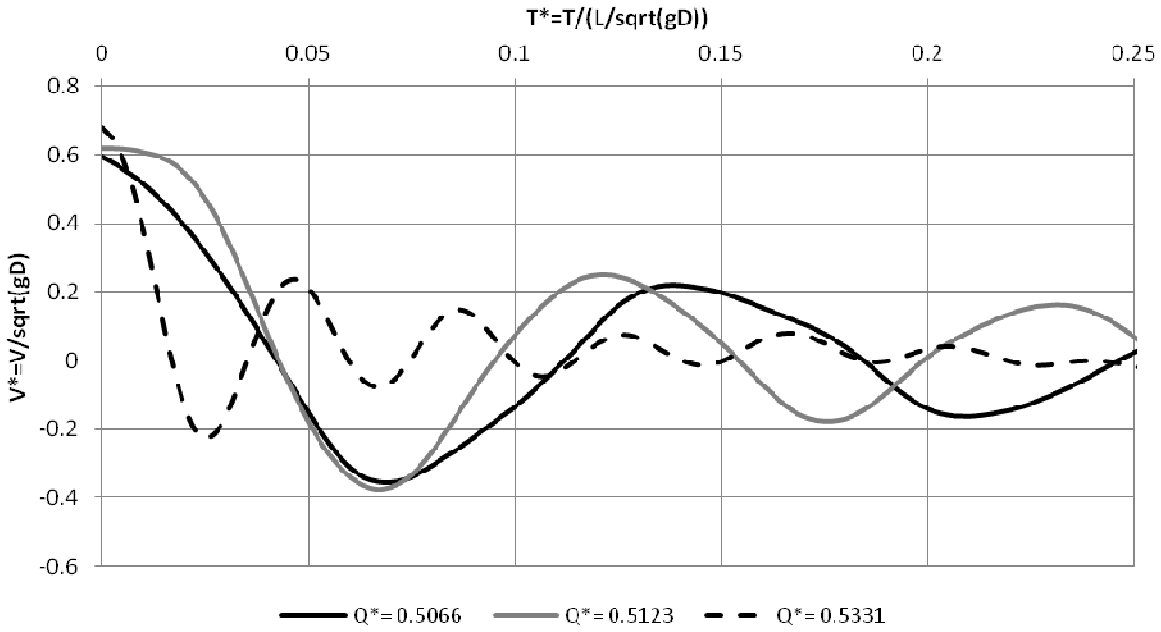

Figure 5.11: Non-dimensional velocity evolution following total obstruction by the knife gate valve, 1.0% favorable slope results.

A comparison between the velocity measurements between the different slopes indicate that the case with the smallest pocket volume and favorable slope presented a more rapid velocity damping then the other cases analyzed. One speculates that this is caused by the motion of this small pocket towards the upstream end of the pipeline following the rapid gate closure. This pocket motion could possibly generate additional energy losses as it would constitute a contraction in the water flow. Such a condition would not be anticipated either in horizontal or adverse slope conditions.

5.1.3.Partial obstruction experiments - Pressure measurements

Experimental conditions involving partial obstruction of the downstream valve enforced obstructions of 81% and 89% by means of a partial obstruction of the knife gate valve. The valve

was quickly closed, but rather than interrupt the flow entirely, wooden pieces blocked the motion of the valve shaft either 13 mm or 8 mm from the valve seat. The resulting gap was measured as 19% and 11% of the valve cross sectional area, respectively.

Figures 5.12 and 5.13 present pressure measurement results at the downstream transducer for the partial valve obstruction for three flow rates, horizontal slope, and valve obstruction of 81% and 89% respectively. In general the results were significantly different from the ones obtained with the full valve obstruction conditions. The significant negative pressure surges were not noticed in these experiments, and no oscillations were noticed for the 81% flow interruption. As Figure 5.12 indicates, few oscillations were noticed in some cases when 89% obstruction occurred, yet the magnitude of those were greatly damped and rapidly dissipated. This behavior is dissimilar from the one observed in the total obstruction experiments.

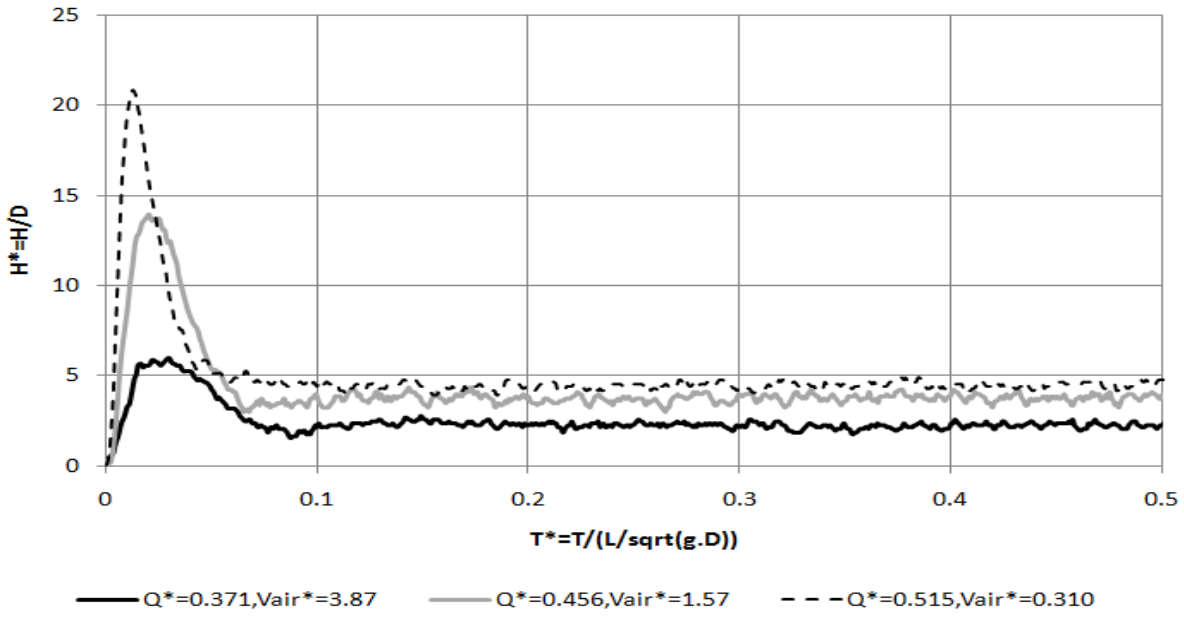

Figure 5.12: Non-dimensional pressure evolution following 81% obstruction by the knife gate valve. (Q*=0.37 to 0.52, horizontal slope)

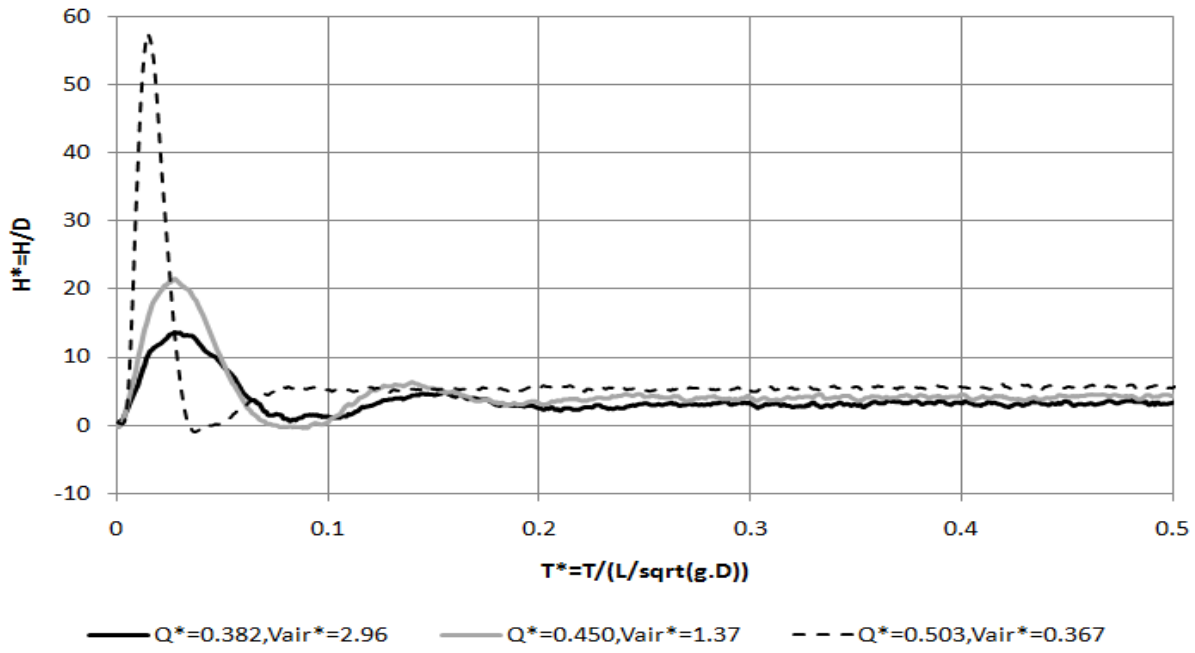

Figure 5.13: Non-dimensional pressure evolution following 89% obstruction by the knife gate valve. (Q*=0.38 to 0.50, horizontal slope)

The three flow rates represented in both Figures 5.12 and 5.13 correspond to the minimum, average, and maximum flow rates tested in the full obstruction experiments under horizontal slope. Other results are omitted for brevity. It's noticeable that the peak flows are much smaller than the ones observed for the complete valve obstruction, as indicated in Table 5.1 below:

Table 5-1- Comparison of peak H*=H/D pressures for horizontal slope experiments averaged between repetitions

Initial flow	Total obstruction	89% obstruction	81% obstruction
Q*≈0.51	H*≈125	H*≈57	H*≈21
Q*≈0.45	H*≈57	H*≈21	H*≈13
Q*≈0.38	H*≈24	H*≈14	H*≈6

As it would be anticipated, the smaller obstruction of 81% yielded smaller pressure peaks upon valve maneuver. The maximum surge peak drop for horizontal cases was 83% for the case of maximum flow (Q*~0.51). On the other hand, the minimum surge peak drop observed for horizontal cases was 42% for the case of minimum flow rate (Q*~0.38) and 89% obstruction. In Table 5.1 one notices that even though the flow rates may be very close between repetitions, the associate variation in air pocket volumes may be more significant due to the large sensitiveness of cavity volumes to flow rates. The same trend presented in Table 5.1 for horizontal slope is also observed for other tested slopes. Figures 5.14 and 5.15 illustrate 81% partial valve obstruction data for the 2.7% adverse and 1.0% favorable slopes respectively.

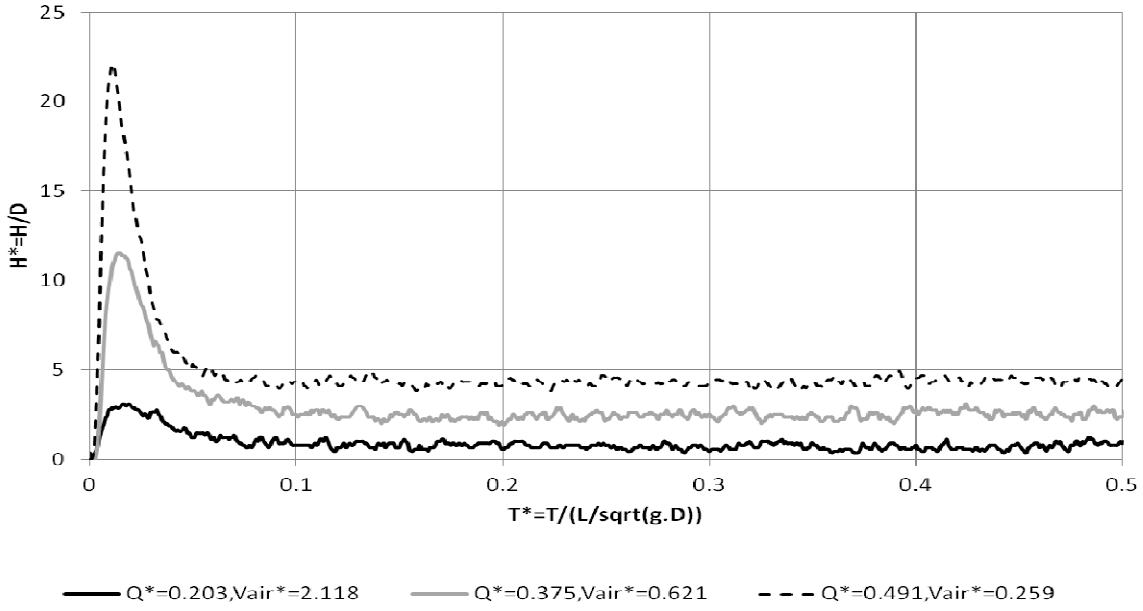

Figure 5.14: Non-dimensional pressure evolution following 81% obstruction by the knife gate valve. (Q*=0.20 to 0.49, 2.7% adverse slope)

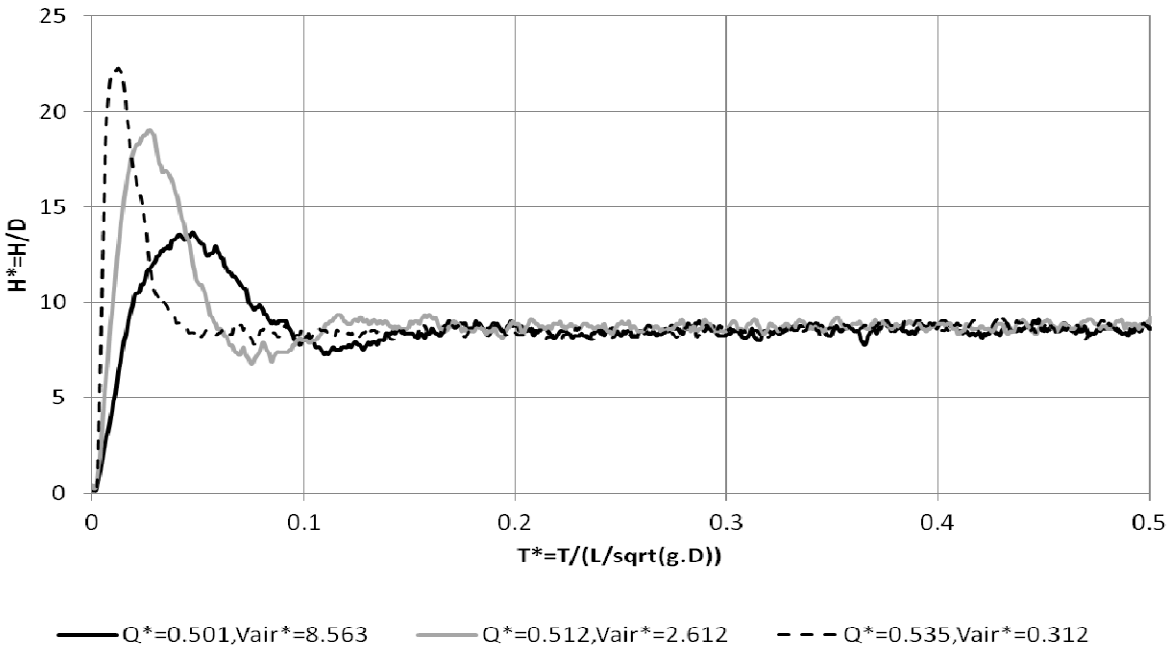

Figure 5.15: Non-dimensional pressure evolution following 81% obstruction by the knife gate valve. (Q*=0.50 to 0.54, 1.0% favorable slope)

Maximum peaks surges for both cases (V_{air}*~0.3) have approximately the same magnitude despite the difference of 8% in the flow rate and 5% in the pocket volume. An interesting feature that is shown in Figure 5.14 is that the peak surges occur at about the same time, regardless of the flow rate and associated air pocket volume. This is not observed in the 81% obstruction, 1% favorable slope case (Figure 5.15), when the larger peak surges tend to occur slightly sooner than the ones associated with larger smaller flow rates and larger air pocket volumes. The explanation for this behavior is related to the associated volume of the air. While the results in Figure 5.14 clearly indicate that there's a single pressure pulse, results obtained with the favorable slope show a slightly oscillation pattern, which is more pronounced for the 89% obstruction results, as presented below.

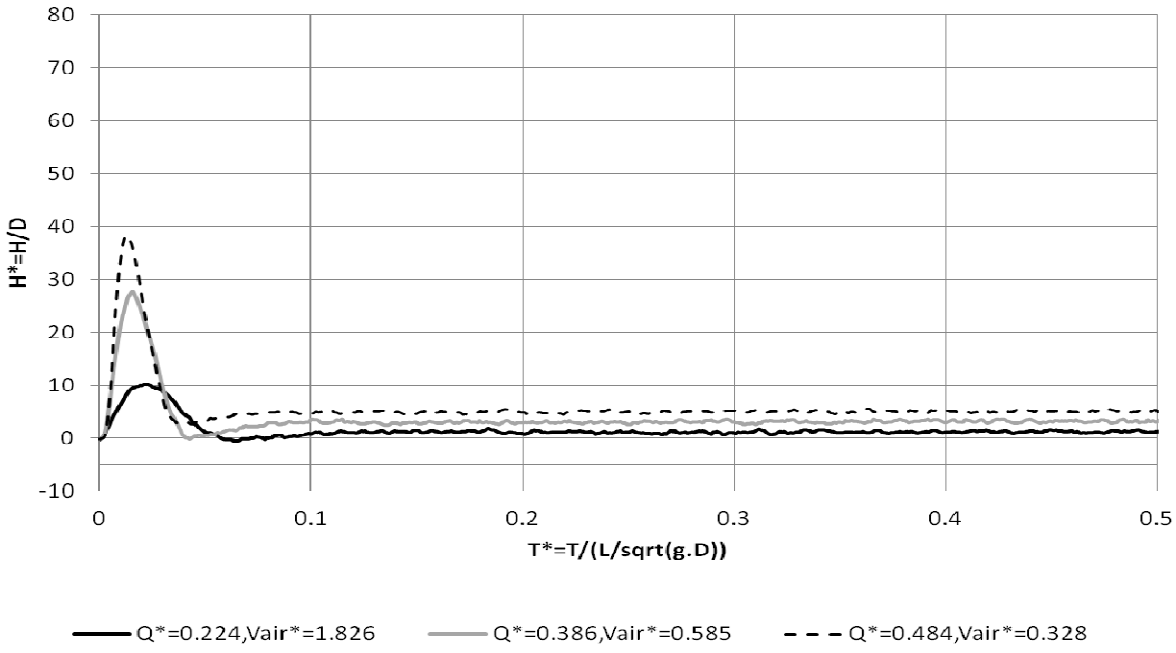

Figure 5.16: Non-dimensional pressure evolution following 89% obstruction by the knife gate valve. (Q*=0.22 to 0.48, 2.7% adverse slope)

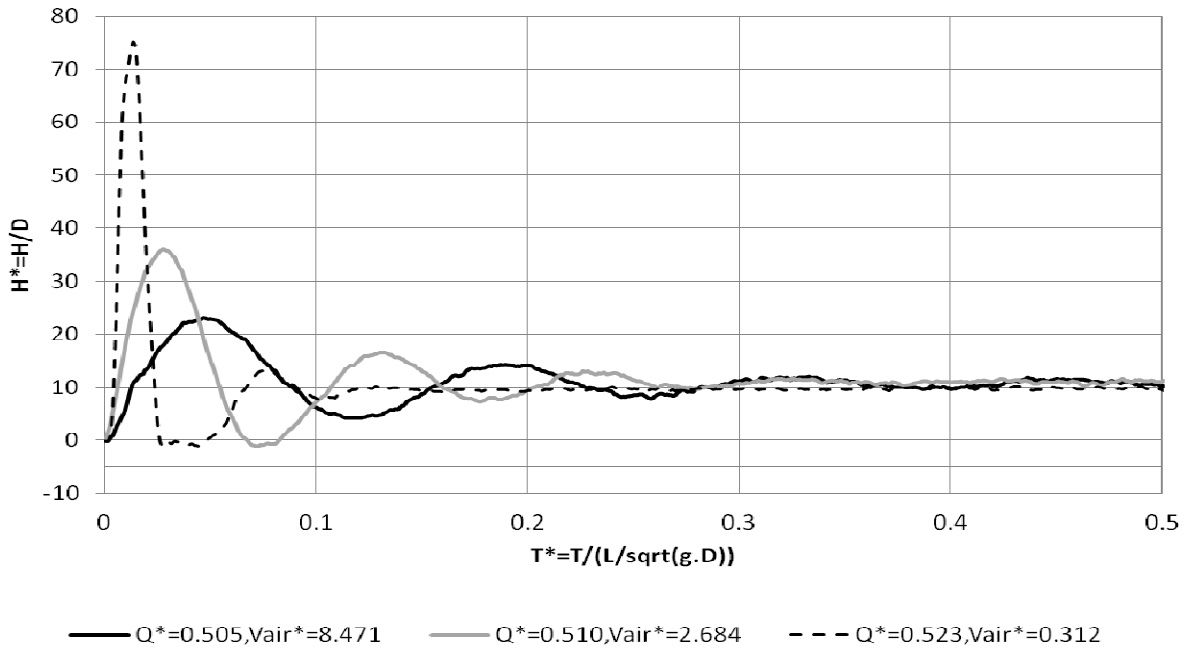

Figure 5.17: Non-dimensional pressure evolution following 89% obstruction by the knife gate valve. (Q*=0.50 to 0.52, 1.0% favorable slope)

Figures 5.16 shows pressure hydrographs for 89%, various flow rates and the largest adverse slope, while Figure 5.17 presents comparable results with the maximum favorable slopes. Unlike the comparison between Figures 5.14 and 5.15, maximum peaks surges for favorable slope and V_{air}*~0.3 is almost twice as large as the one for the adverse slope case (flow rate difference is 7% and 5% in the pocket volume). There is no clear explanation for that. Remarks that were made for Figures 5.14 and 5.15 with regards to the timing of the pressure oscillations are also applicable here. Finally, results obtained with the favorable slope show a moderate oscillation pattern, with quick damping. This oscillation patter is considered as an intermediate case between the full pipe obstruction surge oscillatory pattern and the single-pulse surge pattern observed in most other partial obstruction experiments.

Entrapped air pocket volumes for the adverse slope were much smaller than the comparable ones at horizontal and favorable slopes, and as result the peak flows were larger for the cases with adverse slopes. Figure 5.18 presents the result for the 81% flow obstruction for adverse and horizontal slopes when the flow rate was about Q*~0.4., and even though there was a difference in the air pocket volumes between the two adverse slope conditions, the pressure peak in both cases were fairly similar. At this point we still could not find an explanation for this result, but one speculates that this may be in part due to differences in the knife gate valve maneuvering velocity between conditions. Favorable slope results aren't shown since at these flow rates there were no pressurized flow conditions.

Figure 5.19 results are similar to the Figure 5.18, except that it presents the result for the 89% flow obstruction for different adverse slopes. The same trend is also noticed, with the horizontal slope yielding smaller pressure peaks because of the larger air pocket. The significant differences are that the discrepancy between the horizontal case and the adverse slope is now larger than the case presented in Figure 5.18, and that the pressure peaks, as anticipated, are significantly larger. Likewise, there is no favorable slope results because no pressurized flow could be sustained at flow rates around Q*~0.4.

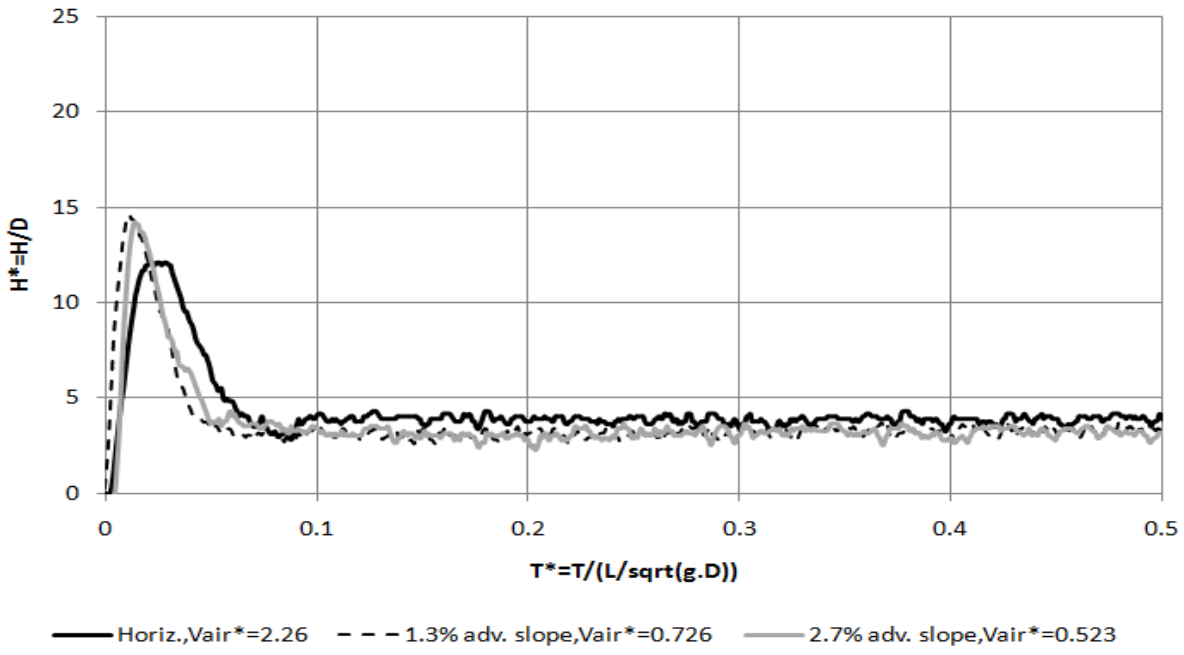

Figure 5.18: Non-dimensional pressure evolution following 81% obstruction by the knife gate valve. (Q*=0.42, varying slopes)

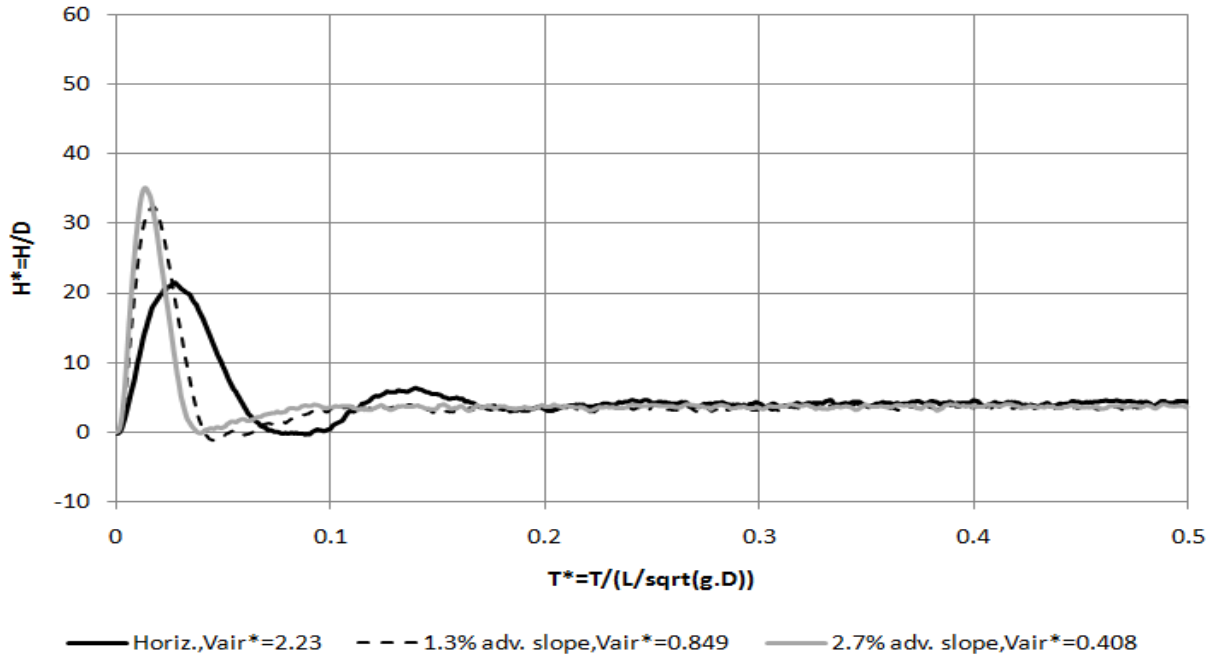

Figure 5.19: Non-dimensional pressure evolution following 89% obstruction by the knife gate valve. (Q*=0.41-0.43, varying slopes)

In order to obtain a comparison of all tested slopes for partial obstruction, one needs to consider a large flow rate (Q*~0.5) so that pressurized flows can be sustained even in favorable slope conditions. Figure 5.20 and 5.21 present such results for all tested slopes using the 81% and 89% flow obstruction respectively. In all tested cases, the air pocket volume was generally small, ranging from Vair*=0.15 up to 0.37. All peak surges observed for the 81% obstruction are very similar (H*~23-27), and all presented the single peak surge pattern. Results for 89% obstruction were consistent except for the favorable slopes, which presented larger peak surges (H*~60 vs. ~85), and the hybrid pattern between single pulse and oscillatory surges.

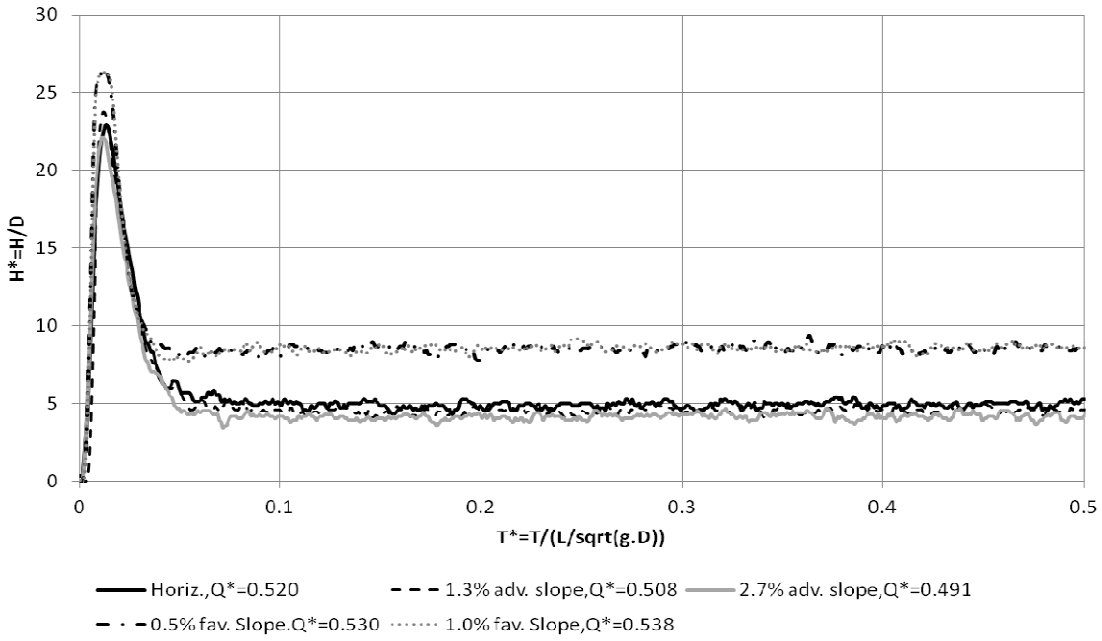

Figure 5.20: Non-dimensional pressure evolution following for 81% obstruction by the knife gate of all the slopes with minimal air pocket volume (Vair*=0.15 to 0.31)

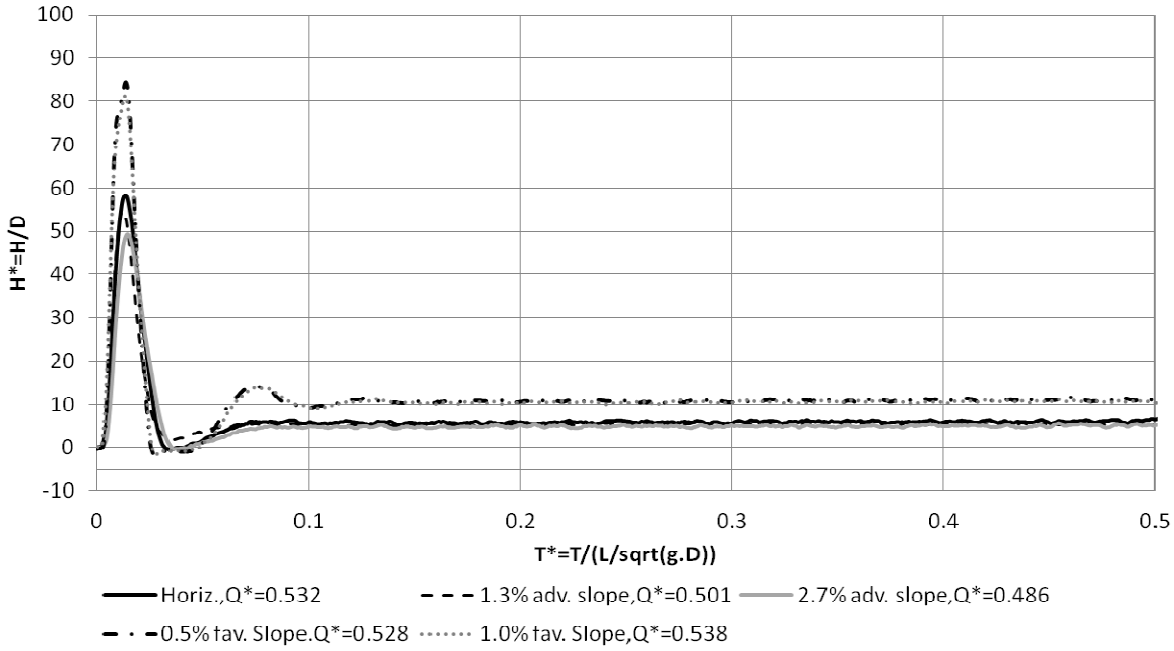

Figure 5.21: Non-dimensional pressure evolution following for 89% obstruction by the knife gate of all the slopes with minimal air pocket volume (Vair*=0.11 to 0.37)

It also maybe noticed in Figures 5.20 and 5.21 that the steady pressure levels obtained for favorable slopes differ slightly from the ones obtained for horizontal and adverse slopes. There is no clear explanation for that but it is speculated that this may be caused by the disassembly and reassembly of the experimental apparatus between the horizontal/adverse and the favorable slope experiments when the apparatus was moved to its current position in the off-campus Hydraulic Research Laboratory at Skyway Drive, Auburn, AL.

5.1.4 Partial obstruction. Experiments - Flow velocity measurements

Flow velocity measurements for the partial obstruction experiments reflected the pressure measurements. Upon valve maneuver, flow decayed rapidly and readjusted to a new steady state

in under 1.2 seconds ($T^*<0.1$). Generally the drop in flow velocity measured by the ADV, and hence flow rate in the pipe, ranged between 50%-64% of the initial flow rate for the case with 81% obstruction; the experiments with 89% obstruction indicated a drop of 72%-80% of the initial flow rate.

Figure 5.22 and 5.25 present velocity measurements for 81% and 89% obstructions and horizontal slope, respectively, with three flow rate ranges represented. It is interesting to notice that, regardless of the initial flow rate, the flow measured after the valve maneuver was very similar between the different cases tested. One may also notice that for the cases with 89% obstruction there was some oscillations on the predicted velocity, which also lasted briefly. There were no noticeable oscillations on the results measured with the 81% obstruction.

Figures 5.23 and 5.26 are analogous to 5.22 and 5.25, but instead present results for the 2.7% adverse slope. Favorable slope (1.0%) results are presented in Figures 5.24 and 5.27 for 81% and 89% obstruction respectively. Velocity results for these slopes are present two interesting features. Adverse slope velocities are significantly different following valve maneuver, which is possibly explained by the larger flow difference between the tested cases when compared with horizontal or favorable slope. Also, velocity measurements in these partial for favorable results present oscillations that are consistent with the pressure measurements presented in Figures 5.15 and 5.17.

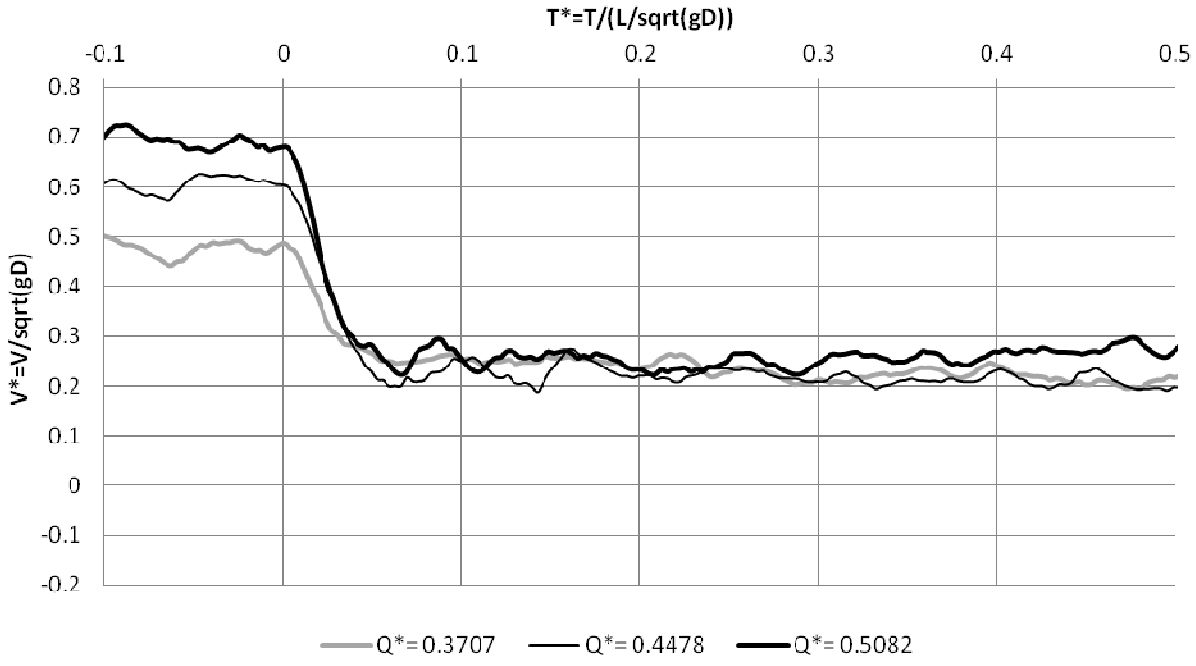

Figure 5.22: Non-dimensional velocity evolution following 81% obstruction by the knife gate valve, horizontal slope results.

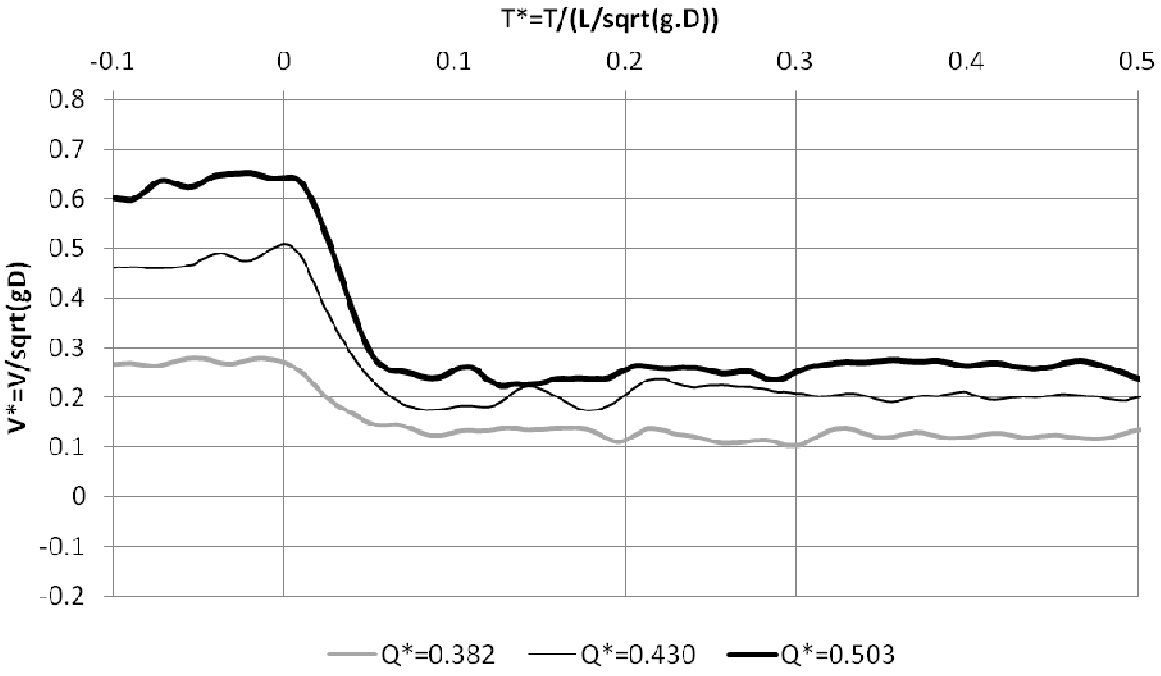

Figure 5.23: Non-dimensional velocity evolution following 81% obstruction by the knife gate valve, 2.7% adverse slope results.

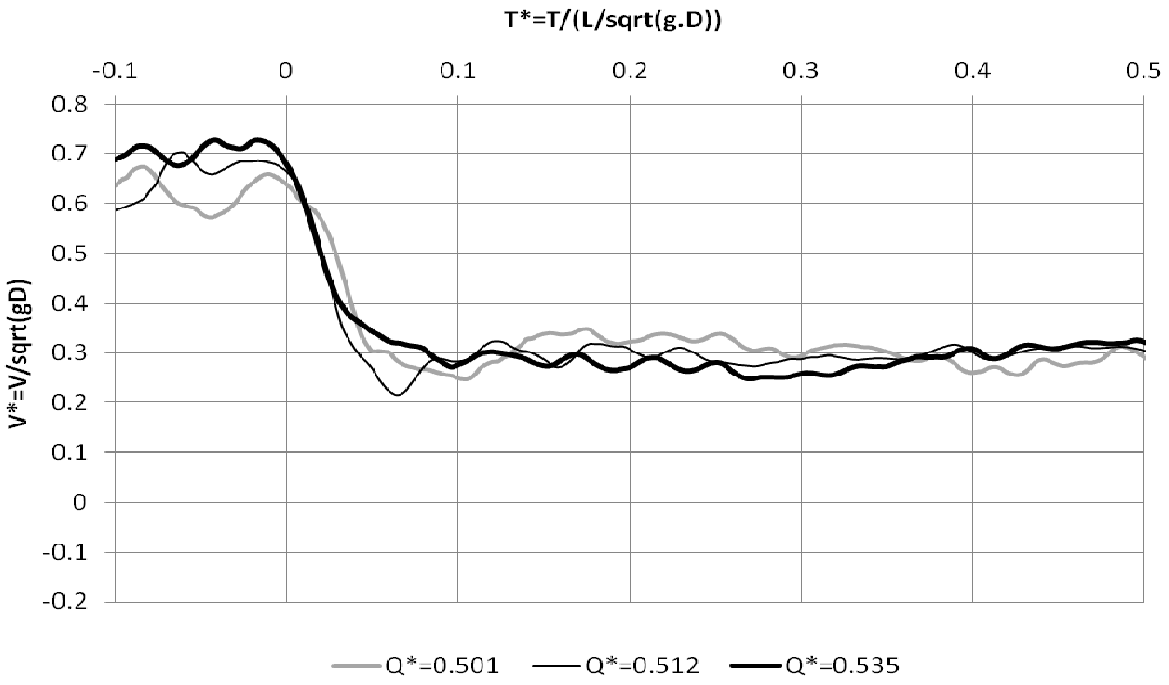

Figure 5.24: Non-dimensional velocity evolution following 81% obstruction by the knife gate valve, 1.0% favorable slope results.

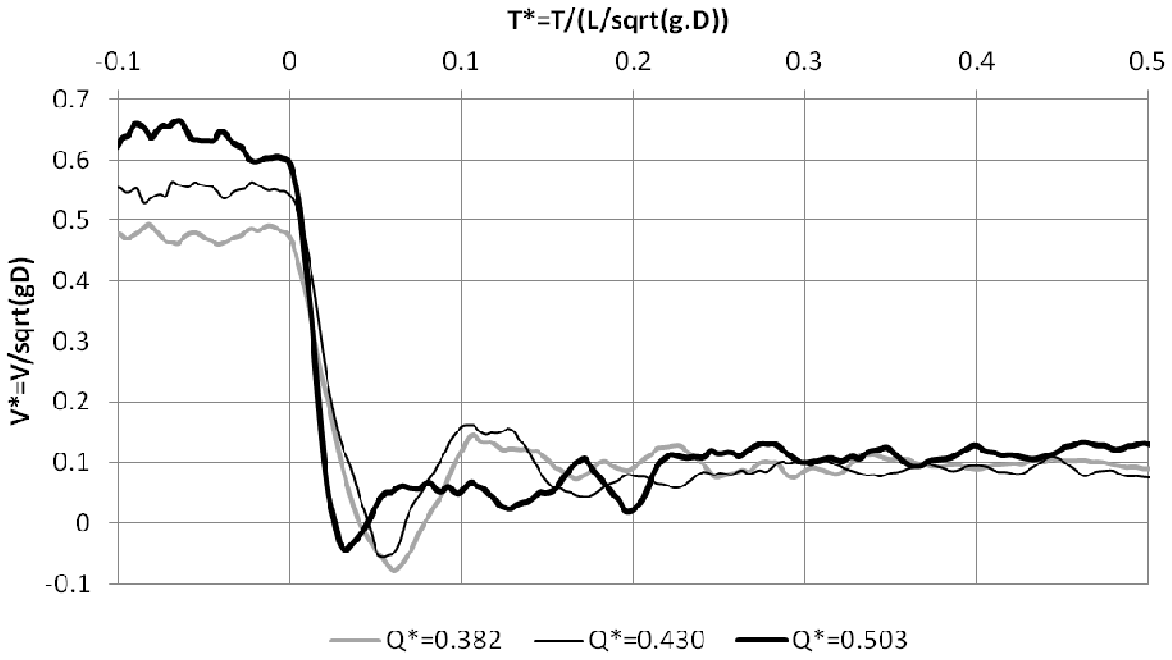

Figure 5.25: Non-dimensional velocity evolution following 89% obstruction by the knife gate valve, horizontal slope results.

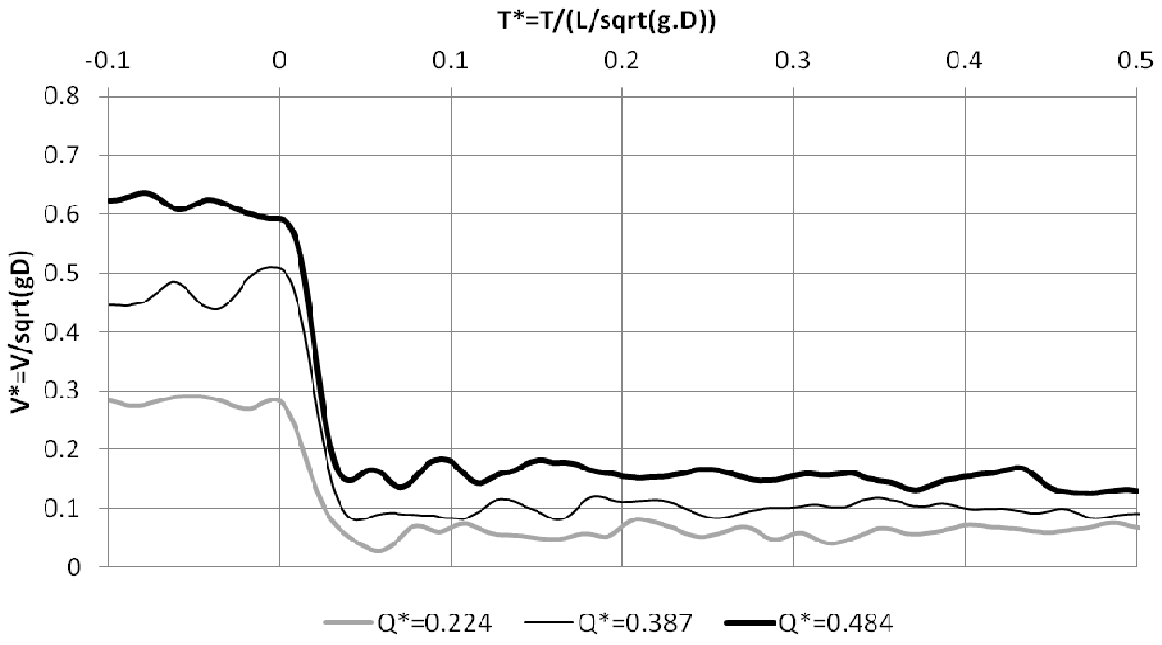

Figure 5.26: Non-dimensional velocity evolution following 89% obstruction by the knife gate valve, 2.7% adverse slope results.

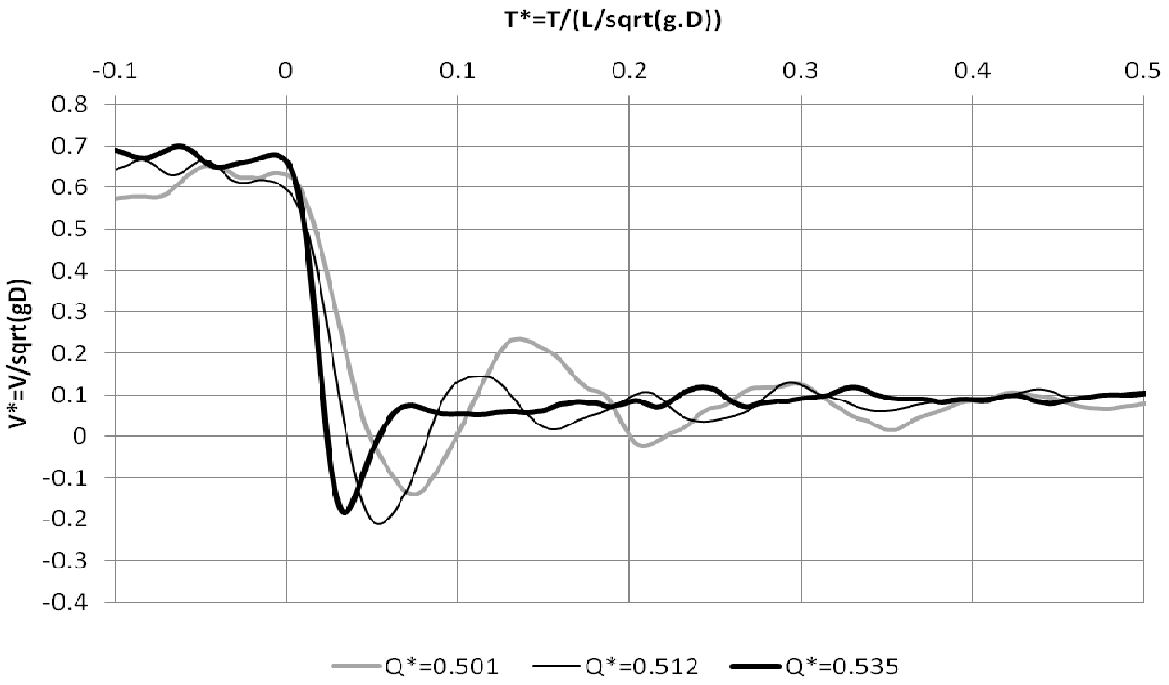

Figure 5.27: Non-dimensional velocity evolution following 89% obstruction by the knife gate valve, 1.0% favorable slope results.

5.1.5 Discussion of experimental results

The initial setup of the experimental apparatus assumed that the upstream reservoir, supported by a wooden platform, was a sufficient anchor to perform the proposed experiments. At the downstream end there was no anchor, but the initial assumption is that any longitudinal deflection on the experimental runs would be negligible. This assumption turned out to be inaccurate as such deflections were noticeable in the experiments involving the smaller pockets, where even the wooden tower would be pushed by the pressure forces generated upon sudden and total obstruction of the knife gate valve.

To assess the extent that this displacement affected the experimental results, experiments were performed with a "single anchor" configuration (only the reservoir weight) and a "dual

anchor" configuration, in which both the extremities of the apparatus were supported against the opposing walls by wooden beams. Peak pressures following total obstruction and horizontal pipeline diameter are presented in Figure 5.28. Pressure measurements are presented for the downstream end of the pipeline (X*=1.0) and for a point halfway through the pipeline length (X*=0.5).

There is a tendency of the dual anchor results to be slightly above the single anchor configurations, particularly for smaller air pocket volumes. Because of these findings, all subsequent experiments adopted dual anchor configuration to minimize any longitudinal displacement, as a means to achieve better comparison with previous investigations and numerical modeling predictions.

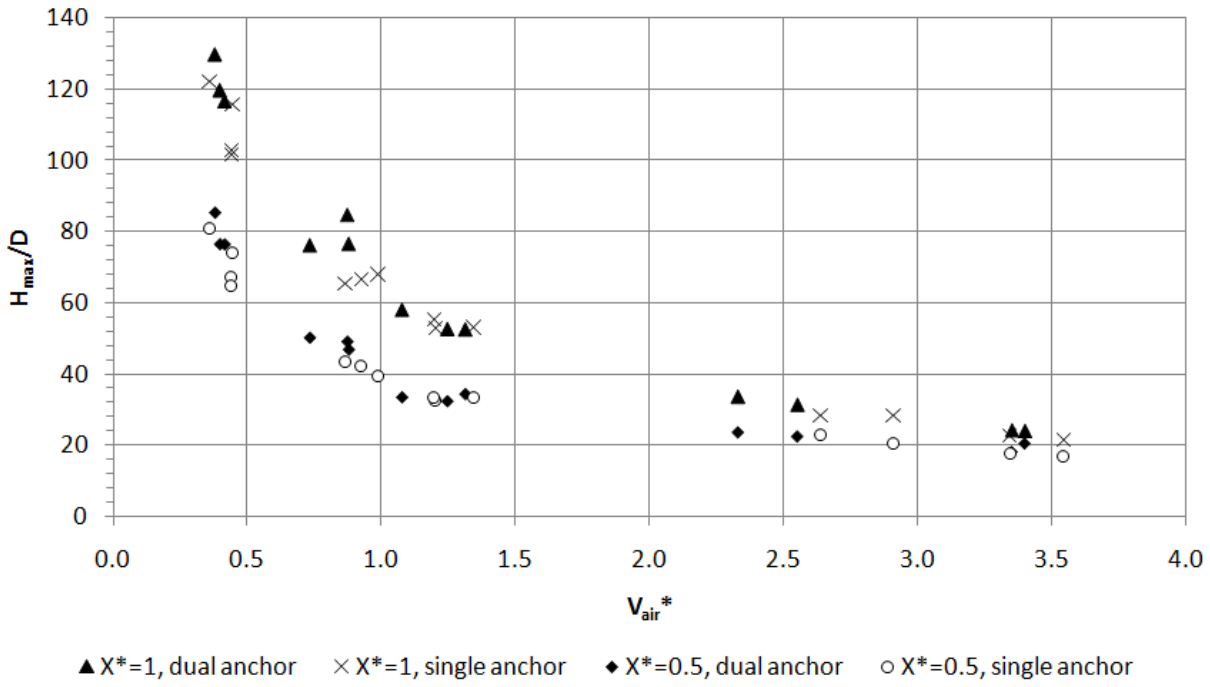

Figure 5.28: Non-dimensional peak pressures measured at two locations along the pipeline (X/L=X*=1.0 and 0.5) for experiments involving complete valve obstruction, horizontal slope and different anchoring schemes

Figures 5.29, 5.30 and 5.31 present all measured peak pressures grouped by slope and obstruction degree; Figure 5.29 (horizontal slope results) also presents the minimum negative pressure observed in the full obstruction conditions. This graph facilitates the comparison between different air pocket volumes and obstruction degrees. In agreement with the data presented in Table 5.1, the pressure peak results with the 89% obstruction are slightly less than half than the ones observed in total valve obstruction for similar air pocket volumes; results from 81% obstruction were about half of the obtained with the 89% obstruction. The scatter in the results is attributed either to small flow rate variations between experimental repetitions and/or to the inability to shut the knife gate valve at the exact same time between the repetitions.

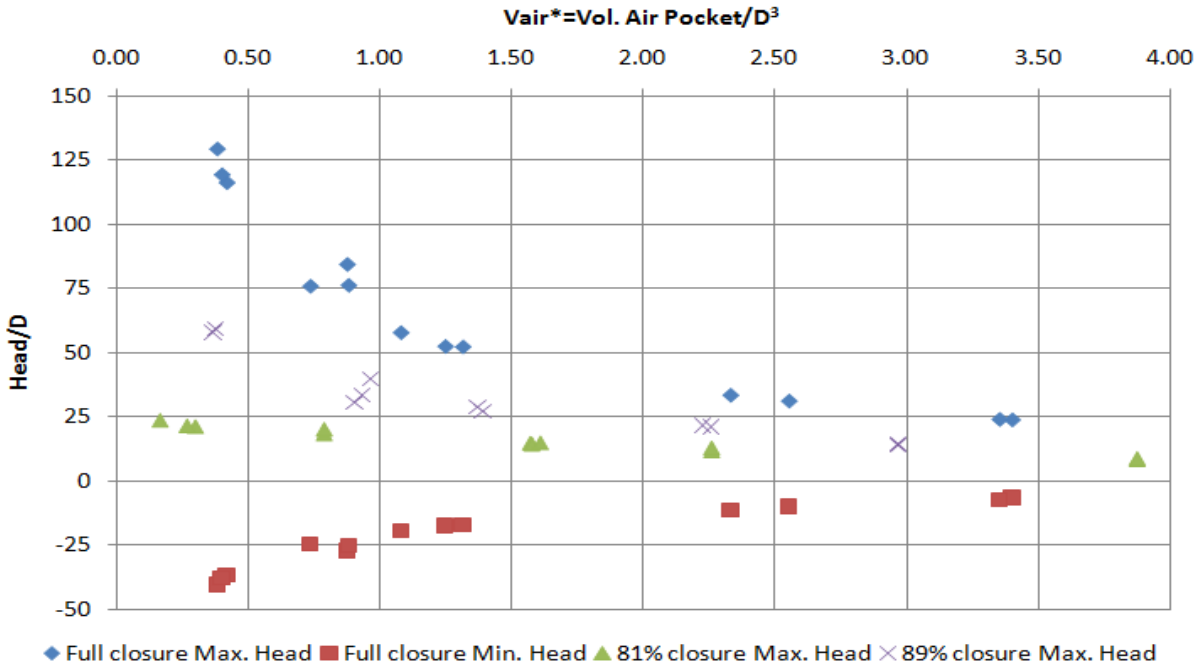

Figure 5.29: Non-dimensional peak pressures as a function of entrapped air pocket volumes, and valve obstruction degree; horizontal slope results shown

Figures 5.30 and 5.31 present measured peak pressures for adverse slopes of 1.3% and 2.7%, respectively. Even though the general trend from Figure 5.29 is also represented, one notices that the pressure drops much more rapidly with larger air pockets than what is observed for horizontal slope results. This result is linked to the geometric characteristics of the upward slope free discharge and the initial flow rate. For steeper adverse slopes conditions, the flow rate required to sustain a certain cavity volume at the downstream end is comparatively smaller than the flow required for shallower or horizontal slopes. Thus, with smaller flow rates, peak surges are also reduced.

This also explains why this trend is reversed for the case of favorable slopes, as indicated in Figures 5.32 and 5.33 for slopes 0.5% and 1.0% respectively. One notices that the rate of the pressure decrease with the size of the air pocket diminishes for larger positive slopes. In such favorable slopes the flow rate required to sustain a certain air cavity at the downstream end of the pipe for favorable slopes is comparatively much larger. Even though the pocket volume is in some cases much larger than the correspondent ones for horizontal and adverse slope cases, the high flow rate still create conditions for large H*=H/D values, above 25 in some conditions.

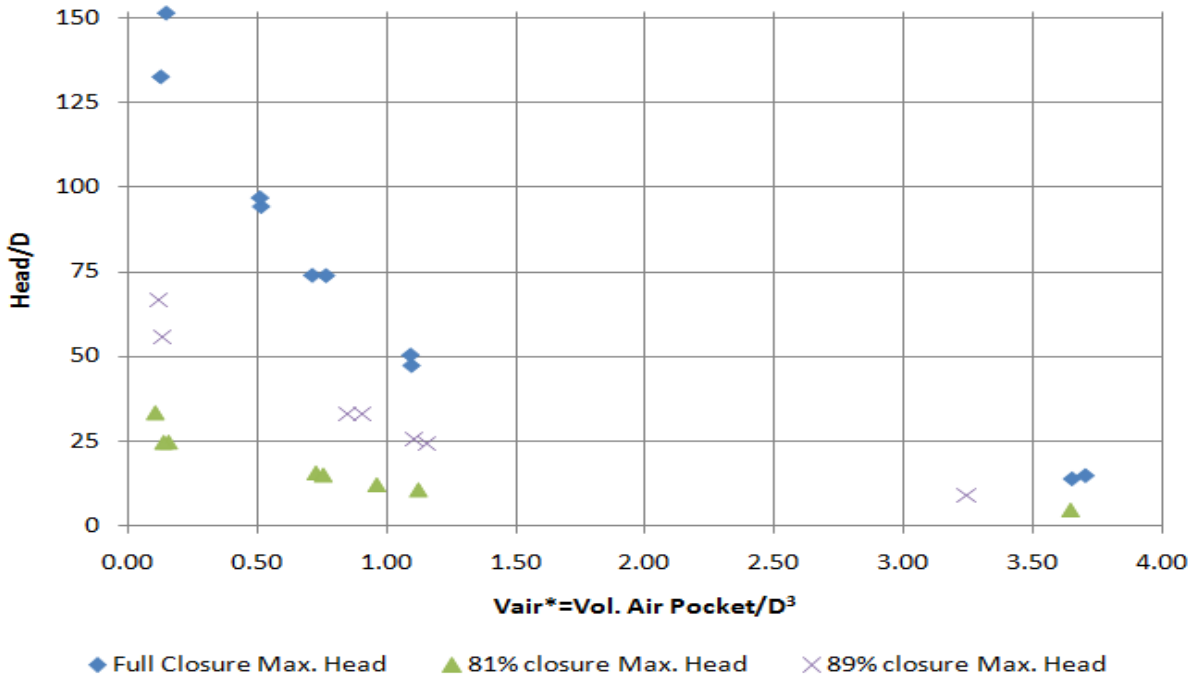

Figure 5.30: Non-dimensional peak pressures as a function of entrapped air pocket volumes, and valve obstruction degree; 1.3% adverse slope results shown

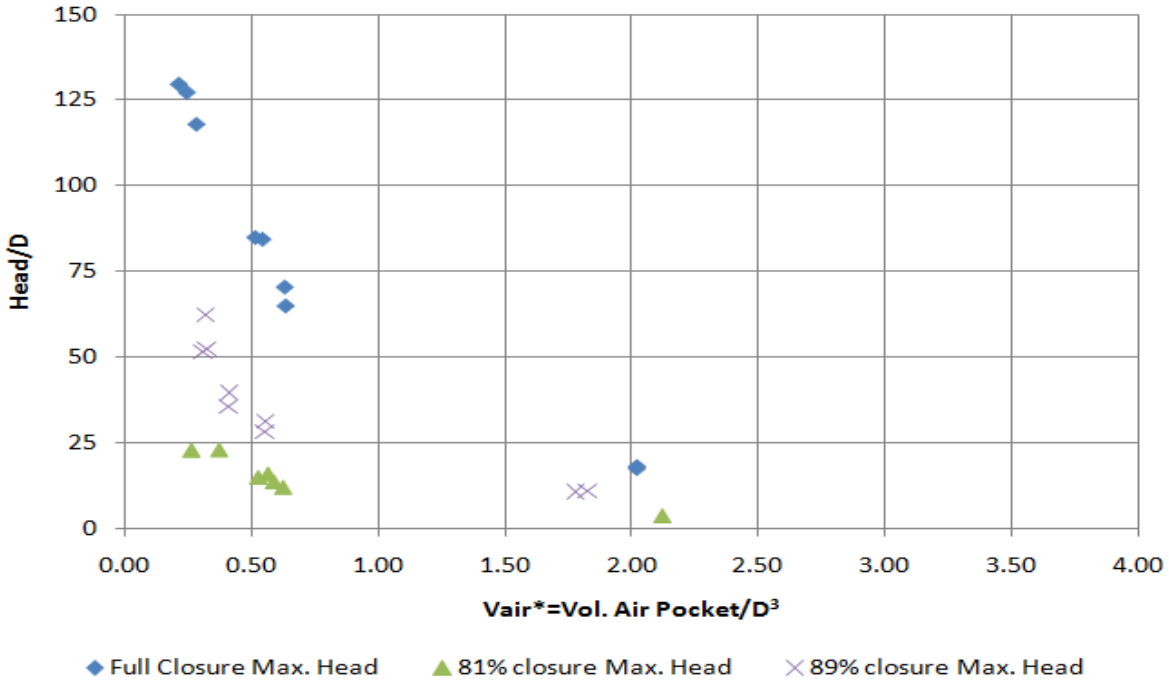

Figure 5.31: Non-dimensional peak pressures as a function of entrapped air pocket volumes, and valve obstruction degree; 2.7% adverse slope results shown

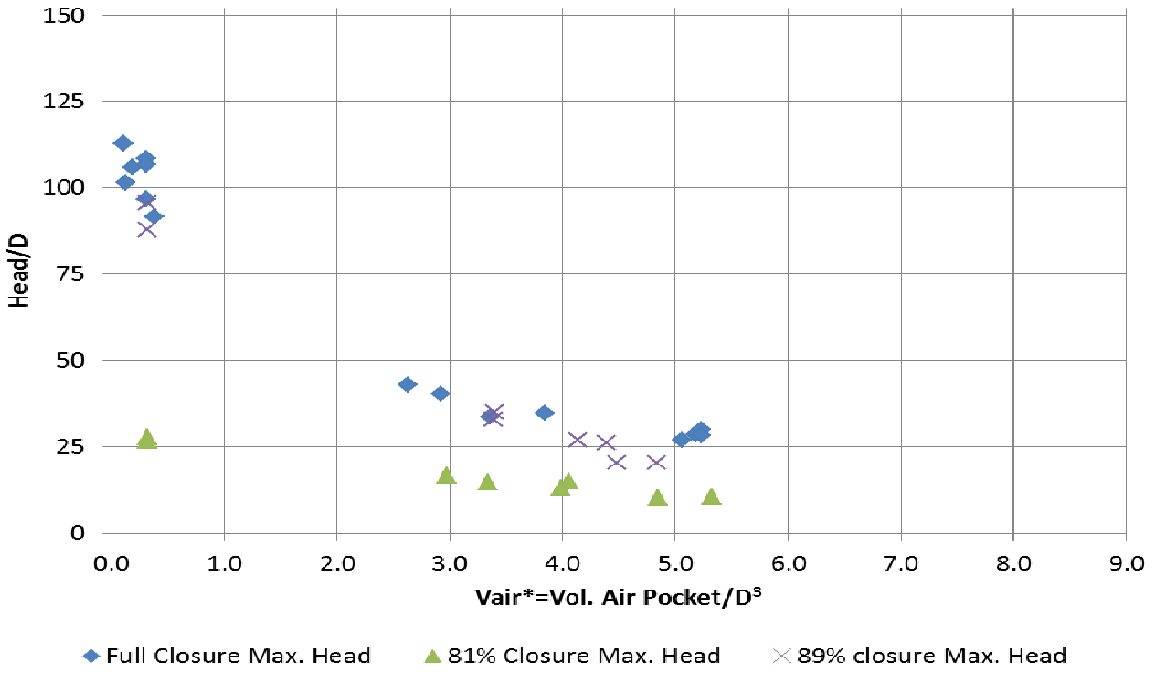

Figure 5.32: Non-dimensional peak pressures as a function of entrapped air pocket volumes, and valve obstruction degree; 0.5% favorable slope results shown

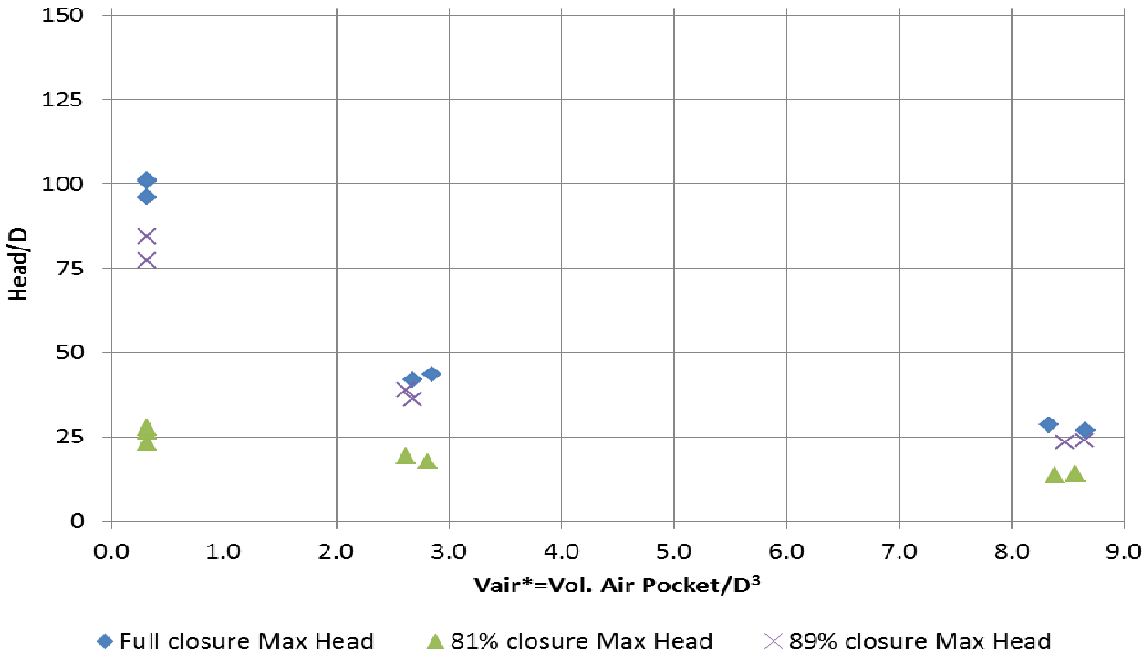

Figure 5.33: Non-dimensional peak pressures as a function of entrapped air pocket volumes, and valve obstruction degree; 1.0% favorable slope results shown

The relationship between surge intensity and initial flow rate is supported by the results presented in Figures 5.34, 5.35 and 5.36, where the peak pressures for different slopes and obstruction types are plotted in terms of the normalized inflow rate $Q^*=Q/(gD^5)^{0.5}$. For instance, while Figure 5.34 indicates that for the horizontal slope a total obstruction will cause a peak pressure $H^*=75$ with a $Q^*=0.5$, this flow rate is smaller for the 1.3% adverse slope results ($Q^*=0.425$) and 2.7% adverse slope ($Q^*\approx0.4$) as indicated in Figures 5.35 and 5.36. Similar comparison can be drawn from partial obstruction experiments. For instance, for the 89% obstruction results at horizontal slope, the peak pressure $H^*=25$ is attained with $Q^*=0.45$, while for 1.3% adverse slope this flow rate is smaller at $Q^*=0.37$.

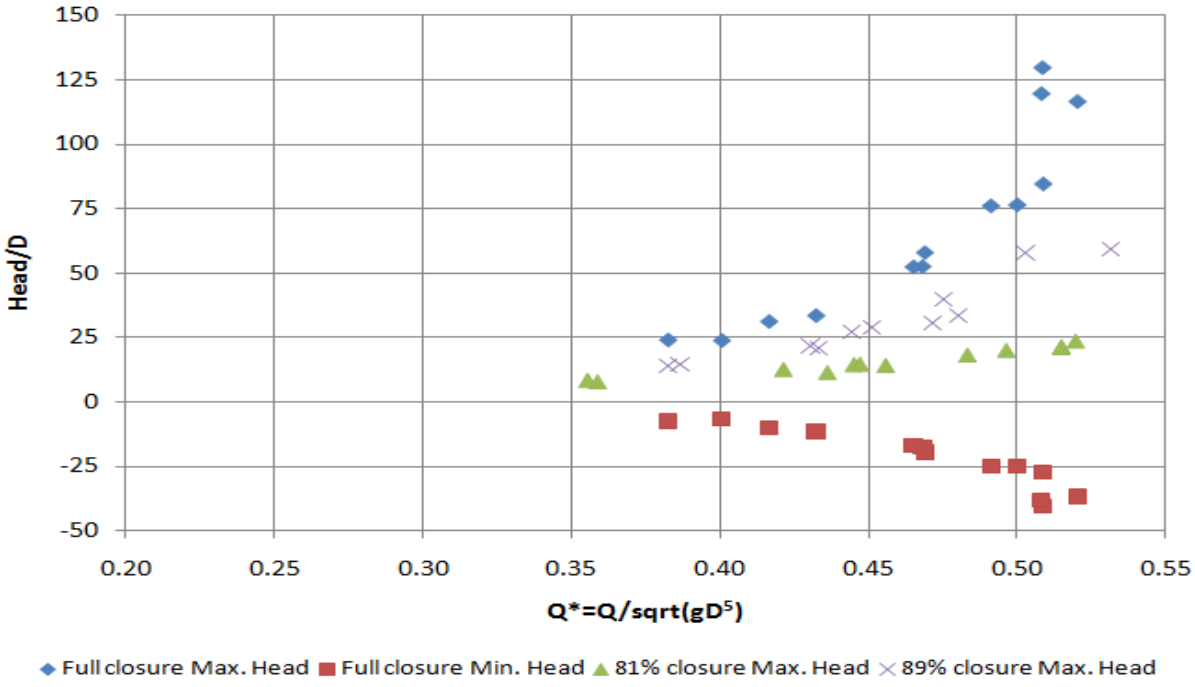

Figure 5.34: Non-dimensional peak pressures as a function of initial flow rate, and valve obstruction degree. Horizontal slope results shown

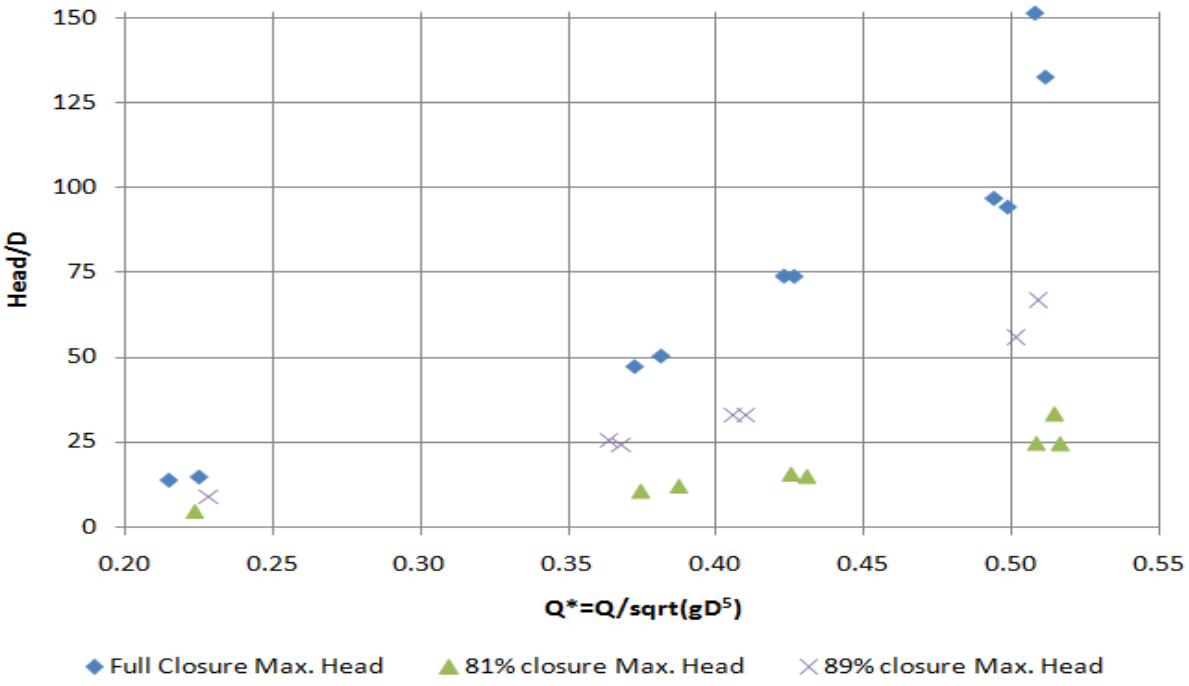

Figure 5.35: Non-dimensional peak pressures as a function of initial flow rate, and valve obstruction degree. 1.3% adverse slope results shown.

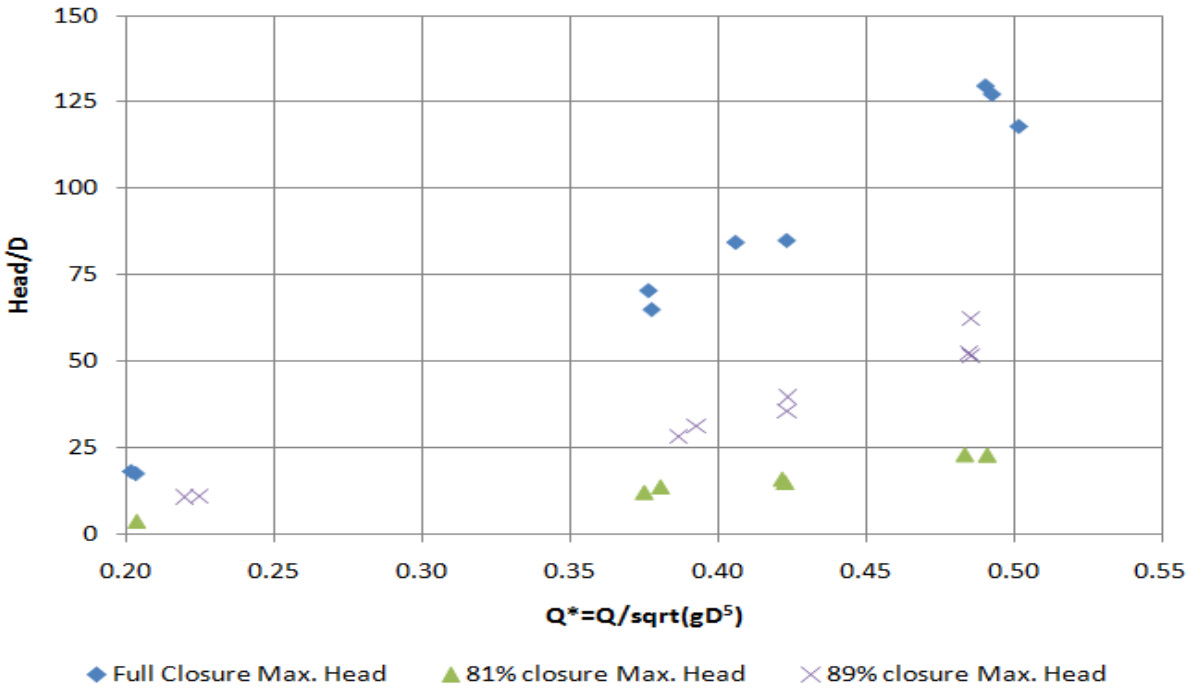

Figure 5.36: Non-dimensional peak pressures as a function of initial flow rate, and valve obstruction degree. 2.7% adverse slope results shown

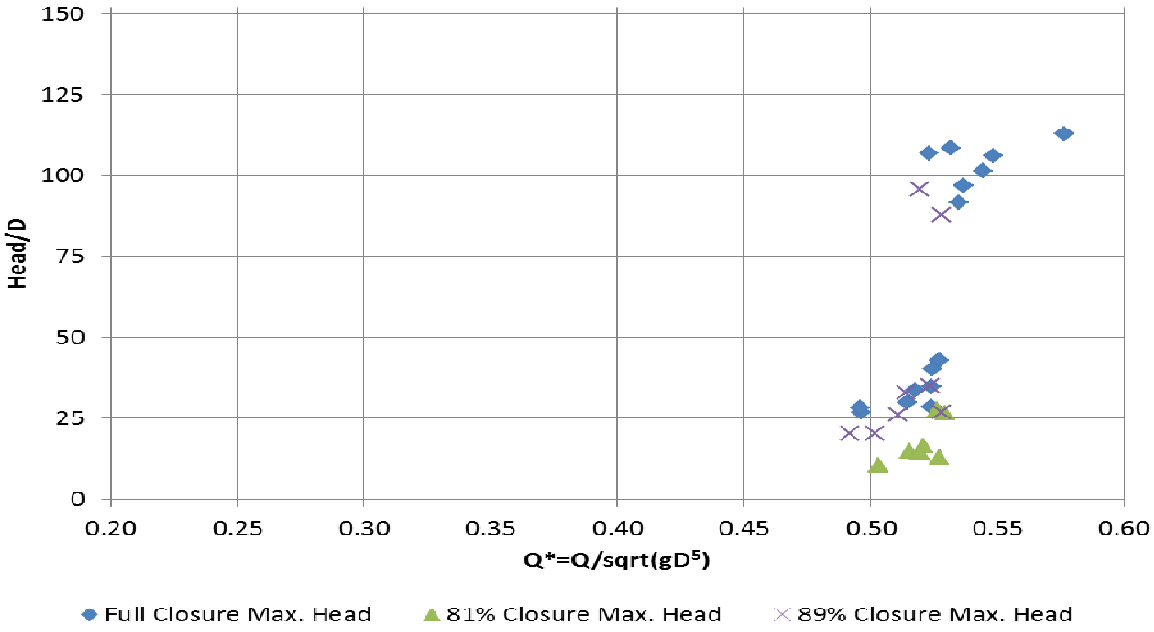

Figure 5.37: Non-dimensional peak pressures as a function of initial flow rate, and valve obstruction degree. 0.5% favorable slope results shown, and are qualitatively similar to the ones obtained with the 1.0% favorable slope

When the relation between the non-dimensional flow rate and peak surge head is considered for favorable slopes, as presented in Figure 5.37, a much weaker relationship between these variables is noticed. The main reason is that for favorable slopes the required flow rate to maintain cavities, even large ones, was generally large. The sensitivity of the cavity volume with the flow rate, as noticed in Figure 5.37, then becomes much smaller. However, in the tested flow range, some conditions also yielded small initial air cavities, associated with large surges.

Figures 5.38, 5.39 and 5.40 present results of the peak pressures for different pipe slopes as a function of the air pocket volume, but this time results are grouped by the obstruction type. Figure 5.38 results include all the maximum and minimum pressures for the total obstruction experiments. Despite the data scatter, one clearly sees the trend of largest pressure peaks for smaller air pockets. Scatter is more pronounced for the partial obstruction experimental results,

and one may notice the tendency of the 1.3% adverse slope peak results to stay between the horizontal results and 2.7% adverse slope results. Favorable slope experiments led to results that were generally larger than the correspondent ones obtained with horizontal or adverse slopes. This separation of the results obtained with different slopes becomes more pronounced for larger air pocket volumes, a result also linked to the differences in the inertia to create air cavities with different flow rates and pipe slopes.

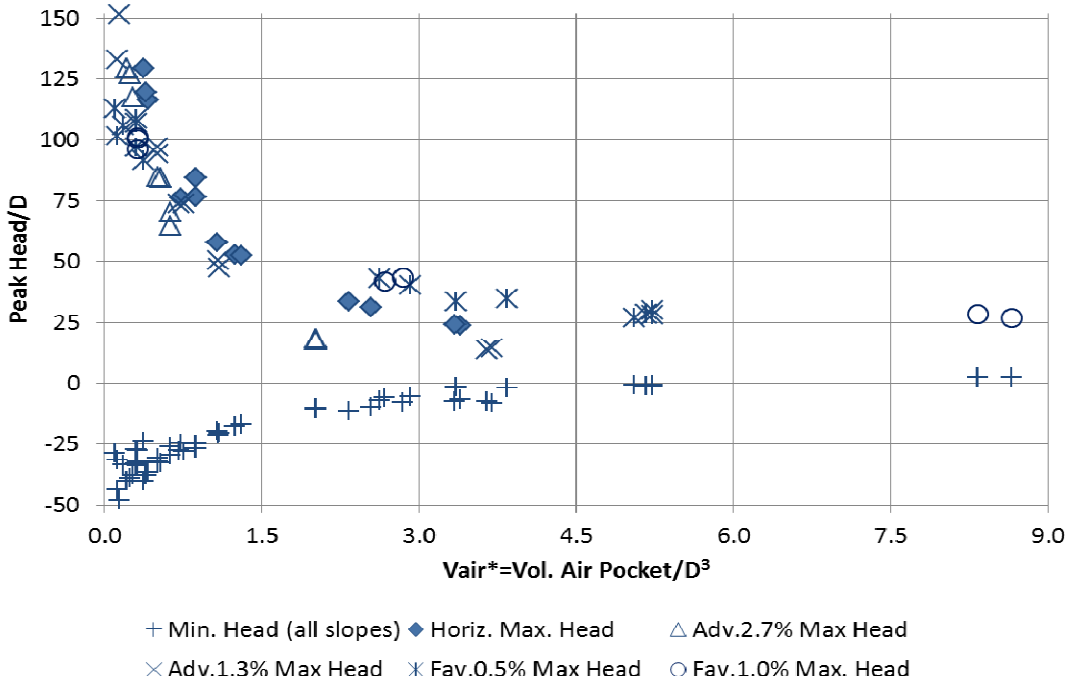

Figure 5.38: Non-dimensional peak pressures as a function of air pocket volume and slope for total obstruction experiments.

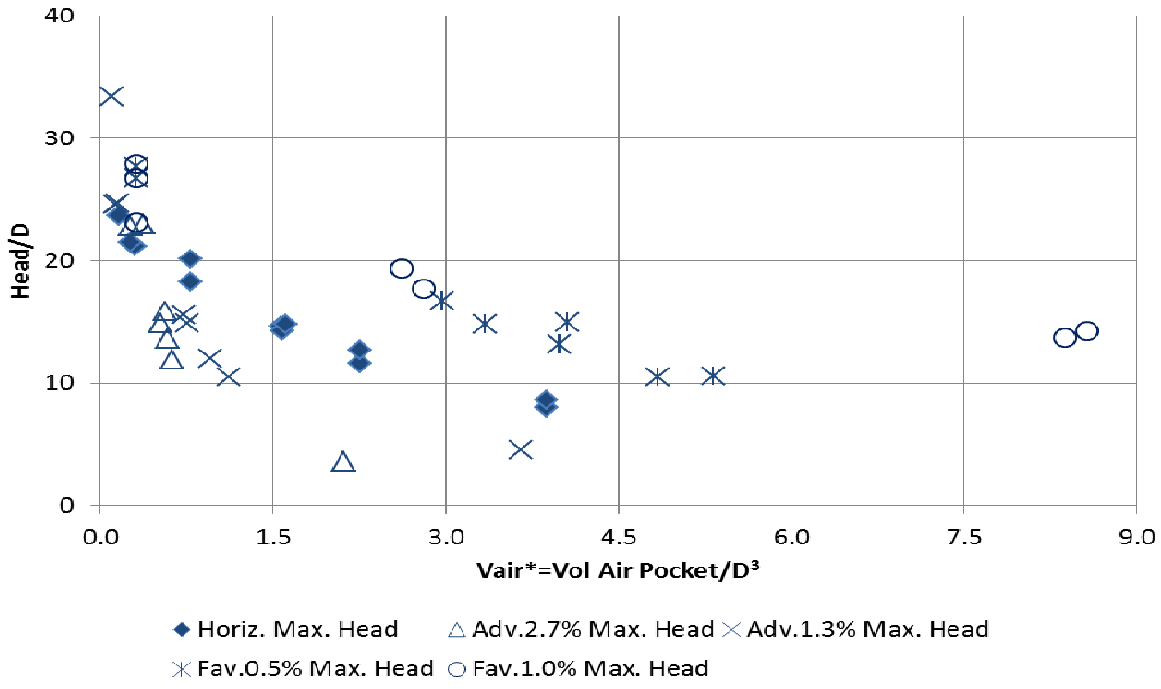

Figure 5.39: Non-dimensional peak pressures as a function of air pocket volume and slope for 81% obstruction experiments.

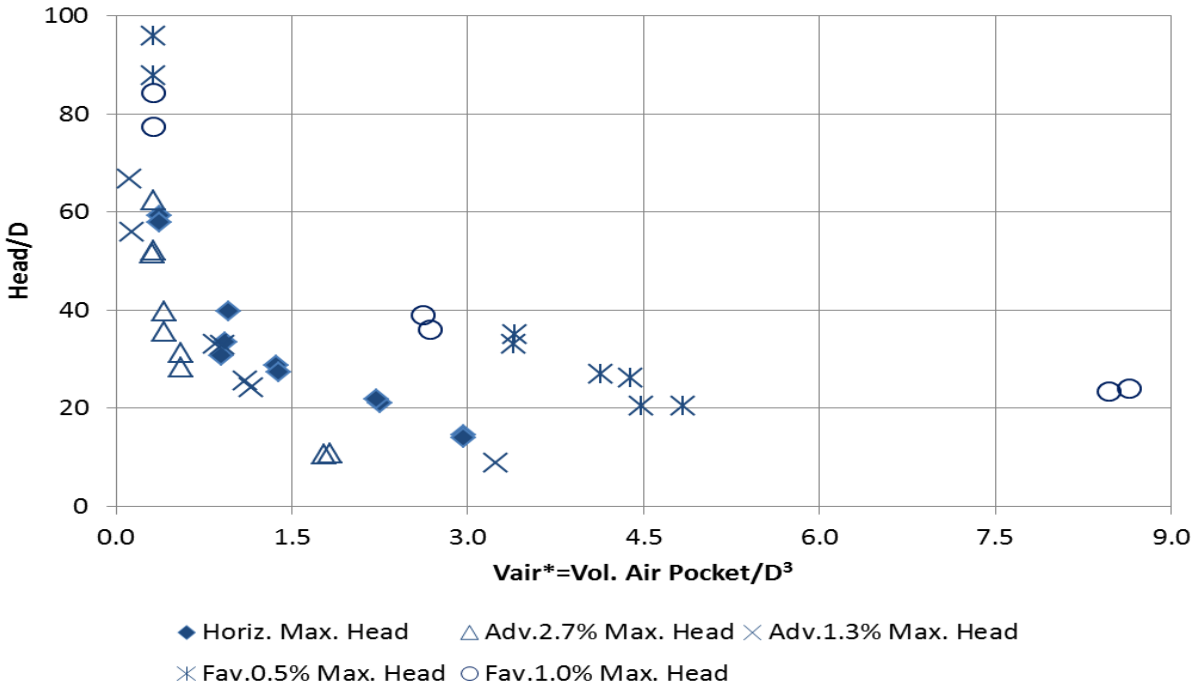

Figure 5.40: Non-dimensional peak pressures as a function of air pocket volume and slope for 89% obstruction experiments.

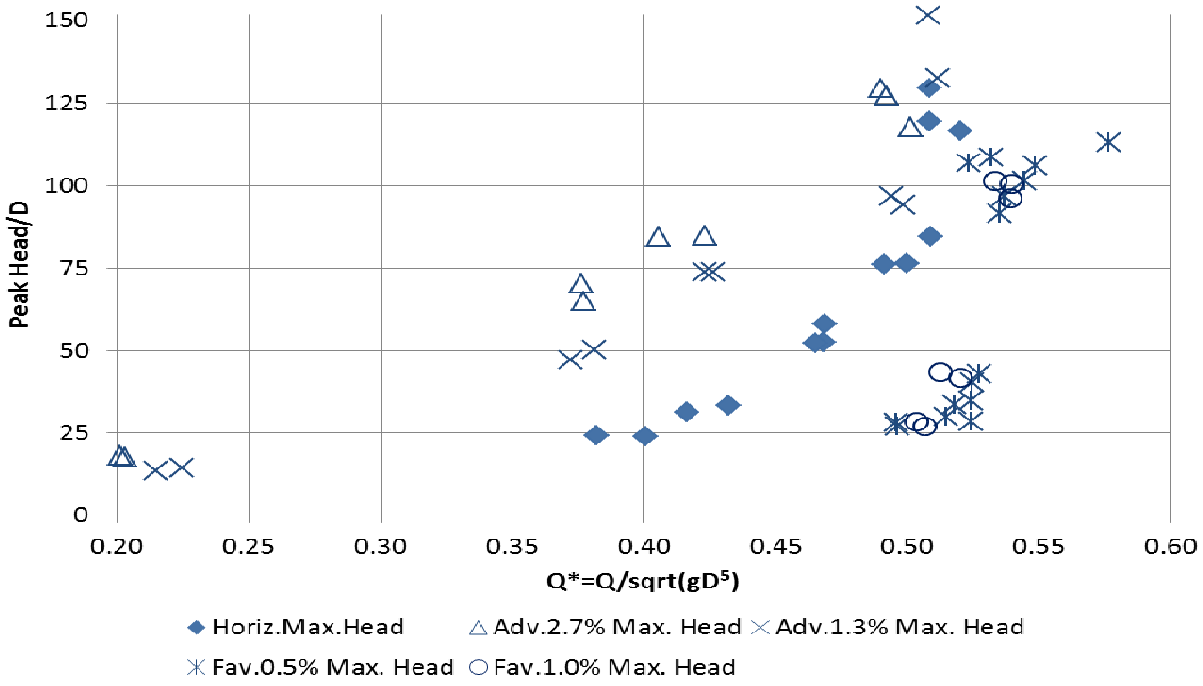

Figure 5.41: Non-dimensional peak pressures as a function of initial flow rate and slope for total obstruction experiments

Figure 5.41 present measured H* for different slopes as a function of Q*, only for total obstruction experiments. While the points are somewhat scattered for larger flow rates (Q*>0.53), the series representing the pipe slopes become clearly separated as the pocket volume increase. One notices clearly that peak surges results for adverse slopes have much more dependency on the initial flow rate when compared to the favorable slope results.

The ratio between the peak pressures measured at the two selected pipe stations (halfway through the pipe length X*=0.5 and at downstream end X*=1.0) is presented in Figure 5.42 for all tested cases, as a function of the air pocket volume. Despite of the data scatter, it noticeable that for horizontal and adverse pipe slopes and smaller air pocket volumes the pressure peak ratio ranged between 0.55 to 0.75, whereas this ratio had a tendency to increase for larger air pocket volumes to value above 0.85. For favorable pipe slopes the ratio between the pressure peaks was

consistently at or above 0.8, even with few cases when the pressure at the upstream transducer was larger than the one measured at the downstream end.

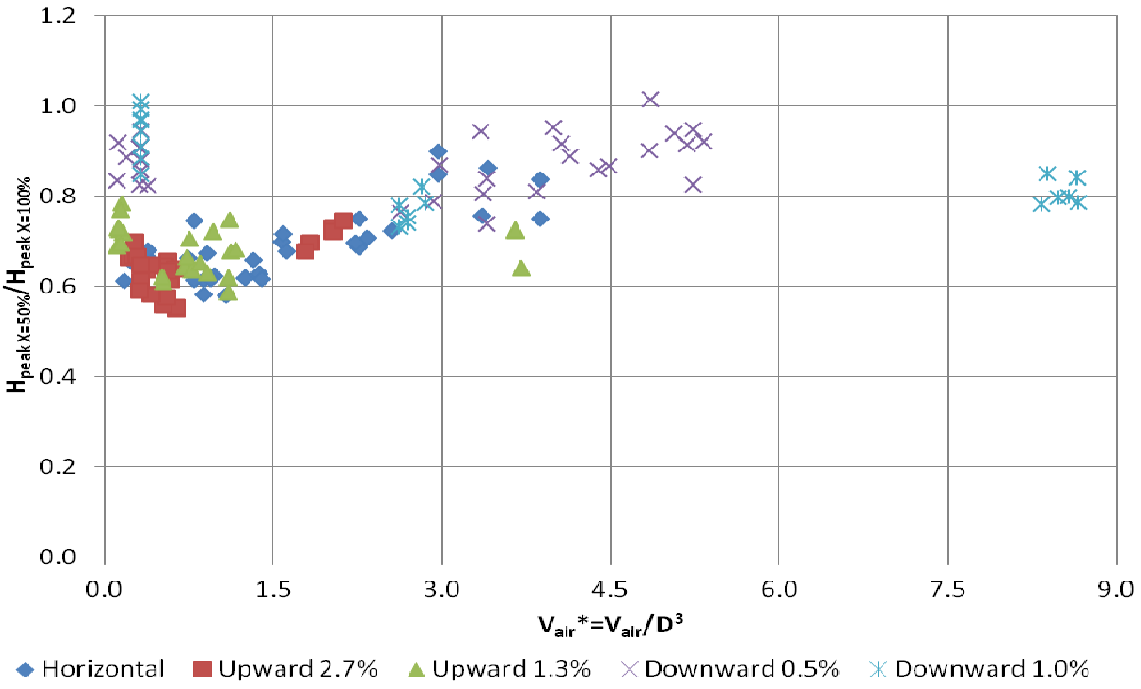

Figure 5.42: Ratio between peak pressures measured at X*=0.5 and X*=1.0 as a function of the entrapped air pocket volume

With regards to the velocity measurements, an interesting remark is that the flow rates are fairly similar right after the valve maneuver within the same obstruction degree, independently of the initial head at the upstream reservoir. There was also a tendency of the measured velocity to increase after valve maneuvering, as result of water level accumulation at the upstream tank. A possible explanation for these similar velocity results, even with different reservoir heads, is that the most of the energy losses upon partial valve obstruction occur at the valve itself. This strong energy loss may by such that differences in reservoir heads (in the order of tens of centimeters) may not have an important impact in the final discharge velocity.

5.2 Numerical modeling results

The pressure head predictions resulting from the numerical model represented by equations 4.3, 4.4 and 4.5 is presented in this section. Figures 5.43 to 5.48 present a comparison between the predicted pressures within the air phase and correspondent measurements. The simulations presented in this section are for the horizontal slope experiments only.

Figures 5.43 and 5.44 presents the comparison between the predicted pressures for the total obstruction and the experimental measurements, with Figure 5.43 presenting the minimum flow rate conditions (largest air pocket entrapped) and Figure 5.44 presenting the maximum pressure condition. It was considered that the valve shut the flow entirely in 0.20 seconds, based on observations of the recorded experiment movies. General trend of the measurements is captured by the numerical model, with a damped pressure oscillation pattern. However, the predicted pressure peaks were larger than the measurements. This may be attributed to some extent to the assumption of the valve closure expression, but in fact the results seem to indicate that the system has more elasticity than actually accounted for in the numerical model. This elasticity in the air-water that mitigates the surges could be due to unaccounted for air volumes, rubber joints used in some pipe connections, larger energy dissipation, among others.

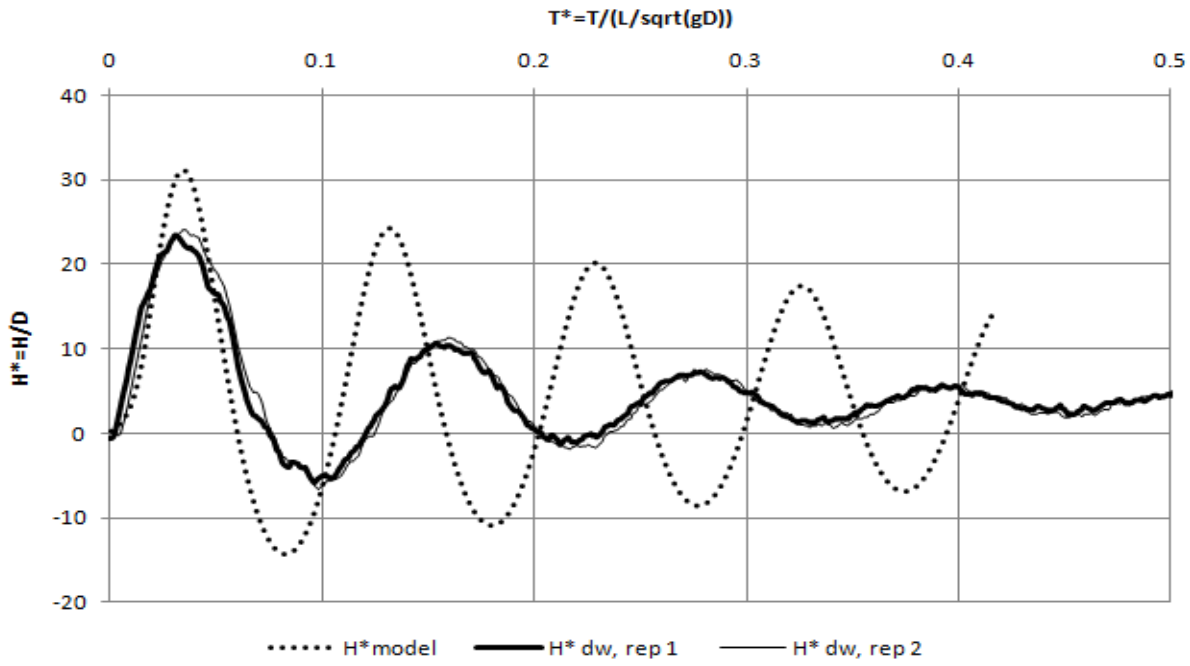

Figure 5.43: Predicted and measured pressure hydrographs for V_{air}*=3.5, Q*=0.38, horizontal slope, and total cross section obstruction condition.

Which is also unclear is the source for the additional pressure damping in the results which is clearly noticed both in Figures 5.43 and 5.44. This behavior was also reported in similar studies, such as Li and McCorquodale (1999). Considering that the cause of this discrepancy could be linked to thermodynamic effects, a modified version of the numerical model based on the work presented by Lee (2005) was developed. This model proposes a thermal damping component in the air phase energy equation, modified from the ideal gas law:

$$\frac{dH_{air}}{dt} = k\frac{H_{air}}{V_{air}}\frac{dV_{air}}{dt} + \frac{(k-1)HA_qH_{air,0}V_{air,0}}{V_{air}M_gR_g}\left(1 - \frac{H_{air}V_{air}}{H_{air,0}V_{air,0}}\right) \quad (5.1)$$

In which: A_q is the contact area between air and water phases, H is the head transfer coefficient, M_g the mass of gas and R_g the gas constant.

However, this modified model has not yielded results that were significantly different from the original version proposed with equations 4.3, 4.4 and 4.5. This discrepancy in the pressure damping thus remains an open question.

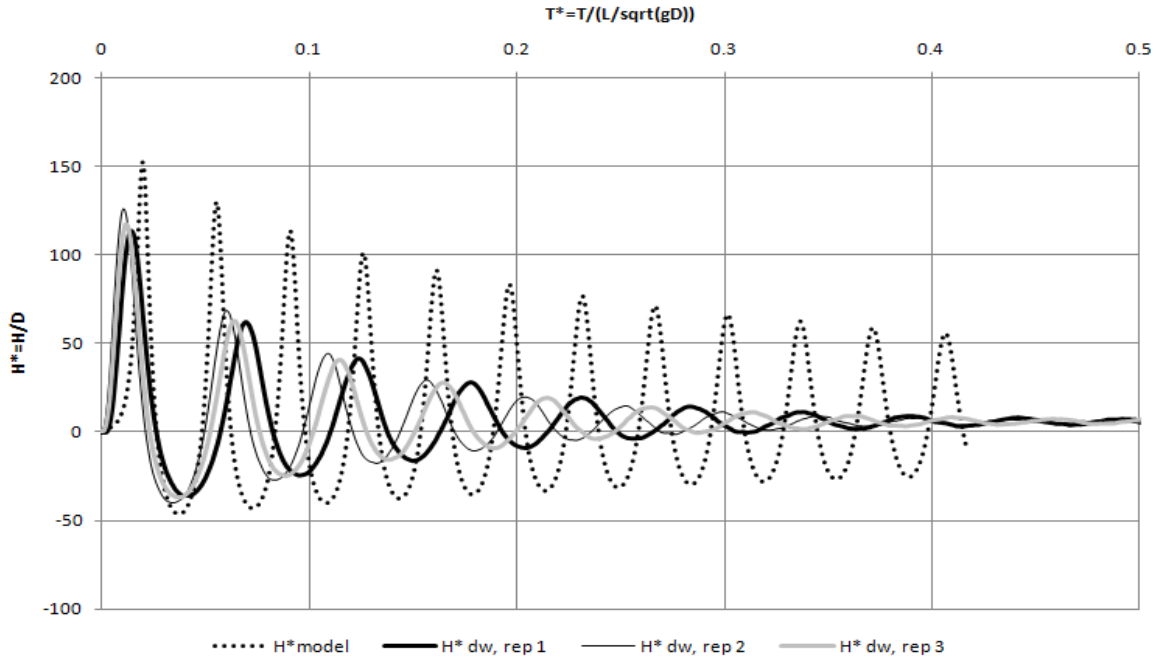

Figure 5.44: Predicted and measured pressure hydrographs for V_{air}*=0.40 Q*=0.51-0.52, horizontal slope, and total cross section obstruction condition

Figures 5.45 and 5.46 present the results of the proposed model in simulating the 81% partial obstruction experimental results for the maximum and minimum tested flow rates. The discharge coefficient of the valve varied from Cd=0.30 to 0.40, calibrated based on observed flow rate after the valve maneuver. The proposed model predicts fairly well the single peak behavior of the system as well the pressure variation following the valve maneuver. The same observation also applies to the comparison with 89% obstruction presented in Figures 5.47 and

5.48. Particularly interesting for the 89% obstruction predictions is the model's ability to capture to some extent the much damped oscillations that are observed following the pressure peak.

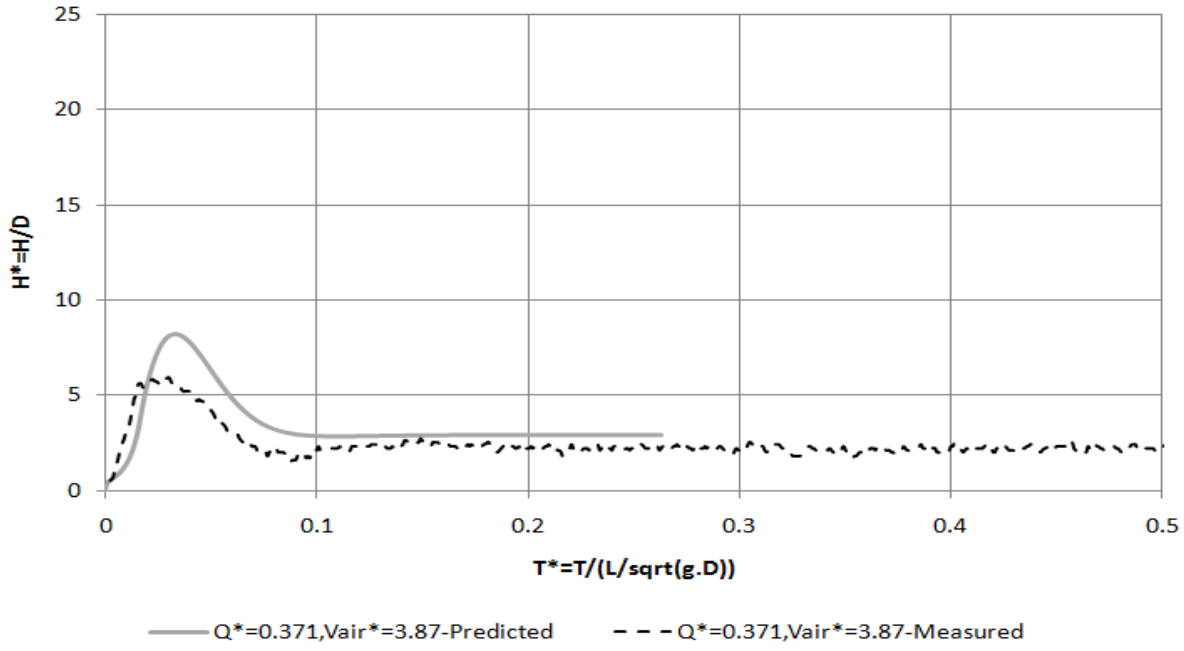

Figure 5.45: Predicted and measured pressure hydrographs, for V_{air}*~3.4, Q*=0.37, horizontal slope, and 81% of cross section obstruction condition

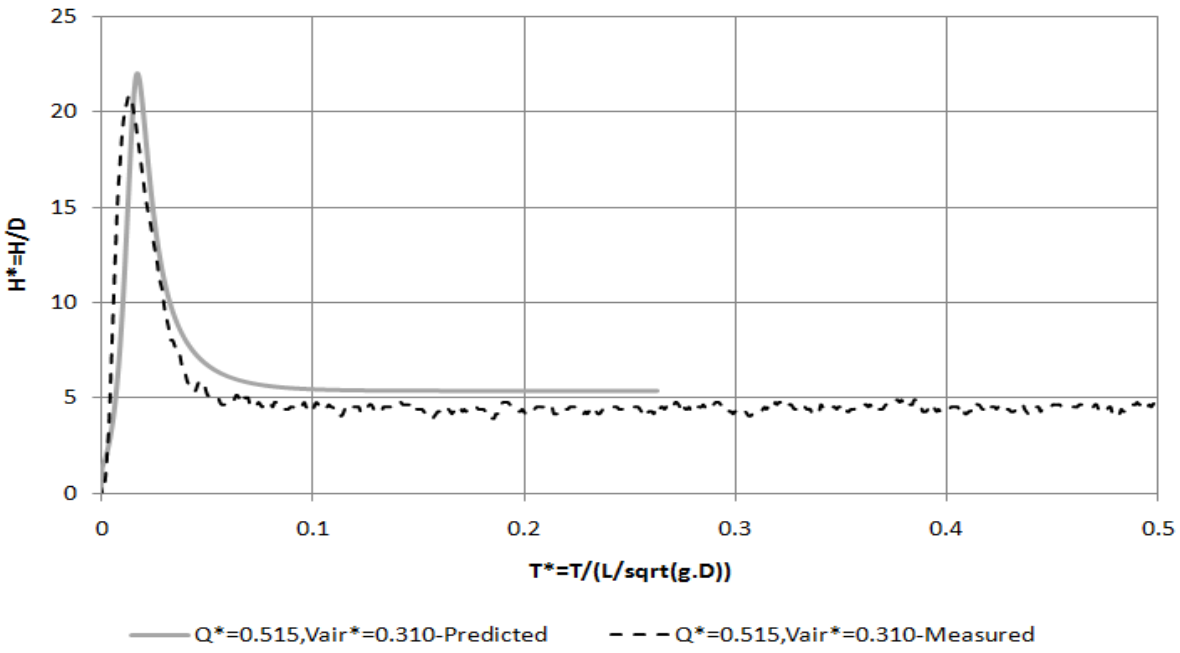

Figure 5.46: Predicted and measured pressure hydrographs, for V_{air}*~0.40, Q*=0.515, horizontal slope, and 81% of cross section obstruction condition

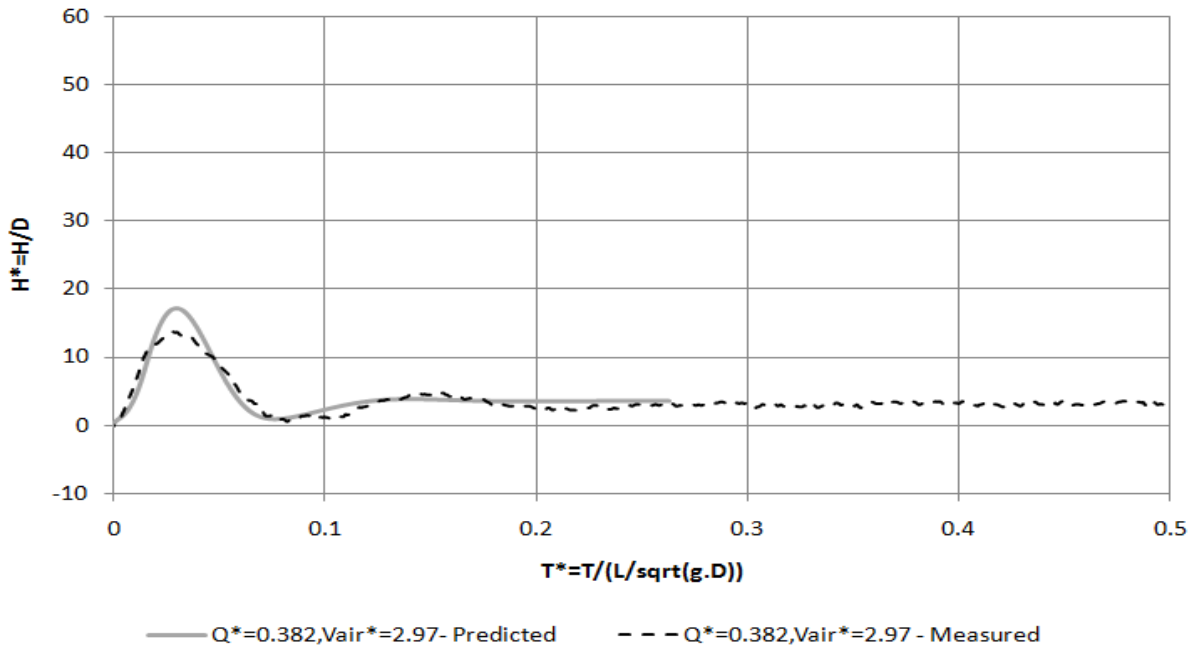

Figure 5.47: Predicted and measured pressure hydrographs, for V_{air}*~2.97, Q*=0.382, horizontal slope, and 89% of cross section obstruction condition

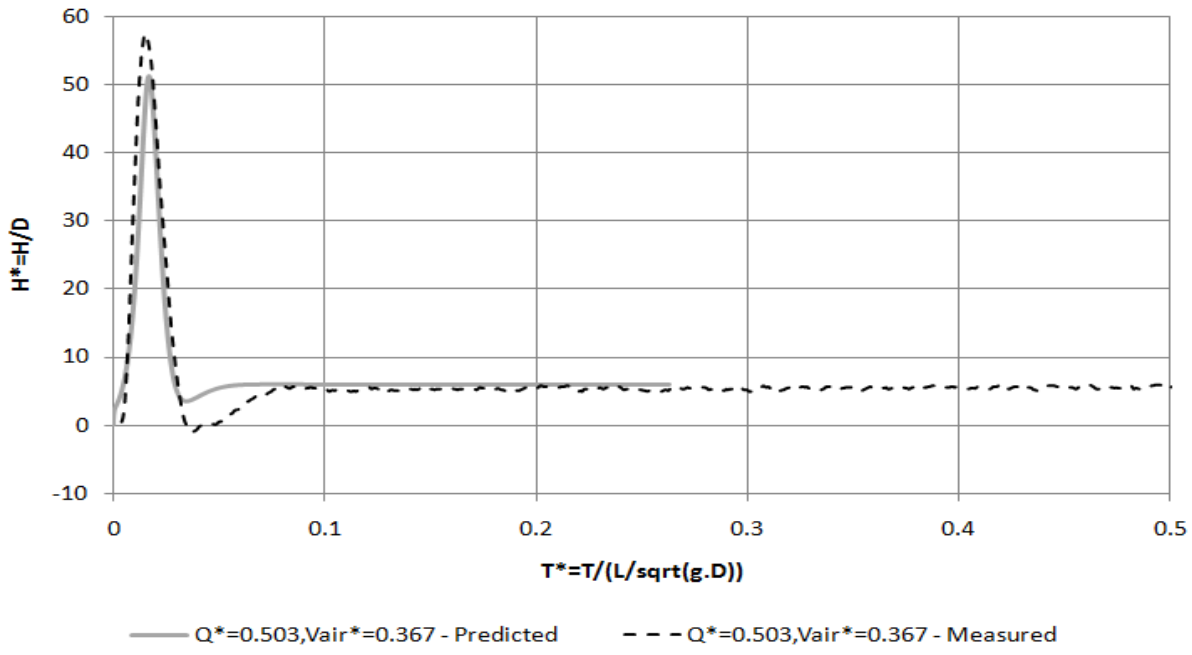

Figure 5.48: Predicted and measured pressure hydrographs, for V_{air}*~0.367, Q*=0.503, horizontal slope, and 89% of cross section obstruction condition.

Chapter six – Conclusions and Recommendations for Future Work

The purpose of this research was to provide further insights in the interactions between air and water in rapid filling pipe flows in the context of large, below grade stormwater tunnels. The focus was in the interactions between entrapped air pockets of various sizes suddenly entrapped in pressurized water flows. Unlike previous investigations, surges that are generated by the compression of air by water are performed both in cases when there is pressure relief, in this instance provided by an orifice, and without pressure relief resembling most previous related investigations. The idea of having this setup was to approximate experimental conditions the anticipated conditions in actual stormwater tunnels. A numerical modeling study was also developed to assess the ability of simplified, one-dimensional models to replicate the results obtained in the experiments.

As results of the research, there are three essential ideas. At the beginning, the collection of valuable experimental data and results on the problem of air pocket entrapment and compression in a fairly wide range of conditions. Then, it was made the numerical modeling of lumped inertia approach to describe this type of interaction in the pipeline. And, finally, with the two first model included it can be arrived a better idea on the physics of the air-water flow interactions and how the experimental and numerical are comparable.

The experimental included essential features present in stormwater storage tunnels. In actual conditions, pressure relief would be provided by structures such as surge shafts and dropshafts that are frequently tens of meters deep. Even in reduced scale experiments replication of these geometric conditions would be difficult, thus the pressure relief was provided by means of an orifice that provides escape for water during the surge process. This orifice was created by the gap of a partially closed knife gate valve. It is thus possible that pressure surges obtained here may be regarded as conservative estimates of air-water surges that would occur in stormwater tunnel systems. This assessment would require more detailed investigations, which would include larger scale experimental apparatus.

The experimental program had a very important task of highlighting the difference between flow characteristics for total and partial flow obstructions. As mentioned, the majority of previous investigations focused in situations involving air entrapped in water flow, in which the flow would compress with little or no air ventilation. The experiments performed with complete obstruction conditions yielded general pressure oscillations with characteristics similar to a spring-mass system. Similarly to observations by previous investigations, these experiments yielded surge oscillations with higher magnitude and frequencies for smaller air pocket volumes. Frequently the pressure oscillations reached sub-atmospheric levels.

The experiments with air pocket compression while allowing for pressure relief presented a pattern that was not reported in previous investigations. To horizontal and adverse, there was observed a single pressure pulse, and in most cases no residual oscillations was detected, an outcome significantly different from the total obstruction systems. To favorable, there was notice that it is a connection between the case with too much opening and the total obstruction by the valve. Moreover, the pressure magnitudes are significantly smaller while negative pressures were not observed in almost all cases. The identification of this distinctive behavior is important so that numerical tools may be constructed to incorporate those observations.

This research also has been useful in isolating the role of the initial flow rate in the surge magnitudes separately from air pocket volumes. Because experiments with comparable pocket volumes were performed with significantly different initial flow rates, it was verified that surge peaks increased with the initial inflow rates, and could be significant even in cases when air pocket volumes were high. Previous comparable studies have not varied systematically the flow rates while performing surge analysis, so these findings are also very useful in the calibration of future numerical models.

While all research objectives were successfully attained, it is recognized that this study is just an initial step to the path of improving our understanding of two-phase flow in stormwater tunnels systems. Clearly there are other relevant topics that should be addressed in future

investigations. Among them is the study of air pocket motion and pocket spreading following entrapment. The study of air pockets migration is very relevant in the design of ventilation points and tunnel filling dynamics. Another relevant topic to be addressed in future investigations is the air entrainment caused by sweeping pipe-filling bores. Depending on the characteristics of the moving bore, the volume of air entrained may be significant, affecting the continuity in the pressurized flow zone. This is study is also relevant because entrained air reduces the acoustic wavespeed, which has impacts in pressure predictions.

Another area that warrants further research is the creation of an improved numerical model able to simulate the filling of stormwater tunnels considering effects of entrapment, compression, motion, and spreading of entrapped air pockets. In order to incorporate in future numerical model, three fundamental gaps will need to be addressed: 1) the air entrainment mechanisms into pipe filling bores; 2) motion of entrapped air pocket due to drag and shear forces; and 3) motion and ventilation of entrapped air pockets.

References

Aimable, R., Zech, Y. (2003). Experimental results on transient and intermittent flows in a sewer pipe model. In: *Proc. XXX IAHR Congress*, Thessaloniki, Greece.

Arai, K. and Yamamoto, K. (2003). Transient analysis of mixed free-surface-pressurized flows with modified slot model 1: Computational model and experiment. In *Proc. FEDSM03 4th ASME-JSME Joint Fluids Engrg. Conf*. Honolulu, Hawaii, Paper 45266.

Baines, W. D. (1991). Air cavity as gravity currents on slope. *J. Hydr. Engrg.* 117 (12), 1600-1615.

Benjamin, T. B. (1968). Gravity currents and related phenomena. *J. Fluid Mech.* 31 (2), 209-248.

Brunner, G. W. (2008) *HEC-RAS, River Analysis System Hydraulic Reference Manual,* US Army Corps of Engineering, Report Number CPD-69

Cardle, J. A., Song, C. S. S. (1988). Mathematical modeling of unsteady flow in storm sewers. *Int. J. Engrg. Fluid Mech.* 1 (4), 495-518.

Cunge, J., Wegner, M., (1964). Integration numerique des equations d'ecoulement de barre de st. venant par un schema implicite de differences finies. application au cas d'une galerie tantot en charge tantot a surface libre. *La Houille Blanche* (1), 33-39.

De Martino, G., Fontana, N., and Giugni, M. (2008). Transient flow caused by air expulsion through an orifice. *J. Hydr. Engrg.*,134(9) p. 1395-1399.

Falvey, H. (1980). Air-water flow in hydraulic structures. NASA STI/Recon Technical Report N, 81:26429.

Fuamba, M.,(2002). Contribution on transient flow modeling in storm sewers. *J. Hydr. Res.* 40 (6), 685-693.

Fuertes, V., Arregui, F., Cabrera, E., and Iglesias, P. (2000). Experimental setup of entrapped air pockets model validation. *BHR Group Conference Series Publication,* V 39, p. 133-146.

Goldring, B., T., (1983). Air voids at downshaft-tunnel bends. *J. Hydr. Engrg.* 109(2) p. 189-198

Guizani, M., Vasconcelos, J. G., Wright, S. J., and Maalel, K. (2005). “Investigation of rapid filling of empty pipes.” International Stormwater and Urban Water Systems Modeling Conference, Toronto, Canada, Ontario, Canada. CHI.

Guo, Q., Song, C. S. S. (1991). Dropshaft hydrodynamics under transient conditions. *J. Hydr. Engrg.* 117 (8), 1042-1055.

Hager W.H., (1999) Cavity outflow from a nearly horizontal pipe. *Int. J. of Multiphase Flow* 25, 349-364

Hamam, M. A., McCorquodale, J. A. (1982). Transient conditions in the transition from gravity to surcharged sewer flow. *Can. J. Civ. Engrg.* (9), 189-196

Holley, E.P., (1969). Surging in laboratory pipeline with steady inflow, *J. Hydr. Engrg.*, 95(3), 961-979.

Issa, R. I., Kempf, M. H. W. (2003). Simulation of slug flow in horizontal and nearly horizontal pipes with the two-fluid model. *Int. J. Multiphase Flow* 29 (1),69-95.

Izquierdo, J., Fuertes, J., Cabrera, E., Iglesias, P. L., and Garcia-Serra, J. (1999). “Pipeline start-up with entrapped air.” *J. Hydr. Res.*, 579-590.

Lautenbach, D.L., Vasconcelos, J.G. Wright, S. J., Wolfe, J. R. , Cassidy, J. F., Klaver, P. R. (2008) “Analysis of Transient Surge in the Proposed District of Columbia Water and Sewer Authority Deep Tunnel System” *Proc. 2008 - WEFTEC Conference*- Pittsburgh, PA

Lee, N. H. (2005) *Effect of Pressurization and Expulsion of Entrapped Air in Pipelines*. Ph.D. Thesis, School of Civil and Environmental Engineering, Georgia Institute of Technology

Li, J. and McCorquodale, A. (1999). "Modeling mixed flow in storm sewers." *J. Hydr. Engrg.,* 125(11), 1170-1180.

Liou, C. P. and Hunt, W. A. (1996). “Filling of pipelines with undulating elevation profiles.” *J. Hydr. Engrg.*. 534-539.

Martin, C.S. (1976). Entrapped air in pipelines. *Proc. of 2nd Intern. Conference on Pressure Surges*, London, England. B.H.R.A. Fluid Engineering, Bedford, England, U.K. pp. 15–28.

Politano, M., Odgaard, A., and Klecan, W. (2007). Case study: Numerical evaluation of hydraulic transients in a combined sewer overflow tunnel system. *J. Hydr. Engrg. 1103, 1110.*

Pozos, O. E. (2007). *Investigation on the Effects of Entrained Air in Pipelines*. PhD thesis, University of Stuttgart, Germany.

Preissmann, A. (1961). Propagation des intumescences dans les canaux et rivieres. In *First Congress of the French Association for Computation*, Grenoble, France, pages 433-442.

Press, W. H., Flannery, B. P., Teukolsky, S. A., Vetterling, W. T., (1989). *Numerical Recipes in Pascal*. Cambridge University Press.

Rossman, L. A. (2004) *Storm Water Management Model User's Manual Version 5.0*, US Environmental Protection Agency

Sanders, B.F. and Bradford, S.F. (2011) A network implementation of the two-component pressure approach for transient flow in storm sewers, *J. Hydr. Engrg.*, 137(2), 158-172

Song, C. S. S., Cardle, J. A., Leung, K. S. (1983). Transient mixed-flow models for storm sewers. *J. Hydr. Engrg.* 109 (11), 1487-1504.

Toro, E. F., (2001). *Shock-Capturing Methods for Free-Surface Shallow Flows*. John Wiley and Sons.

Trindade, B. and Vasconcelos, J. (2011). Numerical simulation of water pipeline filling events with limited ventilation. *Unpublished manuscript submitted in Dec. 2011 to the J. of Hydraulic Engineering*, ASCE

Vasconcelos, J. G. (2007). Mathematical model to simulate the filling of water mains. *Proc. 24º Brazilian Congress of Environmental Sanitation Engineering*, Belo Horizonte, Brazil (in Portuguese).

Vasconcelos, J. G., Marwell, D. T. B. (2011). Innovative simulation of unsteady low-pressure flows in water mains. . *J. Hydr. Engrg.*, 137(11) p.1490-1499

Vasconcelos, J. G., Moraes, J. R. S., and Gebrim, D. V. B. (2009). Field measurements and numerical modeling of a water pipeline filling events. *Proc. 33rd IAHR Congress.* Vancouver, Canada

Vasconcelos, J. G. and Wright, S. J. (2006). Mechanisms for Air Pockets Entrapment in Stormwater Storage Tunnels. *Proc. World Water and Environmental Resources Congress ASCE*, Omaha, NE

Vasconcelos, J. G. and Wright, S. J. (2009). Investigation of rapid filling of poorly ventilated stormwater storage tunnels. *J. Hydr. Res.*,47(5):547-558.

Vasconcelos, J. G. and Wright, S. J. (2011) Geysering generated by large air pockets release through water-filled ventilation shafts,– *J. Hydr. Engrg.*, v. 137, N. 5, 543-555

Vasconcelos, J.G., Wright, S. J., and Roe, P. (2006). Improved simulation of flow regime transition in sewers: Two-component pressure approach. *J. Hydr. Engrg.*, 132(6) p.553-560.

Vasconcelos, J.G., Wright, S. J., and Lautenbach, D. J.. (2011) Modeling Approaches for the Rapid Filling of Closed Conduits with Entrapped Air, *Proc. World Water and Environmental Resources Congress ASCE*, Palm Springs, CA.

Wallis, G. B., (1969). *One-Dimensional Two-Phase Flow*. McGraw-Hill, New York, NY.

Wilkinson, D.L. (1982). Motion of air cavities in long horizontal ducts. *J. Fluid Mech.* 118, 109-122.

Wisner, P.E., Mohsen, F.N. and Kouwen, N., (1975). Removal of air from water lines by hydraulic means. *J. of the Hydr. Div.*, Vol. 101, HY2, pp. 243-25.

Wylie, E. B., Streeter, V. L. (1993). *Fluid Transients in Systems*. Prentice Hall, Upper Saddle River, NJ.

Zhou, F., Hicks, F. E., Steffer, P. M., (2002). Transient flow in a rapidly filling horizontal pipe containing trapped air. *J. Hydr. Engrg.* 128 (6), 625-634.

Zhou, F., Hicks, F. E., Steffer, P. M. (2004). Analysis of effects of air pocket on hydraulic failure or urban drainage infrastructure. *Can. J. Civ. Engrg.* 31, 86-94.